

A Study of Integrated Structural Control Systems for Multi-Hazard
Response Mitigation

*This thesis is dedicated to my parents
for their love, endless support
and encouragement.*

A Study of Integrated Structural Control Systems for Multi-Hazard Response Mitigation

By
Saeedeh Heydari Asl

A Thesis
Submitted to the School of Graduate Studies
In Partial Fulfillment of Requirements
for the Degree of
Master of Applied Science

McMaster University
© Copyright by Saeedeh Heydari Asl, April 2014

Master of Applied Science (2014)
(Civil Engineering)

McMaster University
Hamilton, Ontario

TITLE: A Study of Integrated Structural Control Systems
for Multi-Hazard Response Mitigation

AUTHOR: Saeedeh Heydari Asl

SUPERVISOR: Dr. Michael J. Tait

NUMBER OF PAGES: 143 Pages (i-xi, 1-131)

Abstract

Dynamic Vibration Absorbers (DVA), including Tuned Mass Dampers (TMD) and Tuned Liquid Dampers (TLD) have been successfully employed to reduce excessive wind-induced resonant vibration motions in flexible structures. A limited number of studies have focused on utilizing TMDs in base isolated structures to reduce resonant motions resulting from multi-hazards (both wind and seismic excitation). A recent study has investigated the wind-induced response of a base isolated (BI) structure with a TLD under wind loading, however, its response under seismic excitation was not considered. The focus of this research was on the behaviour of coupled passive structural control base isolation systems under base excitation with particular attention on a BI-building-TLD. A series of shake table tests were conducted on a base isolated scale-model building with a TLD system mounted on its roof. The isolation system comprised of stable unbonded-fiber reinforced elastomeric isolators (SU-FREI). Tests, with and without liquid in the TLD system, were carried out to evaluate the influence of the TLD under both harmonic base excitation and earthquake excitation at various excitation amplitude levels. An existing BI-structure-DVA numerical model was modified to incorporate a multi-parameter isolator model (Backbone Curve model) to simulate the behaviour of a SU-FREI isolation system and was evaluated using results from the shake table study. The BI-structure-DVA numerical model was used to carry out a preliminary investigation on different combinations of linear and nonlinear base isolators with linear and nonlinear DVA under harmonic excitation. An iterative updating scheme was added to the numerical model to simulate the amplitude dependent behaviour of SU-FREI under earthquake excitation and this updated model was then used to investigate the performance of the BI-building-TLD and a linear BI-building-TLD under different earthquake ground motions.

Acknowledgements

I would like to gratefully and sincerely express my deepest gratitude to my supervisor, Dr. Michael Tait, for his tremendous support, understanding and patience throughout this study. Without his encouragement and guidance this project would not have been materialized.

I would also like to thank fellow graduate students Dr. Shayne Love, Barry Foster and Niel Van Englen who helped with the experimental phase of this research.

Finally, and most importantly, I would like to thank my parents for their unconditional love and care throughout my life, for their support in all my pursuits and for giving me the strength to pursue my goals and chase my dreams. I would not have made it this far without them. My sisters, my best friends all my life, deserve my wholehearted thanks as well for all their love and encouragement.

Table of Contents

Chapter 1 Introduction..... 1

 1.1 Introduction 1

 1.2 Research Subject 3

 1.3 Research Objectives 3

 1.4 Structure of Thesis 4

Chapter 2 Literature Review..... 6

 2.1. Theory of Base Isolation..... 6

 2.1 Base Isolated Structures Subjected to Wind and Earthquake Loads..... 8

 2.2 Base Isolation Systems..... 9

 2.2.1 Sliding Base Isolation Systems..... 9

 2.2.2 Elastomeric Isolators..... 11

 2.3 Fiber-Reinforced Elastomeric Isolators (FREI) 12

 2.3.1 Scragging 13

 2.3.2 Stable Unbonded Application of FREI..... 14

 2.4 Modelling of SU-FREI..... 16

 2.4.1 Backbone Curve Model 17

 2.4.2 Bouc-Wen Model..... 18

 2.5 Dynamic Vibration Absorbers 19

 2.6 Tuned Mass Damper (TMD)..... 19

 2.6.1 TMD Design 20

 2.6.2 Performance of TMDs under Earthquake Excitation..... 23

 2.7 Tuned Liquid Damper 25

 2.7.1 Background..... 25

2.7.2	Shallow Water TLD	26
2.7.3	Deep Water TLD and Damping Screens	27
2.7.4	Hardening and Softening Behaviour.....	27
2.7.5	Linearized TLD Properties	28
2.7.6	TLD Design Parameters.....	34
2.7.7	Modal Expansion Model.....	36
2.8	Base Isolation-Structure-Dynamic Vibration Absorber Systems.....	38
Chapter 3	Shake Table Test of a BI-Building-TLD System	41
3.1	Shake Table Test Set-up.....	41
3.2	Building Model	42
3.3	Base Isolation System	45
3.4	Tuned Liquid Damper	45
3.5	Test Results	47
3.5.1	Harmonic Base Excitation Tests.....	47
3.5.2	Natural Frequencies and Modes Shapes	49
3.5.3	Frequency Response Plots	52
3.5.4	Earthquake Excitation Tests	57
3.6	Summary	62
Chapter 4	BI-Structure-DVA Systems under Harmonic Excitation.....	64
4.1	Introduction	64
4.2	Base Isolation-Structure-DVA Model.....	65
4.3	Structure Module.....	68
4.4	Base Isolation Module.....	69
4.4.1	SU-FREI Models	69
4.5	Dynamic Vibration Absorber (DVA) Module	78

4.5.1	Tuned Liquid Damper Model	79
4.6	Input Excitation	81
4.7	Model Evaluation	81
4.8	Linear Base Isolation System Model	87
4.9	Linear DVA –Linear Tuned Mass Damper Model	87
4.10	Response of Linear and Nonlinear Base Isolation and DVA Systems.....	88
4.10.1	BI-Structure-TMD System.....	88
4.10.2	LBI-Structure-TLD System	91
4.10.3	LBI-Structure-TMD System	92
4.11	Summary.....	93
Chapter 5	BI-Structure-TLD under Earthquake Excitation.....	95
5.1	Introduction	95
5.2	Evaluation of BI-Structure-TLD Model for Earthquake Excitation	96
5.3	Nonlinear Base Isolation-Structure-TLD Subjected to Earthquake Excitation	101
5.4	Linear Base Isolation-Structure-TLD Subjected to Earthquake Excitation	109
5.5	Summary	113
Chapter 6	Summary and Recommendations	115
6.1	Overview of the Research	115
6.2	Shake Table Tests.....	116
6.3	Numerical Base Isolation-Structure-Dynamic Vibration Absorber Model.....	117
6.3.1	Base Isolation-Building-DVA Subjected to Harmonic Excitation	118
6.3.2	Base Isolation-Building-DVA Subjected to Earthquake Excitation.....	118
6.4	Recommendations for Future Studies	119
References	121

List of Figures

FIGURE 2-1 UNIFORM HAZARD SPECTRA (UHS) FOR FOUR MAJOR CANADIAN CITIES (5% DAMPING) NBC 2010 [8]	7
FIGURE 2-2 LATERAL DEFORMATION IN BASE ISOLATED STRUCTURE COMPARED TO FIXED BASED STRUCTURE	7
FIGURE 2-3 LOAD DISPLACEMENT HYSTERESIS FROM CYCLIC LATERAL TESTING ON AN UNSCRAGGED SU-FREI BEARING	14
FIGURE 2-4 GRAPHICAL DEPICTION DISPLAYING THE SOFTENING AND HARDENING BEHAVIOUR DUE TO ROLLOVER DEFORMATION OF SU-FREI.....	15
FIGURE 2-5 ROLLOVER DEFORMATION OF SU-FREI AT THREE DISPLACEMENT AMPLITUDES [43]	16
FIGURE 2-6 BILINEAR MODEL OF A SU-FREI (FIGURE FROM [44]).....	16
FIGURE 2-7 SCHEMATIC OF A STRUCTURE-TMD	21
FIGURE 2-8 INFLUENCE OF H/L AND NORMALIZED FLUID RESPONSE AMPLITUDE (η/h) ON TLD FREQUENCY RESPONSE [77]	28
FIGURE 2-9 SCHEMATIC OF STRUCTURE-TLD.....	29
FIGURE 2-10 TLD TANK DIMENSIONS.....	29
FIGURE 2-11 EQUIVALENT MECHANICAL LINEARIZED STRUCTURE-TLD.....	32
FIGURE 2-12 SCHEMATIC OF BI-STRUCTURE-TLD	39
FIGURE 3-1 SHEMATIC ELEVATION VIEW OF TEST BUILDING.....	42
FIGURE 3-2 SCHEMATIC PLAN VIEW OF TEST BUILDING	43
FIGURE 3-3 PHOTOGRAPH OF SHAKE TABLE TEST SETUP	43
FIGURE 3-4 PHOTOGRAPH OF SU-FREI.....	45
FIGURE 3-5 SCHEMATIC OF THE TLD.....	46
FIGURE 3-6 RESPONSE HISTORY PLOTS OF (A) ISOLATOR DISPLACEMENT, (B) ROOF ACCELERATION AND (C) TLD FREE SURFACE MOTION (EXCITATION AMPLITUDE=3.8 MM, EXCITATION FREQUENCY=1.22 Hz).....	48
FIGURE 3-7 APPROXIMATE MODE SHAPE OF (A) BI-BUILDING, (B) BI-BUILDING-TLD.....	51
FIGURE 3-8 FREQUENCY RESPONSE OF BI-BUILDING AND BI-BUILDING-TLD (A) ISOLATOR DISPLACEMENT AND (B) ROOF ACCELERATION AT AN EXCITATION AMPLITUDE OF 1.3 MM.....	53
FIGURE 3-9 FREQUENCY RESPONSE OF BI-BUILDING AND BI-BUILDING-TLD (A) ISOLATOR DISPLACEMENT AND (B) ROOF ACCELERATION AT AN EXCITATION AMPLITUDE OF 2.5 MM.....	54
FIGURE 3-10 FREQUENCY RESPONSE OF BI-BUILDING AND BI-BUILDING-TLD (A) ISOLATOR DISPLACEMENT AND (B) ROOF ACCELERATION AT AN EXCITATION AMPLITUDE OF 3.8 MM.....	55
FIGURE 3-11 FREQUENCY RESPONSE OF TLD FREE SURFACE MOTION	57
FIGURE 3-12 ACCELERATION TIME HISTORY OF INPUT EXCITATION FOR EL CENTRO EARTHQUAKE (PGA = 0.3 G)	58
FIGURE 4-1 BI-STRUCTURE-TLD MODEL.....	66
FIGURE 4-2 4DOF BI-STRUCTURE- DVA MODEL.....	66
FIGURE 4-3 INDIVIDUAL MODULES COMPRISING THE BI-STRUCTURE-TLD MODEL.....	67
FIGURE 4-4 FORCE AND ACCELERATION TRANSMISSION BETWEEN DIFFERENT MODULES.....	67
FIGURE 4-5 SCHEMATIC OF THE SU-FREI WITH THEORETICAL DIMENSIONS (UNITS MM)	70

FIGURE 4-6 DISPLACEMENT TIME HISTORY OF THE LATERAL CYCLIC TEST	70
FIGURE 4-7 MEASURED FORCE-DISPLACEMENT (HYSTERESIS) LOOPS FROM LATERAL CYCLIC TEST	71
FIGURE 4-8 HYSTERESIS LOOPS AT 100% T_R AND 200% T_R (A) EXPERIMENTAL, (B) BOUC-WEN MODEL	74
FIGURE 4-9 HYSTERESIS LOOPS (A) EXPERIMENTAL, (B) BOUC-WEN MODEL AND (C) BACKBONE CURVE MODEL (100% T_R)	77
FIGURE 4-10 INPUT HARMONIC BASE ACCELERATION TIME HISTORY (3.8 MM EXCITATION AMPLITUDE).....	81
FIGURE 4-11 BI-BUILDING ISOLATOR DISPLACEMENT AT (A) 1.3 MM (B) 2.5 MM AND (C) 3.8 MM EXCITATION AMPLITUDE	83
FIGURE 4-12 BI-BUILDING-TLD ISOLATOR DISPLACEMENT AT (A) 1.3 MM (B) 2.5 MM AND (C) 3.8 MM EXCITATION AMPLITUDE	85
FIGURE 4-13 BI-BUILDING-TLD FREE SURFACE RESPONSE AT (A) 1.3 MM AND (B) 3.8 MM EXCITATION AMPLITUDE.....	86
FIGURE 4-14 BI-BUILDING-TMD AND BI-BUILDING-TLD ISOLATOR DISPLACEMENT AT (A) 1.3 MM, (B) 2.5 MM AND (C) 3.8 MM EXCITATION AMPLITUDE.....	90
FIGURE 4-15 LBI-BUILDING-TMD ISOLATOR DISPLACEMENT AT (A) 1.3 MM AND (B) 3.8 MM EXCITATION AMPLITUDE	91
FIGURE 4-16 LBI-BUILDING-TMD ISOLATOR DISPLACEMENT AT (A) 1.3 MM AND (B) 3.8 MM EXCITATION AMPLITUDE	93
FIGURE 5-1 NORMALIZED ISOLATION DISPLACEMENT, ROOF ACCELERATION AND NORMALIZED WAVE HEIGHT TIME HISTORIES, BI- STRUCTURE-TLD MODEL COMPARED TO SHAKE TABLE TEST RESULTS, EL CENTRO EARTHQUAKE, PGA = 0.1 G.....	100
FIGURE 5-2 NORMALIZED ISOLATION DISPLACEMENT, ROOF ACCELERATION AND NORMALIZED WAVE HEIGHT TIME HISTORIES, BI- STRUCTURE MODEL COMPARED TO SHAKE TABLE TEST RESULTS, EL CENTRO EARTHQUAKE, PGA = 0.1 G	101
FIGURE 5-3 PSUEDO ACCELERATION RESPONSE SPECTRA OF EARTHQUAKES	103
FIGURE 5-4 PSUEDO ACCELERATION RESPONSE SPECTRA OF EARTHQUAKES	104
FIGURE 5-5 RESPONSE HISTORY OF ISOLATION DISPLACEMENT FOR (A) KOBE (B) EL CENTRO AND (C) SAN FERNANDO AT PGA = 0.1 G	105
FIGURE 5-6 RESPONSE HISTORY OF TLD WAVE HEIGHT FOR (A) KOBE EARTHQUAKE (B) EL CENTRO EARTHQUAKE AND (C) SAN FERNANDO EARTHQUAKE AT PGA = 0.1 G	107
FIGURE 5-7 RESPONSE HISTORY OF ISOLATION DISPLACEMENT FOR LINEAR BASE ISOLATION SYSTEM FOR (A) KOBE EARTHQUAKE (B) EL CENTRO EARTHQUAKE AND (C) SAN FERNANDO EARTHQUAKE AT PGA = 0.1 G.....	111
FIGURE 5-8 RESPONSE HISTORY OF WAVE HEIGHT FOR LINEAR BASE ISOLATION FOR (A) KOBE EARTHQUAKE (B) EL CENTRO EARTHQUAKE AND (C) SAN FERNANDO EARTHQUAKE AT PGA = 0.1 G	112

List of Tables

TABLE 3-1 STIFFNESS PROPERTIES OF FB BUILDING	44
TABLE 3-2 DAMPING PROPERTIES OF FB BUILDING.....	44
TABLE 3-3 MASS PROPERTIES OF FB BUILDING (INCLUDING TLD TANK MASS).....	44
TABLE 4-1 UNSCRAGGED BOUC-WEN PARAMETERS (UNITS N M).....	73
TABLE 4-2. BACKBONE CURVE MODEL PARAMETERS [7]	76
TABLE 4-3 EQUATIONS TO CALCULATE D_i COEFFICIENTS	80
TABLE 4-4 LINEARIZED EQUIVALENT TLD PARAMETERS AT THE FREQUENCY OF EXCITATION EQUAL TO NATURAL FREQUENCY OF THE TLD	88
TABLE 4-5 RATIO OF PEAK ISOLATOR DISPLACEMENT	92
TABLE 5-1 RELATIVE PERCENTAGE DIFFERENCE BETWEEN PREDICTED AND MEASURED BI-BUILDING-TLD PEAK ISOLATOR DISPLACEMENT AND ROOF ACCELERATION VALUES	98
TABLE 5-2 GROUND MOTION RECORDS.....	102
TABLE 5-3 REDUCTION IN PEAK ISOLATOR DISPLACEMENT FOR NONLINEAR BI-BUILDING WITH THE ADDITION OF A TLD.....	108
TABLE 5-4 REDUCTION IN PEAK ROOF ACCELERATION FOR NONLINEAR BI-BUILDING WITH THE ADDITION OF A TLD	108
TABLE 5-5 RATIO OF LBI-BUILDING-TLD PEAK ISOLATOR DISPLACEMENT TO BI-BUILDING-TLD PEAK ISOLATOR DISPLACEMENT	110
TABLE 5-6 RATIO OF LINEAR BI-BUILDING-TLD PEAK ROOF ACCELERATION TO SU-FREI BI-BUILDING-TLD PEAK ROOF ACCELERATION..	110
TABLE 5-7 PERCENT DECREASE IN PEAK ISOLATOR DISPLACEMENT RESPONSE FOR LBI-BUILDING WITH ADDITION OF TLD	113
TABLE 5-8 PERCENT DECREASE IN PEAK ROOF ACCELERATION RESPONSE FOR LINEAR LBI-BUILDING WITH ADDITION OF TLD	113

Chapter 1 Introduction

1.1 Introduction

In order to minimize loss of life and mitigate damage due to major earthquakes it is important to design and build earthquake resistant structures and to protect the vibration-sensitive contents of structures with critical functions. Conventional seismic design is based on dissipation of seismic energy through stable inelastic mechanisms such as flexural hinging of beams, columns and walls, axial tension yielding, compression buckling of brace elements and shear hinging of elements. Although these mechanisms can dissipate sufficient energy resulting in acceptable seismic performance, if properly designed, a major drawback with this design philosophy is that the dissipated energy corresponds directly to structural damage.

In the last two decades significant research effort has focused on increasing seismic performance levels utilizing innovative earthquake resistant systems. The majority of these systems can be divided into two main categories, supplemental damping devices that dissipate seismic energy, and base isolation systems, which limit the transmission of seismic energy to the structure. Seismic control, which can be implemented through the addition of supplemental damping devices and base isolation systems to the main structure, reduces the dynamic response of the structure as a result of the combination of structural period shift and added energy dissipation.

Base isolation decouples the motion of the structure from the ground motion by introducing a low stiffness layer between the structure and its foundation. This changes both the fundamental

frequency of the structure and the structural mode shape. The reduction in the natural frequency of a base isolated structure shifts the natural frequency of the structure away from the high frequency content of expected earthquakes in the region the structure is located. In a base isolated structure, the majority of lateral deformation during wind or earthquake excitation occurs in the isolation layer rather than the superstructure. As a results the structure responds in a near rigid body motion [1] leading to a reduction in structural damage.

Studies have indicated that base isolated structures perform efficiently under seismic loading. However, the increased deformability at the base of the structure and the increased flexibility of the base isolated structure make it more susceptible to wind induced vibrations. This can lead to serviceability issues such as excessively large base displacements and floor accelerations [2], [3]. Furthermore, if the bearings have low damping the addition of the isolation system could amplify resonant motions produced by wind excitations [3].

Several recent studies, have introduced dynamic vibration absorbers as a solution for the serviceability problem in base isolated structures [4], [5]. Dynamic vibration absorber (DVA) is a supplemental damping device mounted at a certain location on the structure. These devices reduce the dynamic response of the structure by absorbing and dissipating a portion of input energy. Dynamic vibration absorbers are efficient solutions for wind induced serviceability issues [5]. Studies have been carried out on dynamic vibration absorbers and their efficiency in suppressing wind and earthquake structural vibrations and several buildings in world are equipped with these devices [6].

The use of dynamic vibration absorbers in base isolated structures is a relatively new concept and the efficiency of this type of device is still being investigated. Structures equipped with both base isolation and dynamic vibration absorbers are often referred to as hybrid structural systems [3]. Nearly all the current studies of hybrid systems focus on the application of TMDs on base isolated structures. In 2011 Love et al. [3] introduced a TLD as an effective control system for wind induced base isolated structures. The study showed that a TLD could be employed to control structural vibrations in wind induced base isolated structures.

1.2 Research Subject

In this research study the response of a structure equipped with a base isolation system and a set of TLDs is experimentally investigated under two different types of excitation. The TLD, which is a nonlinear device, is coupled with a nonlinear base isolation system where the properties of both TLD and base isolation are amplitude dependent. A building model of this system was tested on a shake table under both harmonic and earthquake excitation.

While a TLD is considered a nonlinear dynamic vibration absorber with amplitude dependent stiffness and damping properties, a TMD on the other hand represents a linear device with linear damping and stiffness properties. This research investigates and compares the performance of both linear and nonlinear DVAs (i.e. TMDs and TLDs, respectively) on a base isolated structure subjected to harmonic base excitation and earthquake loading. Furthermore, additional studies were conducted in order to investigate the performance of the combination of linear or nonlinear DVAs with a linear or nonlinear isolation system. Base isolation systems having different linear stiffness values were studied.

The nonlinear base isolation systems studied and tested in this research utilized a stable unbonded fiber reinforced elastomeric isolator that has nonlinear amplitude dependent effective stiffness and effective damping. A scaled-model building equipped with stable unbonded fiber reinforced elastomeric isolators and a set of TLDs was utilized [7] and shake table tests were carried out to study the behaviour of these two nonlinear amplitude dependent control devices when used in combination. In this research different configurations of the above mentioned linear and nonlinear systems are studied and the performance of hybrid systems under harmonic and earthquake loading is investigated.

1.3 Research Objectives

The main objectives of this research were as follows:

- Conduct experimental shake table tests on a quarter scale base isolated building equipped with tuned liquid dampers; Study the response of a base isolated building equipped with

tuned liquid dampers subjected harmonic base excitation and earthquake excitation and compare the results to the response of the base isolated building without the TLDs.

- Select a model to simulate nonlinear stable unbonded fiber reinforced elastomeric bearings that were used in the shake table tests.
- Develop and evaluate a numerical model of a base isolation-structure-DVA system subjected to harmonic and seismic excitation.
- Investigation of performance of different combinations of linear/nonlinear base isolation systems with linear/nonlinear dynamic vibration absorbers subjected to harmonic base excitation and earthquake loading.

1.4 Structure of Thesis

The structure of this thesis is organized into seven chapters.

Chapter 1 provides a brief introduction and background information on BI-structure-DVA systems as well as an overview of the objectives of the research and the structure of the thesis.

Chapter 2 presents a literature review of both base isolation systems and dynamic vibration absorbers. This chapter begins with a brief overview of the theory of base isolation and performance of base isolated buildings under earthquake and wind excitation. Different base isolation systems are subsequently discussed and the isolators used in this research (stable unbonded fiber reinforced elastomeric isolator) are introduced. In addition, the properties of this type of isolator and two numerical models for SU-FREI are described. The second part of the chapter focuses on dynamic vibration absorbers. The design and performance of both tuned mass dampers (TMD) and tuned liquid dampers (TLD) are reviewed. Linearization of tuned liquid dampers and a modal expansion method to solve sloshing water problem in these devices are presented. Finally, buildings equipped with both a base isolation system and a dynamic vibration absorber are presented and discussed.

Chapter 3 presents a shake table test program. This chapter begins with a description of the shake table test setup and the scaled-model building used in this study. A detailed description of the tuned liquid dampers and isolation system are then presented. The types of base excitation employed in

this study are discussed and the time histories and response spectra are presented. Finally the shake table test results are presented and discussed.

Chapter 4 focuses on the numerical modelling of the base isolation BI-structure-DVA under harmonic base excitation. The SU-FREI are modelled using both a Bouc-Wen model and a Backbone Curve model. An existing BI-building-TLD program, developed for wind excitation, is modified in order to model and analyze a BI-structure-DVA under different levels of harmonic base excitation. The model is evaluated by comparing shake table harmonic excitation test results to model results. In addition, a preliminary investigation of different combinations of linear and nonlinear base BI and DVA systems subjected to harmonic base excitation is carried out. The parametric study comprises of different combinations of a linear and nonlinear base isolation (BI) and dynamic vibration absorbers (DVA) systems. The combinations are as follows:

- Nonlinear BI - Nonlinear DVA
- Nonlinear BI - Linear DVA
- Linear BI - Linear DVA
- Linear BI - Nonlinear DVA

Chapter 5 focuses on the modelling of BI-building-TLD subjected to earthquake excitation. Three different modelling methods are investigated and evaluated for earthquake excitation by comparing shake table test results with model results for El Centro earthquake at three different peak ground accelerations (PGA). The response of BI-building-TLD, using SU-FREI and TLD is then studied under 8 different earthquake ground motion records at 4 different PGA. Two linear base isolation building-DVA systems are also studied using the same earthquake ground motion records at two different PGA.

Chapter 6 provides a summary of the research work in this thesis and recommendations for future research on BI-structure-DVA systems.

Chapter 2 Literature Review

2.1. Theory of Base Isolation

A base isolation system is intended to protect a building from earthquake forces by reducing the transmission of horizontal acceleration into the building, providing a means of energy dissipation leading to reduced transmitted acceleration. Base isolation decouples the motion of structure from ground motion during an earthquake event. The isolation layer in the base isolated building modifies the first mode of the structure resulting in a reduction in or elimination of seismic induced damage compared to conventional fixed-based design [1].

Uniform Hazard Spectra (UHS) for 4 major Canadian cities is provided in Figure 2-1. It can be observed from this figure that the highest spectral acceleration during an earthquake commonly occurs in periods lower than 0.5 seconds. This period range corresponds to the fundamental periods of common low-rise structures. Such structures amplify earthquake accelerations, which leads to increased inter-story drift, resulting in structural damage. Increasing the fundamental period of the structural system can shift the structural period towards lower spectral acceleration values as shown in Figure 2-1 [1].

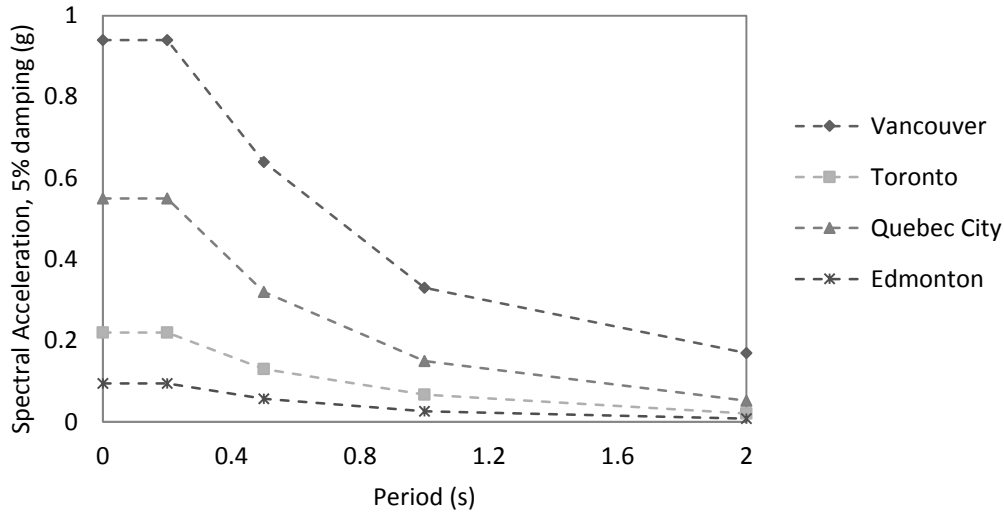


Figure 2-1 Uniform Hazard Spectra (UHS) for four major Canadian cities (5% damping) NBC 2010 [8]

The fundamental period of a properly designed isolated structure is much higher than the fundamental period of the fixed-base structure. The objective of a base isolation system is to shift the fundamental period of structural vibration to a value higher than the predominant energy containing periods of the earthquake. When the fundamental period of a building is within the low period range of expected earthquakes in a region, base isolation is expected to be effective. The isolation system modifies the fundamental period of the structural system by introducing a layer of low lateral stiffness between the foundation and superstructure. The majority of the lateral deformation therefore occurs in the isolation layer and the structure itself moves as a rigid body during the lateral excitation. This is illustrated in Figure 2-2.

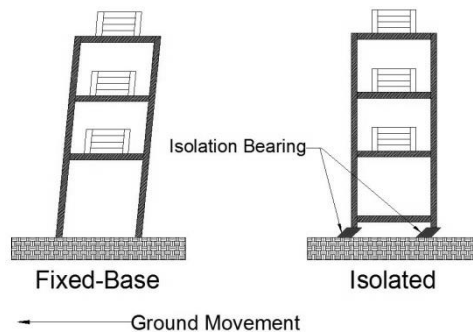


Figure 2-2 Lateral deformation in base isolated structure compared to fixed based structure

The first base isolated structure using elastomeric bearings was a three-storey building built in 1969 and located in the former Yugoslavia [1]. However, the bearings were found to possess insufficient vertical stiffness, which resulted in a rocking type response. In the last two decades, particularly after the introduction of steel reinforced elastomeric bearings, base isolation has gained acceptance as a viable solution for seismic mitigation [9]. The first base isolated building in United States was the Foothill Communities Law and Justice Center in San Bernardino (completed in 1985), which was designed to withstand a magnitude of 8.3 earthquake. The bearings used in this building consisted of natural rubber isolators reinforced with steel plates [9].

Base isolation is also an effective solution for the seismic retrofit of existing structures. As an example, the San Francisco City Hall, designed in 1911, experienced significant damage during the Loma Prieta (1989) earthquake. The building was subsequently retrofitted with 530 lead-plug rubber bearings, which were installed between the foundation and the structure. The bearings are expected to decrease the seismic vulnerability of the building under similar earthquakes and suppress structural deformation and damage.

An isolation system needs to have sufficient lateral flexibility to decrease the lateral stiffness and increase the period of structure. On the other hand, the bearings should be designed properly to have sufficient lateral stiffness in order to limit the effect of the isolation layer on the response of the isolated building under minor wind or earthquake loads. Moreover, the energy dissipation of the isolation system provided by the damping of the bearings or supplementary dampers must limit the displacements at the isolation level to an acceptable level.

2.1 Base Isolated Structures Subjected to Wind and Earthquake Loads

Ideally, the stiffness of the isolators should be relatively high when subjected to wind loading or low level earthquakes. As the load increases it is desirable that the stiffness of the isolators decreases, which lengthens the structural period. This type of behaviour results in base isolated structures that perform effectively under both wind loads and strong earthquakes.

Vulcano [10] numerically studied the dynamic response of base isolated buildings subjected to strong earthquake and wind loads and attempted to find an optimal base isolation system that

operates effectively under both load types. This study revealed that due to floor accelerations exceeding the comfort threshold, serviceability problems may occur during strong wind loads in buildings equipped with flexible base isolation systems with rather high isolation ratio values (i.e. greater than 4). Isolation ratio is defined as the ratio of fundamental vibration period of the isolated structure to the period of the fixed-base structure. An increase in the isolation ratio results in larger displacements under both earthquake and wind loads. This increase in the isolation ratio decreases seismic induced floor accelerations while increasing the floor accelerations under wind loads. The effect of wind loads on base isolated buildings, particularly tall buildings that are more vulnerable to the wind loads, is reported on Liang et al. [11] in which the acceleration response of buildings and the habitability of structures is studied under wind loading. Findings from this study indicate that increasing the damping ratio of the isolation system can control the acceleration response while it is not sufficient in controlling displacement demands. Furthermore, it was reported that increasing the horizontal stiffness of the isolation system is an efficient way to control the habitability of the base isolated structure and to keep accelerations in the human comfort level.

2.2 Base Isolation Systems

The basic types of the isolation systems that are in use today are divided into two major categories. Elastomeric bearings are the most common type in use in which the elastomeric material provides a restoring force to counter the earthquake forces. The other category is low-friction sliding systems that work by placing a low friction material between the structure and ground.

2.2.1 Sliding Base Isolation Systems

An attractive feature of this type of isolation system is the use frictional forces as an energy dissipation source. These devices are used in simple forms such as pure friction devices and more advanced devices involving pure friction elements in combination with laminated rubber bearings. Some examples of sliding systems include the following systems:

Sliding Friction or Pure Friction (P-F): The concept of sliding base isolation systems dates back to the 19th century just after catastrophic earthquakes in India and China [12], [13]. One or several friction plates are used to isolate the structure from the ground. Even a layer of sand separating the structure from the foundation can be utilized as a simple P-F base isolator [13], [14]. These devices reduce the seismic force transmission to the structure by limiting shear transfer across the sliders. Once the friction threshold is exceeded the structural response is governed by frictional characteristics of the sliding interface [15]. Sliding base isolation is a simple and low cost system with features such as stable properties, high performance-price ratio and non-resonant characteristics and is a suitable and applicable method for low cost structures [16]. However, the lack of a restoring force (self-centering) in these devices leads to undesirable permanent displacements of the structure after an earthquake event [7]. Advanced types of isolators have subsequently been introduced to overcome this drawback.

Friction Pendulum: This device has a concave sliding surface. The gravity force induced by the lifting of the structure due to lateral motion on the concave surface provides the restoring force to re-center the bearings. This feature results in the structure returning to its original position [17] after a seismic event. The material used for the sliding surface of these devices is primarily Teflon. The damping provided by frictional effects is, however, dependent on velocity, temperature, cleanliness and wear of the surface [9].

Resilient Friction (R-F): These devices were proposed by Mostaghel [18]. Among various friction devices, the resilient friction base isolation (R-FBI) system is the most common [19], [20] and has been found to be effective in reducing accelerations without undergoing large base displacements [21], [22]. This isolator type consists of several layers of Teflon coated friction plates with a central core of rubber in which the rubber provides the restoring force while the friction forces that develop between the plates provides an energy dissipation mechanism. An extensive study on this type of isolator was carried out by Mostaghel and Khodaverdian [23].

Sliding Resilient –Friction (SR-F): This system is a R-F unit with an additional upper friction plate. For low ground accelerations there is no sliding in the upper friction plate and the SR-F base isolator behaves as a R-F unit. For large ground accelerations, sliding in the upper friction plate occurs, which provides an additional energy dissipation mechanism and increases the overall effectiveness of the isolation system [24].

2.2.2 Elastomeric Isolators

The first elastomeric bearings produced were large rubber blocks consisting of either natural gum rubber or neoprene [25]. The vertical stiffness of these bearings was comparable to their horizontal stiffness. As a result, as the bearings were subjected to the weight of the structure large vertical deformations occurred in the bearings [25].

In addition to the low vertical stiffness of these bearings, under axial loads these bearings were found to exhibit significant bulging. Structural application of elastomeric bearings requires the vertical stiffness to be significantly larger than the horizontal stiffness in order to support the substantial structural weight. In order to increase the vertical stiffness while maintaining a low horizontal stiffness, reinforcing layers were introduced. The use of reinforcing sheets in rubber bearings not only significantly increases the vertical stiffness without changing the horizontal stiffness, but it also limits bulging under axial loading.

Another challenge with the natural rubber or synthetic rubber (neoprene) bearings is the low damping of these materials. Although the use of natural rubber leads to simplified manufacturing and modelling, the damping is often insufficient for base isolation application. As a result, additional supplementary damping is often required [25], which results in additional cost. The introduction of high damping natural rubber or neoprene materials and/or the use of a lead-plug core has resolved the low damping issue. These solutions eliminate the need for supplementary damping devices, which can be costly.

Steel Reinforced Elastomeric Isolator (SREI): this type of isolator is comprised of alternating layers of rubber and steel and rely on vulcanization to adhere the rubber to the steel plates. The manufacturing process of the SREI consists of cutting the steel plates, sand blasting and then acid cleaning. The steel plates are then placed in a mold together with the compounded sheets of rubber and are vulcanized by heating for several hours under high pressure. The steel reinforcement is near rigid in both extension and flexure and the bearings are flexible in the horizontal direction (capable of resisting wind forces with little or no deformation), and stiff in vertical direction.

High Damping Rubber Bearing (HDRB): These bearings are comprised of specially formulated high-density rubber elastomer, which possess significant levels of damping. However, the use of

this bearing type results in an increase in the accelerations transferred to the superstructure, which is undesirable for buildings that have sensitive equipment [26].

Lead Plug Laminated Rubber Bearing (LRB or New Zealand): this type of isolator was first introduced in 1975 in New Zealand [9]. A cylindrical lead-plug is placed in a hole located at the center of the bearing. The reason for selecting lead as the material is its high energy dissipating capacity compared to other readily available materials [27]. The lead core is used to reduce the lateral displacement and to offer an additional mechanism for energy dissipation, while flexibility and restoring forces are provided by the elastomer. The performance of this type of isolator is reported in [28], [29], [30]. Furthermore, work by [31] and [32] represent the mechanical behaviour of the hysteretic behaviour of this type of isolator.

2.3 Fiber-Reinforced Elastomeric Isolators (FREI)

As mentioned previously, the high cost and weight of the SREI have limited their use, particularly in common, normal importance buildings. As a more versatile and affordable alternative to steel reinforcement, cloth fiber has been introduced as an alternative reinforcement material, which is both flexible and light-weight. Fiber reinforcement comprises a large number of individual fibers that are grouped into strands, woven into a fabric, and embedded into a thin polymer matrix. The thin layers of fiber reinforcement used in a FREI are more flexible under extension and have negligible flexural rigidity compared to steel reinforcement [33]. Woven carbon fiber is the material primarily used as fiber reinforcement. Other materials such as glass fibers or Kevlar can also be used but are less common [34], [35]. Initial studies indicate that it is possible to achieve adequate vertical and horizontal stiffness in FREIs. Moreover, FREI have other advantages such as potentially low manufacturing cost, light-weight, and the possibility of being produced in long rectangular strips or large sheets and subsequently modified to the required size [36].

Several studies have compared the performance of carbon-FREI to SREI; concluding that while the effective stiffness of the SREI and carbon-FREI are comparable, the FREI provided almost twice the effective damping of SREIs for the same elastomer [37], [38]. When an FREI is subjected to lateral displacement, tension is developed in the reinforcement through the curvature of the

bearing. As a result, the individual strands in each fiber bundle slip against each other and produce frictional damping. This frictional damping adds to the natural damping of the elastomer [33]. This added damping can be compared to the added damping in SREI by using lead-plug [39].

2.3.1 Scragging

An elastomeric material in its natural untested virgin state is defined as being in its unscragged state. When an unfilled or particle reinforced rubber, in its unscragged state, is subjected to cyclic loading at a constant amplitude under tensile, compressive, or shear loading its stiffness reduces. Due to this reduction in stiffness the stress required on reloading is less than that of the initial loading for deformations up to a maximum of those previously achieved [40]. The mechanism, which results in this reduction of the stiffness is defined as scragging. Part of the reduction in stiffness will be recovered over time. The micro-mechanical structural behaviour that is responsible for this loss of stiffness is the breaking of weak crosslinks that are found in elastomers [40].

Once the material is deformed to a certain elongation level, it is scragged up to that elongation level [8]. The material is only scragged up to the largest amplitude to which it has been subjected to. Cycling the bearing at greater amplitudes than those previously tested will result in unscragged behaviour.

The difference between scragged and unscragged load displacement hysteresis is illustrated in Figure 2-3. The unscragged loop in Figure 2-3 is shown as solid line and the scragged loops corresponding to the second and third cycles are the dashed and dotted lines, respectively. As can be seen in Figure 2-3, a noticeable drop in effective stiffness occurs between the first and second cycles as a result of the scragging phenomena. However, it can also be observed that significantly less change is noted between the second and third cycles. Often, the effects of scragging on the hysteretic behaviour are greatest in the first cycle and become negligible after two to three cycles [41], which is in agreement with the results shown for the bearings considered in this study

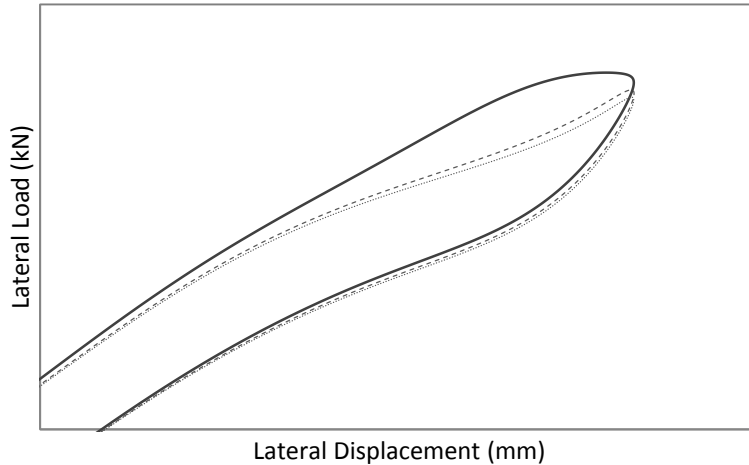


Figure 2-3 Load displacement hysteresis from cyclic lateral testing on an unscrapped SU-FREI bearing

2.3.2 Stable Unbonded Application of FREI

The connection of the isolators (steel reinforced or fiber reinforced) to the building (super-structure) and the base or foundation (substructure) is typically accomplished using thick steel plates to which the isolators are bonded. The use of these steel plates results in an isolator that is both heavy and costly. A more convenient installation method is to place the isolators directly underneath the structure with no connection to it or the structure and this also negates the need for the thick steel plates. This unbonded type of application reduces the cost and effort of installation and has been shown to be a low-cost and light-weight alternative to current seismic isolation practices [42].

Toopchi-Nezhad et al. [42] studied the behaviour of unbonded FREIs. An FREI satisfying the requirements of stability is denoted a stable unbonded fiber reinforced elastomeric isolator (SU-FREI). SU-FREIs with different aspect ratios under cyclic lateral tests were investigated by Toopchi-Nezhad [42]. It was found that SU-FREIs could be effectively used for seismic isolation purposes based on ASCE 7-05 design provisions. It was also demonstrated through experimental testing that SU-FREIs show suitable behaviour for seismic isolation purposes.

As the fiber reinforcement in the FREI has almost no flexural or bending rigidity, when the unbonded bearing is subjected to lateral displacements a unique deformation occurs, which was first referred to as rollover deformation by Toopchi-Nezhad et al. [42]. The stiffness of the isolators decreases as the rollover deformation occurs. This reduction in stiffness can result in an unstable response if the isolator is not properly designed. In the case of large lateral displacements, the two vertical faces of the bearing, perpendicular to the direction of excitation, make contact with the upper and lower support surfaces. As a result, the lateral stiffness begins to increase and hardening occurs in the bearing [43]. The graphical illustration of the softening and hardening due to the rollover deformation is shown in Figure 2-4. Figure 2-5 illustrates the rollover deformation of a SU-FREI.

As the isolator begins to rollover, the lateral stiffness decreases resulting in an increased period for the base isolated structure. An increased period increases the efficiency of an isolation system thereby mitigating the seismic response of a structure. The reduction in stiffness is considered acceptable as long as stability is maintained (i.e. the tangential lateral stiffness remains positive [42]). This contact phenomenon occurs in elastomeric bearings with flexible reinforcement in an unbonded application. As contact occurs the resultant hardening limits the extreme displacement of the isolator [41].

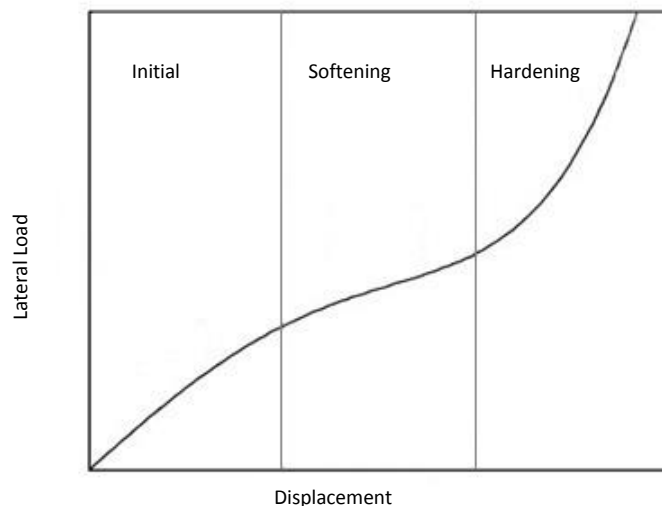


Figure 2-4 Graphical depiction displaying the softening and hardening behaviour due to rollover deformation of SU-FREI

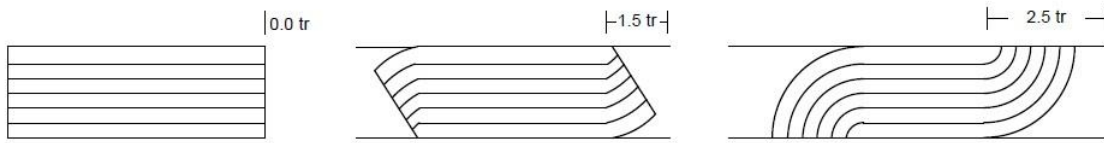


Figure 2-5 Rollover deformation of SU-FREI at three displacement amplitudes [43]

2.4 Modelling of SU-FREI

Various models have been introduced to simulate the behaviour of SU-FREIs. A proper model should simulate both the softening and hardening behaviour of this type of isolator. Simple models such as a bilinear model or more complex multi-parameter models have been utilized. Toopchi-Nezhad et al. [44] used a bilinear model to simulate the force-displacement behaviour of SU-FREI. This model simulates the idealized form of the unscragged load-displacement hysteresis loops of the SU-FREIs [44]. The parameters that represent this model include: elastic stiffness (K_1), post-yield stiffness (K_2) and strength (q). As shown in Figure 2-6, K_1 is selected in order to satisfy damping ratio at a given amplitude, K_2 is determined from the tangent stiffness at zero displacement [9] and the strength, q , is taken as the average of q_1 and q_2 .

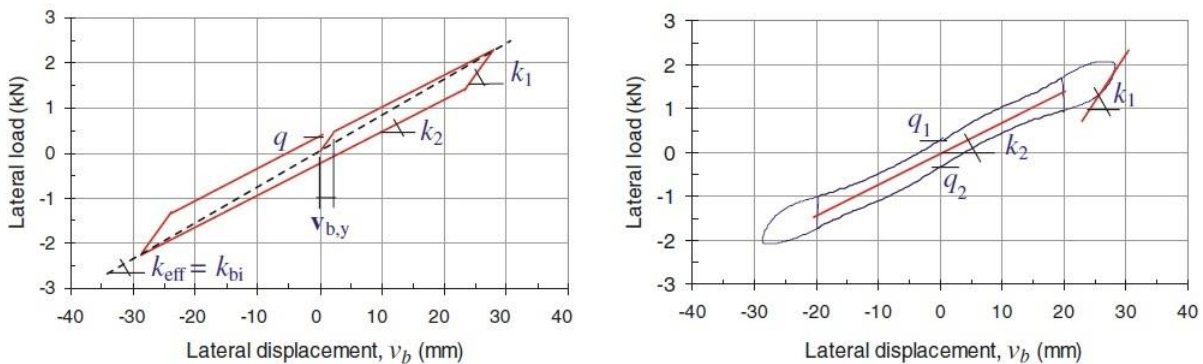


Figure 2-6 Bilinear model of a SU-FREI (Figure from [44])

Toochi-Nezhad et al. [44] also evaluated a complex 10-parameter rate and amplitude dependent stiffness and damping model to predict the lateral response of SU-FREIs. The constants and parameters of this model are evaluated by a least square fit to the lateral load-displacement

hysteresis loops of the isolators. Although this model was unable to capture the unscragged behaviour of the isolators, it is in a good agreement with scragged loops [44].

In another study Toopchi-Nezhad et al. investigated the use of a backbone curve model to simulate the hysteresis behaviour of SU-FREI [45]. This model utilizes a polynomial of order 5 and equivalent viscous damping to model the hysteresis loops. The parameters are determined by applying a least squares fit to the experimental data. Finally, Love et al. [3] used a modified Bouc-Wen model to simulate the behaviour of a SU-FREI. The Bouc-Wen model utilizes two time dependent variables to form two coupled equations simulating the hysteresis behaviour of the isolators.

2.4.1 Backbone Curve Model

The Backbone Curve model is a 5th order polynomial function that can be used to fit experimentally obtained lateral force-displacement response data. The lateral force in an individual bearing can be expressed as

$$f_{b,i}(t) = f_{sb,i}(t) + f_{db,i}(t) \quad 2-1$$

$f_{sb,i}(t)$ and $f_{db,i}(t)$ are the stiffness force and the damping force in bearing respectively. Where the stiffness force can be expressed as

$$f_{sb,i}(t) = k_{b,i}(v_b(t))v_b(t) \quad 2-2$$

where $v_b(t)$ is the displacement and $k_{b,i}(v_b(t))$ is the effective lateral stiffness of the bearing (secant stiffness) and is modelled as a 4th order polynomial

$$k_{b,i}(v_b(t)) = b_0 + b_1v_b(t) + b_2v_b^2(t) + b_3v_b^3(t) + b_4v_b^4(t) \quad 2-3$$

A least squares fitting method can be used to fit the 5th order model in order to determine the five parameters of the model b_0 to b_4 based on the experimental data of the lateral load displacement.

The equivalent viscous damping force of the hysteresis models of the individual bearings is also expressed as Rayleigh damping idealization and is calculated from the equation

$$f_{db,i}(t) = C_{b,i}(t)\dot{v}_b(t) \quad 2-4$$

$C_{b,i}(t)$ is the damping coefficient at any time instant and is defined as

$$C_{b,i}(t) = 2\zeta_{eff} \sqrt{\frac{k_{b,i}(v_b(t))P}{g}} \quad 2-5$$

where P , g and ζ_{eff} are the applied load on an individual bearing, the acceleration due to gravity and constant effective damping values respectively [42].

2.4.2 Bouc-Wen Model

A common model used to represent the hysteretic systems subjected to random excitation is the Bouc-Wen model. This model can be used for base isolation bearings subjected to wind and earthquake loadings.

The model utilizes two time dependent variables to form two coupled equations. X is the displacement variable representing the displacement of the bearing, and Z is a hysteretic variable that has no physical meaning. The Bouc-Wen model introduced by Chen and Ahmadi has the form of [3]:

$$p = c\dot{X} + a_1X + a_2|X|X + a_3X^3 + b\left(1 - \frac{\beta}{A}|z|^n\right)z \quad 2-6$$

$$Y\dot{z} = -\gamma|\dot{X}|z|z|^{n-1} - \beta\dot{X}|z|^n + A\dot{X} \quad 2-7$$

The cubic polynomial in the above equation enables the softening behaviour of the bearing to be modelled by altering the backbone curve of the load-displacement plots.

In order to capture the softening and subsequent hardening behaviour as the bearing is displaced laterally a fifth order polynomial is introduced [3]:

$$p = c\dot{X} + a_1X + a_2|X|X + a_3X^3 + a_4|X|X^3 + a_5X^5 + b\left(1 - \frac{\beta}{A}|z|^n\right)z \quad 2-8$$

The above modified Bouc-Wen model describes the behaviour of a non-linear isolation system such as the SREIs in the case of elastomeric isolators [3]. The parameters were determined by least square fitting of the model to experimental force-displacement test data.

Both the Backbone Curve model and Bouc-Wen model that will be used to simulate the force-displacement behaviour of the isolators used in this study are presented in more detail in Chapter 4.

2.5 Dynamic Vibration Absorbers

Over the past several decades, advanced analysis tools together with modern construction techniques and the development of new construction materials have led to both light-weight and flexible structures. However, structures having the above characteristics often experience excessive deformations and accelerations due to wind-induced vibration leading to serviceability limit state issues. Consequently, the lateral displacement becomes a more prevalent issue and serviceability requirements, including limiting the deflections and accelerations, can govern the design [5]. In order to meet the serviceability requirements, a significant number of tall buildings and towers are fitted with a variety of supplemental damping systems. Supplemental damping systems are intended to consume a portion of the wind or seismic energy input into a structure. The mechanical energy dissipation in the supplemental damping device reduces the energy dissipation demand on the structural system, thereby reducing the dynamic response of the structure. The two most common types of dynamic vibration absorbers are tuned mass dampers and tuned liquid dampers [4].

2.6 Tuned Mass Damper (TMD)

A conventional TMD includes a relatively small auxiliary mass attached to the main structure. TMDs were introduced by Frahm in 1909 [46]. In its simplest form a TMD, which is an assembly of a mass, a spring and a viscous damper, is placed at a certain location in the building. The absorber is usually installed near the roof level of the building. The main task of the device is to counter the effect of the lateral excitation forces by absorbing a portion of the vibration energy from the structure. These systems are capable of significantly reducing the dynamic response of the structure and have shown to be particularly effective in reducing wind-induced vibrations and

limiting the floor vibrations in high-rise buildings [46]. The principle of operation is to transfer the vibration energy from structure to the auxiliary mass. The auxiliary mass dissipates the vibration energy by vibrating out of phase with structural motion and absorbs a portion of the input energy thus reduces the dynamic response of main structure.

Although TMDs are highly efficient their use has some drawbacks. Although the mass of the TMD is a small fraction of the main structure mass, it requires a relatively large space for installation. In addition, the TMD is normally designed to be in resonance with the building and can undergo relatively large lateral displacements. Thus, large clearances must be provided to accommodate these displacements at the installation location. Furthermore, the TMD must be capable of having free motion during vibration. As a result it must be mounted on a smooth, near friction free, surface to allow free motion [46] or installed as a suspended mass.

The first recorded application of a TMD in a building was the Centerpoint Tower in Australia [47] in 1987. Another one of the earliest TMD applications was in Citicorp building in New York. The building is 278 meters tall and the installed TMD consists of a 410 ton concrete block. The TMD system, located on the 63rd floor, has a dimension of $9.14 \times 9.14 \times 3.05$ m. The mass is attached to two sets of spring damping mechanisms [6]. One of the world's largest TMDs is installed in Taipei 101 tower, which was constructed in 2004. The 101 storey building is 508 meters high and is equipped with a TMD. The mass is 660 tons and is suspended from the 92nd floor. The pendulum sways to offset building motions that are caused by strong winds. Its sphere, the largest damper sphere in the world, consists of 41 circular steel plates, each with a height of 125 mm being welded together to form a 5.5 m diameter sphere [48].

Additional examples of TMD applications include the CN Tower in Toronto (1975), Huis Ten Bosch Domtoren in Nagasaki (1992) and Washington National Airport Tower in Washington D.C. (1997) [6].

2.6.1 TMD Design

A simple TMD-structure system could be illustrated as a two degree of freedom mass-spring-dashpot system as shown in the Figure 2-7.

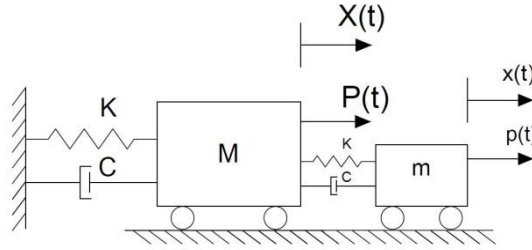


Figure 2-7 Schematic of a Structure-TMD

For the system subjected to base excitation, applying Newton's second law of motion on each of the masses yields the two equations of motion for this two degree of freedom system [4]:

$$M\ddot{X}(t) + C\dot{X}(t) + KX(t) - [c\{\dot{x}(t) - \dot{X}(t)\} + k\{x(t) - X(t)\}] = P(t) \quad 2-9$$

$$m\ddot{x}(t) + c\{\dot{x}(t) - \dot{X}(t)\} + k\{x(t) - X(t)\} = p(t) \quad 2-10$$

m , c and k are the mass, damping and stiffness parameters of TMD. In the above equations no simple closed-form expression can be derived for the optimum damper parameters. One approach to determine the optimum parameter values is by numerical trial and error; that is to investigate different combinations of damper parameters ξ_{TMD} and f in a systematic manner to get the combination that minimizes the maximum response [49]. Numerous studies over the past several decades have used this method to develop design graphs for obtaining optimum damper parameters. Randall et al. [50] developed such design graphs for damped SDOF structures under wind-type excitation.

Den Hartog [51], solved the structure-TMD equations of motion to minimize the steady-state response of an undamped main structure subjected to harmonic base or main mass excitation. In this study a closed form expressions for the optimum design parameters of the TMD attached to an undamped structure was developed.

Assuming m as the absorber mass and M as the main structure mass, the mass ratio μ is defined as

$$\mu = \frac{m}{M} \quad 2-11$$

If ω_{TMD} is the frequency of the damper mass and ω is the natural frequency of the main structure mass, the frequency ratio f is defined as

$$\Omega_{opt} = \frac{\omega_{TMD}}{\omega} \quad 2-12$$

Den Hartog [52] studied the variation of the amplitude ratio a_1/x_{st} as a function of the forcing frequency ratio for a TMD tuned to the primary structure. He defined a_1 as the amplitude of the sinusoidal steady-state response and x_{st} is the static displacement of primary structure, respectively. The optimum frequency ratio, Ω_{opt} , and optimum damping ratio of TMD, ξ_{opt} , for the case of harmonic excitation acting the main structure mass where found to be a function of the mass ratio.

$$\Omega_{opt} = \frac{1}{1 + \mu} \quad 2-13$$

$$\xi_{opt} = \sqrt{\frac{3\mu}{8(1 + \mu)}} \quad 2-14$$

Furthermore, when the harmonic excitation is applied on the base of the structure the optimum parameters were determined to be [53]:

$$\Omega_{opt} = \frac{1}{1 + \mu} \sqrt{\frac{2 - \mu}{2}} \quad 2-15$$

$$\xi_{opt} = \sqrt{\frac{3\mu}{8(1 + \mu)}} \sqrt{\frac{2}{2 - \mu}} \quad 2-16$$

The optimization carried out by Den Hartog was based on minimizing the relative displacement amplitude of the primary structure in an undamped linear single-degree-of-freedom structure subjected to harmonic dynamic force.

Warburton and Ayorinde [54] found that if the damping of main structure is small the effect of the structural damping on optimal parameters is negligible. They determined the optimal parameters for an undamped structure under random base excitation as follows:

$$\Omega_{opt} = \frac{1}{1 + \mu} \sqrt{1 + \frac{\mu}{2}} \quad 2-17$$

$$\xi_{opt} = \sqrt{\frac{\mu(4 + 3\mu)}{8(1 + \mu)(2 + \mu)}} \quad 2-18$$

Asami et al. [55] determined a numerical solution for a damped structure subjected to unit input acceleration from ideal white noise with optimization criterion aimed at minimizing the mean square acceleration response. Asami et al. [56] published a series of optimal solutions for damped structure subjected to sinusoidal excitation and random white noise excitation.

2.6.2 Performance of TMDs under Earthquake Excitation

Several researchers have investigated optimum TMD design parameters including the frequency ratio and damping of TMD for a given mass ratio in order to reduce the structural response under earthquake loading. However, there is no general agreement on the design parameters of TMDs for seismic excitation [57]. In some early studies, TMDs were found to be ineffective in reducing the seismic response of structures. Gupta and Chandrasekaren [58] found that the use of TMDs in reducing response of structure subjected to earthquake excitation is not as effective compared to the case of harmonic excitation. Kaynia et al. [59] investigated the effect of TMD on the fundamental mode response, concluding that TMDs are less effective in reducing seismic response than previously assumed. A total of 48 different earthquake records were used in this study. Findings showed that optimum reduction in response was achieved at the frequency ratio of unity ($\Omega = 1$). It was concluded that increasing the period and damping of structure would reduce the efficiency of the TMD. Sladek and Klingner [60] used the parameters introduced by Den Hartog for harmonic loading and studied the response of a 25-storey building under the El Centro earthquake. Findings indicate that TMDs are not effective in reducing the response of the building. Later more successful studies were carried out showing the efficiency of TMDs in buildings subjected to seismic excitation. Wirsching and Yao [61] obtained considerable response reduction for a TMD with a certain mass ratio and tuning ratio of $\Omega = 1$ by changing the damping ratio for a structure under non-stationary ground acceleration. Wirsching and Campbell [62] showed the efficiency of TMDs by calculating TMD parameters for a building subjected to white noise base acceleration using an optimization method. Ohno et al. [63] minimized the mean square

acceleration response of main structure subjected to earthquake ground motion. Villaverde [64], [65], Villaverde and Koyama [66] and Villaverde and Martin [67] also studied the applicability of TMDs for seismic application. They found that when the damping ratio of the first two complex modes of vibration of structure-TMD system is equal to the average damping ratios of structure and TMD, the TMD performance is greatest. To achieve this damping ratio the TMD should be in resonance with the main structure and the damping ratio should be equal to:

$$\xi = \beta + \phi\sqrt{\mu} \quad 2-19$$

where β is the damping ratio of the structure, ϕ is the amplitude of mode shape at TMD location and μ is the ratio of TMD mass to the generalized mass of structure in given mode. β and ϕ are computed for a unit modal participation factor. The method was found to be effective after being used in several numerical and experimental 2D and 3D analysis of buildings and cable-stayed bridges under different ground excitations. Miyama [68] showed that it is possible to obtain 80 percent energy absorption with a mass ratio of 5 percent and argued that TMDs with a mass less than 2 percent of the first mode of the generalized mass are not effective. Sadek et al. [57] introduced an improvement to the method presented by Villaverde and numerically illustrated the effectiveness of this improved method in determining the TMD parameters for seismic application.

Studies have also showed that one of the inherent limitations of TMD systems is lack of robustness against deviations in design parameters [69], [70]. High dependence on the earthquake frequency content and impulsive character of the earthquake excitation are mentioned as other limitations on the efficiency of TMDs for seismic loading [52], [71]. It was also found that improved control performance can be attained by increasing the mass ratio to enhance robustness and seismic effectiveness.

TMDs that are designed for harmonic or wind excitation can be optimized to maximum the reduction of the resonant response. However, a TMD that is tuned for optimum response reduction for a specific earthquake may not lead to maximum response reduction for other earthquakes. In other words, in the case of earthquake excitation, unlike harmonic and wind excitation, an optimum design that works for a general earthquake loading cannot be determined. Therefore, for earthquake loading the design approach should focus on improving the overall TMD performance for general seismic excitation instead of optimizing TMD parameters for a specific earthquake.

Villaverde [72] has reported significant reduction in the structural response under earthquake excitation using a resonant TMD approach that results in two of the modal damping coefficients being approximately equal to the average of damping ratios of the resonant modes of the building and the TMD. Sadek et al. [57] also reported considerable reduction of the response of structure subjected to earthquake loading by designing the TMD to obtain equal damping and frequencies for the first and third complex modes of vibration. Miranda [73] demonstrated that the optimum parameters for an efficient TMD correspond to a specific tuning which defines an energetic balance between the building and the TMD. This study presented a theoretically approximate energy-based model for a two-degree of freedom mechanical system. Miranda investigated the use of a TMD as a means to substantially increase modal damping in order to decrease seismic response of the structure and determined optimum TMD parameters that maximize the modal damping of the TMD through an iterative procedure.

2.7 Tuned Liquid Damper

2.7.1 Background

A tuned liquid damper (TLD) consists of a rigid tank partially filled with a fluid, which is typically water. Lateral excitation of the structure will cause sloshing motion of the liquid inside the TLD tank. A TLD reduces the response of the structure utilizing the fluid sloshing motion to absorb and dissipate the lateral excitation energy. In order to maximize the amount of energy dissipation, TLDs are normally designed to operate at the resonant frequency of the structure. By tuning the natural frequency of the sloshing motion to the natural frequency of the structure the liquid motion transmits inertia forces approximately anti-phase to the external excitation force, suppressing the structural vibration [74].

TLDs have been utilized to mitigate the lateral vibration of tall and flexible buildings since the 1980s. Some of the advantages of TLDs compared to other vibration dampers are low cost of installation and maintenance and their simple design. Additionally, the necessity of installing water

tanks for fire suppression purposes in current building codes creates an opportunity for using the same tanks as TLDs to meet both objectives.

The idea of using a liquid tank as a TLD was proposed almost 100 years ago by Frahm in 1909 [51] and at that time was primarily used for reducing rolling in ships. In 1960s it was also used in space applications to reduce satellite oscillations [75], [76]. Since 1980s, several existing buildings that suffered from vibration problems had been outfitted with TLD systems, simply through modifying existing water storage tanks. Some recent applications of this device include One King West Tower in Toronto, Canada, completed in 2005 and One Rincon Hill Tower in San Francisco, U.S., completed in 2009.

At larger response amplitudes the sloshing motion of the water inside the tank is often characterized as highly non-linear [74]. The amplitude of the sloshing motion depends on the amplitude and frequency of the excitation forces as well as the geometry of the tank, properties of the contained liquid and depth of the liquid inside the tank [74].

2.7.2 Shallow Water TLD

TLDs are categorized based on the ratio of water depth to tank length denoted as the fluid depth ratio. TLDs with a fluid depth ratio of less than 0.1 are categorized as shallow water TLDs and TLDs with larger water depth ratio are categorized as deep water TLDs.

In shallow water systems, energies dissipate through wave breaking at the fluid surface and viscous dissipation in the boundary layer at the walls and at the bottom of the tank. While in deep water TLDs wave breaking does not typically occur [77]. The damping caused by the wave breaking can be an order of magnitude higher than the damping ratio achieved in deep water TLDs. Sun et al. [77] showed that damping in deep water TLDs is too low to be sufficiently effective while the shallow water TLDs normally have sufficiently high damping.

Although the larger damping of shallow water TLDs is advantageous, using shallow water TLDs has some major drawbacks. Studies have shown that the effectiveness of TLDs is proportional to their mass ratio, which is defined as ratio of effective mass of the fluid inside the TLD tank to the total mass of the building. A TLD with larger mass works better in terms of energy dissipation

through sloshing force [77]. Therefore, for shallow water TLDs a larger number of tanks must be used to achieve a reasonable mass ratio, which can lead to space limitation issues. Another issue with shallow water TLDs is the fact that the occurrence of wave breaking leads to extremely nonlinear and unpredictable response behaviour.

2.7.3 Deep Water TLD and Damping Screens

Due to the drawbacks of using shallow water TLDs, deep water TLDs can be utilized with mechanisms to increase the inherent damping ratio. Deep water TLDs permit suitable mass ratios to be achieved and do not have the same level of nonlinearities as shallow water TLDs. Increased damping can be obtained by installing damping screens inside the tank. The use of screens is an economical and simple way to increase and control the damping of a TLD. The damping can be adjusted by changing the screen solidity ratio, which is defined as the ratio of blocked area to open area in the screen [78].

Adding damping devices to TLDs was first introduced in 1950's by introducing ring baffles to the tank walls by Miles [79], Bauer [80], and Abramson [81]. In later studies submerged nets and screens were placed inside the TLD tanks in order to induce energy dissipation [82], [83]. Studies have also been carried out on the effect of number of screens and location within a TLD [84]. The deciding criterion for the best arrangement was determined based on the amount of energy absorbed by the TLD.

2.7.4 Hardening and Softening Behaviour

The natural frequency of liquid sloshing is amplitude dependent and therefore is nonlinear. Studies show that the liquid depth to length ratio, h/L , affects the nonlinear type of sloshing. In shallow liquid TLDs, studies show that as the amplitude of excitation increases, the natural frequency of liquid becomes higher that is hardening type nonlinearity. Experiments show that this hardening behaviour is strong when the depth ratio is around 0.1. As the depth ratio increases the nonlinearity becomes weaker. At the depth ratio of 0.3, the behaviour of the liquid sloshing is almost linear. At

this depth ratio the amplitude dependency of the frequency of sloshing is minimum. At the depth ratios higher than 0.4 the behaviour of sloshing liquid becomes softening [77].

Hayama [85] reported the critical value of depth ratio at 0.335. According to his study, the liquid motion is hardening when $h/L < 0.335$ and it is softening when $h/L > 0.335$. The liquid motion is linear at $h/L = 0.335$. It is shown in Figure 2-8 for liquid depth ratios below 0.3 the frequency response curve bends to high frequency side and liquid sloshing becomes hardening. For depth ratio of 0.4 the fluid sloshing is softening with the frequency response curve bending to low frequency side. For critical depth, the frequency of liquid does not depend on the excitation amplitude. At this depth ratio the fluid sloshing becomes linear and the peak fluid response stays at the frequency ratio of 1.00 [77].

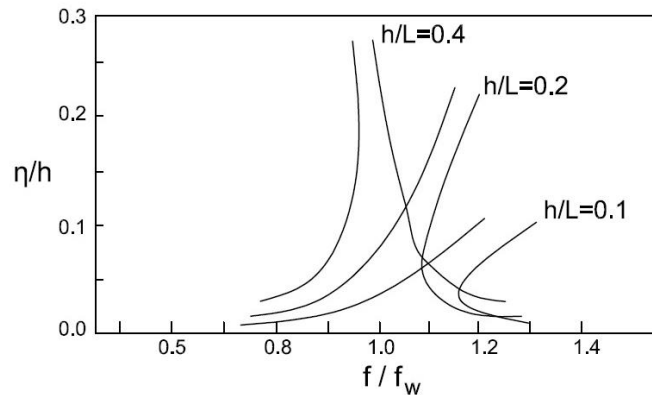


Figure 2-8 Influence of h/L and normalized fluid response amplitude (η/h) on TLD frequency response [77]

2.7.5 Linearized TLD Properties

2.7.5.1 Generalized Properties of TLD

By restricting the fluid response to small amplitudes the TLD can be modelled as an equivalent TMD. It has been found that the response of a structure equipped with a TLD can be predicted with reasonable accuracy using this type of model [86].

Figure 2-9 shows a schematic of a TLD-structure system. Assuming a rigid tank and inviscid, incompressible, irrotational fluid flow and negligible surface tension, the velocity of a liquid particle relative to the tank can be represented by the gradient of velocity potential $\Phi(x, z, t)$.

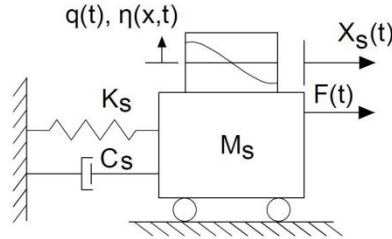


Figure 2-9 Schematic of Structure-TLD

For the TLD consider a rigid rectangular tank of length L in the direction of excitation, width b perpendicular to excitation and height H , filled with water to a stationary depth h is shown in Figure 2-10.

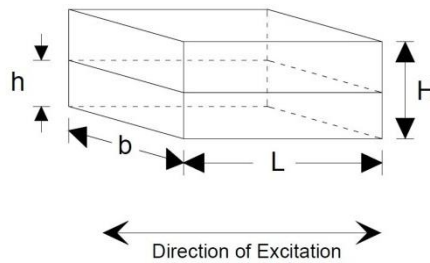


Figure 2-10 TLD tank dimensions

Considering the kinematic continuity of incompressible flow leads to the following requirement [86]

$$\frac{\partial^2 \Phi}{\partial x^2} + \frac{\partial^2 \Phi}{\partial z^2} = 0 \quad 2-20$$

The solution satisfying equation above can be expressed as

$$\Phi(x, z, t) = \sum_{n=1}^{\infty} \dot{q}_n(t) \cos\left(\frac{n\pi x}{L}\right) \frac{\cosh\left(\frac{n\pi(z+h)}{L}\right)}{\left(\frac{n\pi}{L}\right) \sinh\left(\frac{n\pi h}{L}\right)} \quad 2-21$$

The generalized coordinate $q_n(t)$ and its derivative are functions of time and its associated spatial function represents the velocity potential function of the n^{th} sloshing mode.

The amplitude of liquid sloshing is assumed to be sufficiently small so that the linearized free surface condition is satisfied by

$$\left[\frac{\partial \Phi}{\partial z} \right]_{z=0} = \frac{\partial \eta}{\partial t} \quad 2-22$$

The generalized coordinate $q_n(t)$ can physically be described as free-surface sloshing amplitude of the n^{th} mode at $x = 0$ as follows

$$\eta(x, t) = \sum_{n=1}^{\infty} q_n(t) \cos\left(\frac{n\pi x}{L}\right) \quad 2-23$$

The corresponding Lagrange's equations of this system take the form of

$$\frac{d}{dt} \left(\frac{\partial T}{\partial \dot{q}_n} \right) - \frac{\partial T}{\partial q_n} + \frac{\partial V}{\partial q_n} = Q_n, \quad n = 1, 2, 3, \dots \quad 2-24$$

where Q_n accounts for non-conservative forces and T is the kinetic potential energy and V is gravitational potential energy of the sloshing liquid.

Therefore, the equation of motion for the structure-TLD system shown in Figure 2-9 can be expressed as

$$m_n^* \ddot{q}_n(t) + c_n^* \dot{q}_n(t) + m_n^* \omega_n^2 q_n(t) = \gamma_n^* \ddot{X}(t), \quad n = 1, 2, 3, \dots \quad 2-25$$

where generalized mass and stiffness properties are

$$m_n^* = \frac{1}{2} \frac{\rho b L^2}{n\pi \tanh\left(\frac{n\pi h}{L}\right)} \quad 2-26$$

$$k_n^* = \frac{\rho b L g}{2} \quad 2-27$$

and γ_n^* the excitation factor is defined as

$$\gamma_n^* = \rho b L^2 \frac{(1 - \cos(n\pi))}{(n\pi)^2} \quad 2-28$$

The linearized generalized damping can be determined by minimizing the error between the actual damping force and the linearized generalized damping force [87]

and C_l is loss coefficient and is defined as

$$C_l = SC_d \quad 2-29$$

in which $S = \frac{A}{bh}$ with A being is the area of screen normal to the flow and C_d is the drag coefficient.

The value of c_{eq}^* is excitation dependent, and the linearized generalized damping coefficient has been determined for both random and sinusoidal excitation [86].

While the above equivalent damping accounts for the damping due to the damping screens, the energy dissipation through the fluid viscosity is also estimated as

$$\xi_w = \left(\frac{1}{2h}\right) \sqrt{\frac{\nu}{2\omega_n}} \left(1 + \frac{2h}{b} + SC\right) \quad 2-30$$

Where SC is defined as surface contamination factor and is usually taken as unity.

2.7.5.2 Structure-TLD System

The equation of motion for an equivalent linear two degree of freedom structure-TMD system can be expressed as [86]:

$$\begin{bmatrix} (M_s + m) & m \\ m & m \end{bmatrix} \begin{bmatrix} \ddot{X}_s \\ \ddot{x}_r \end{bmatrix} + \begin{bmatrix} C_s & 0 \\ 0 & c \end{bmatrix} \begin{bmatrix} \dot{X}_s \\ \dot{x}_r \end{bmatrix} + \begin{bmatrix} K_s & 0 \\ 0 & k \end{bmatrix} \begin{bmatrix} X_s \\ x_r \end{bmatrix} = \begin{bmatrix} F(t) \\ 0 \end{bmatrix} \quad 2-31$$

The equation of motion of the structure equipped with TLD shown in Figure 2-9 according to Lagrange's equations is in the form of

$$\begin{bmatrix} (M_s + \rho bhL) & \gamma^* \\ \gamma^* & m^* \end{bmatrix} \begin{bmatrix} \ddot{X}_s \\ \ddot{q} \end{bmatrix} + \begin{bmatrix} C_s & 0 \\ 0 & c_{eq}^* \end{bmatrix} \begin{bmatrix} \dot{X}_s \\ \dot{q} \end{bmatrix} + \begin{bmatrix} K_s & 0 \\ 0 & k^* \end{bmatrix} \begin{bmatrix} X_s \\ q \end{bmatrix} = \begin{bmatrix} F(t) \\ 0 \end{bmatrix} \quad 2-32$$

Therefore, substituting x_r the equation of motion of the TLD-structure system will have the form of

$$\begin{bmatrix} (M_s + m_w) & m_{eq} \\ \gamma^* & \gamma^* \end{bmatrix} \begin{bmatrix} \ddot{X}_s \\ \ddot{x}_r \end{bmatrix} + \begin{bmatrix} C_s & 0 \\ 0 & c_{eq}^* \Gamma \end{bmatrix} \begin{bmatrix} \dot{X}_s \\ \dot{x}_r \end{bmatrix} + \begin{bmatrix} K_s & 0 \\ 0 & k^* \Gamma \end{bmatrix} \begin{bmatrix} X_s \\ x_r \end{bmatrix} = \begin{bmatrix} F(t) \\ 0 \end{bmatrix} \quad 2-33$$

thus the motion of the equivalent TMD-structure system of Figure 2-11 is described as

$$\begin{bmatrix} (M'_s + m_{eq}) & m_{eq} \\ m_{eq} & m_{eq} \end{bmatrix} \begin{bmatrix} \ddot{X}_s \\ \ddot{x}_r \end{bmatrix} + \begin{bmatrix} C_s & 0 \\ 0 & c_{eq} \end{bmatrix} \begin{bmatrix} \dot{X}_s \\ \dot{x}_r \end{bmatrix} + \begin{bmatrix} K_s & 0 \\ 0 & k_{eq} \end{bmatrix} \begin{bmatrix} X_s \\ x_r \end{bmatrix} = \begin{bmatrix} F(t) \\ 0 \end{bmatrix} \quad 2-34$$

2.7.5.3 Equivalent Linear TMD

Since the basic principle of vibration control used in a TLD is the same as used for a TMD, it is possible to apply the TMD analogy in investigating the characteristics and modelling of TLDs. An equivalent mechanical model enables the sloshing fluid system in the TLD to be represented as a single degree of freedom mass-spring-dashpot system. This linearized model is more convenient to use and analyze.

The relationship between design parameters of a TLD for the objective response level and optimum tuning parameters of a TMD can be easily determined; therefore, substituting a TLD as an equivalent TMD has the advantage of obtaining optimal parameters. Sun et al. [88] utilized TMD analogy to find out that effective mass of a TLD is always smaller than the actual liquid mass. Suggesting that for the same amount of damper's mass, the TMD would be more efficient than a TLD. Figure 2-11 shows a schematic of equivalent linearized TLD-structure system.

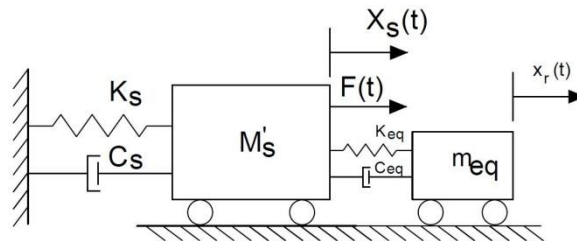


Figure 2-11 Equivalent mechanical linearized Structure-TLD

In order to express a TLD as an equivalent TMD, an equivalent displacement variable x_r is introduced as

$$q = \Gamma x_r \quad 2-35$$

where q is the generalized coordinate relating to the free surface motion and is also a measure of relative motion with respect to the horizontal motion of the structure. The modal participation factor (Γ) relates the relative motion of the equivalent mechanical system shown in Figure 2-11 to the actual free surface response amplitude of the fundamental sloshing mode.

$$\Gamma_n = \frac{2}{n\pi} (1 - \cos(n\pi)) \tanh\left(\frac{n\pi h}{L}\right) \quad 2-36$$

The mass of the structure can be modified as follows to account for the non-participating component of the liquid associated with the fundamental sloshing mode

$$M'_s = M_s + (\rho b h L - m_{eq}) \quad 2-37$$

The equivalent mass, damping and stiffness, corresponding to the fundamental sloshing mode, are used to represent an equivalent mechanical system, which develops dynamic forces equal to the forces exerted by sloshing fluid. The equivalent mass and stiffness representing the sloshing fluid in a rectangular tank are given by [89], [90].

$$m_{eq} = \frac{8\rho b L^2}{\pi^3} \tanh\left(\frac{\pi h}{L}\right) \quad 2-38$$

$$k_{eq} = \frac{8\rho b L g}{\pi^2} \tanh^2\left(\frac{\pi h}{L}\right) \quad 2-39$$

The normalized equivalent mass indicates the amount of fluid that participates in the sloshing motion. The amplitude dependent equivalent damping coefficient and equivalent damping ratio are determined for random or sinusoidal excitation for a given value of σ_r or x_r , respectively. The following equations are introduced for amplitude-dependent equivalent damping coefficient and damping ratio for random excitation.

$$c_{eq} = C_l \frac{16\rho b L}{\pi^3} \sqrt{\frac{32}{\pi^3}} \tanh^3\left(\frac{\pi h}{L}\right) \Delta E \omega \sigma_r \quad 2-40$$

$$\xi_{eq} = C_l \sqrt{\frac{32}{\pi^3}} \tanh^2\left(\frac{\pi h}{L}\right) \Delta E \frac{\sigma_r}{L} \quad 2-41$$

where

$$\Delta = \left(\frac{1}{3} + \frac{1}{\sinh^2\left(\frac{\pi h}{L}\right)} \right) \quad 2-42$$

$$\Xi = \sum_{j=1}^{ns} \left| \sin^3\left(\frac{\pi x_j}{L}\right) \right| \quad 2-43$$

For sinusoidal excitation the following equations are used to determine the amplitude-dependent equivalent damping coefficient and damping ratio.

$$c_{eq} = C_l \frac{256\rho bL}{3\pi^5} \tanh^3\left(\frac{\pi h}{L}\right) \Delta \Xi \omega x_r \quad 2-44$$

$$\xi_{eq} = C_l \frac{16}{3\pi^2} \tanh^2\left(\frac{\pi h}{L}\right) \Delta \Xi \frac{x_r}{L} \quad 2-45$$

Once a target response amplitude has been selected a loss coefficient that provides the required TLD damping ratio can be calculated.

2.7.6 TLD Design Parameters

As a TLD operates analogous to a TMD, therefore, the same design parameters (mass ratio, tuning ratio and TLD damping ratio) are utilized.

Unlike a TMD, there is a non-contributing mass of liquid, m_0 , that does not participate due to the formation of recirculation zones. The non-contributing or inactive mass (m_0) acts as a rigid mass attached directly to the building [91]. The portion of the liquid mass that does participate as a result of the liquid sloshing motion is defined as the equivalent mass, m_{eq} . The equivalent mass can be estimated using potential flow theory [90].

The effective mass of the liquid inside the TLD tanks is usually indicated with the parameter of mass ratio. Assuming M^* as the generalized mass of the structure and m_{TLD} as the effective mass of the liquid inside the tank, the mass ratio is then defined by μ [92]

$$\mu = \frac{m_{TLD}}{M^*} \quad 2-46$$

As discussed in previous section, effective mass of TLD is the portion of fluid mass that contributes to the fundamental sloshing mode.

Lamb [93] introduced an equation to calculate the frequency of TLD based on the linear wave theory:

$$f_{TLD} = \frac{1}{2\pi} \sqrt{\frac{\pi g}{L} \tanh\left(\frac{\pi h}{L}\right)} \quad 2-47$$

The ratio of the natural frequency of the TLD, f_{TLD} , to the natural frequency of the structure, f_s , is defined as the tuning ratio, Ω , which is an important parameter influencing the performance of TLD:

$$\Omega = \frac{f_{TLD}}{f_s} \quad 2-48$$

The inherent damping ratio of sloshing fluid inside the tank (ξ_{TLD}) is another parameter that influences the performance of TLD. The damping coefficient, C_{TLD} , is defined as a measure of energy dissipation in TLD in one complete cycle of vibration expressed as

$$C_{TLD} = 2 m_{TLD} \omega_{TLD} \xi_{TLD} \quad 2-49$$

in which ω_{TLD} is the natural angular frequency of the TLD ($\omega_{TLD} = 2 \pi f_{TLD}$), and ξ_{TLD} is the damping ratio of TLD [94]. The main source of inherent damping in a TLD is the viscous energy dissipation in solid boundaries of the tank and free surface contamination. However, for TLDs equipped with damping screens, Tait [86] showed that when a slat-type damping screen is installed inside the deep water tank the resulting damping ratio is dependent on the amplitude of sloshing as the damping of screens is proportional to the square of fluid velocity. The damping of a TLD equipped with damping screens will be discussed in more details in the modelling section in Chapter 4.

2.7.7 Modal Expansion Model

Several studies have proposed various methods to solve the sloshing water problem in rectangular TLD tanks. In the case of small fluid response amplitudes, the simplest approach is to neglect the non-linear terms of the free-surface boundary conditions. When the sloshing fluid response amplitude is large, the nonlinearity conditions cannot be neglected. In such cases, the non-linear free surface boundary conditions can be included through modal expansion of the coupled modes [82], [95]. The accuracy of this model increases with an increase in the number of sloshing modes included in the modal expansion. The number of modes incorporated defines the order of modal expansion model. A third order model refers to a modal expansion that considers three sloshing modes. It should be noted that the linearized model takes into account only the first mode, also referred to as first order model. Kaneko and Yoshida [82] introduced a 3rd order modal expansion model based on the Galerkin, which considered the damping of the fundamental mode due to fluid drag on damping screens. In this study a modal expansion method based on the Bateman-Luke introduced by Love and Tait [96] is used to model the TLD. This model incorporates the modal damping arising from the viscous fluid and the added energy dissipation due to the installation of damping screens is considered for all the modes.

The equation of motion of the m th sloshing mode is [3]

$$\ddot{q}_m + 2\omega_m(\xi_{\omega,m} + \xi_{s,m})\dot{q}_m + \omega_m^2 q_m + P_m \ddot{X} + d_1^m \ddot{q}_1 q_2 + d_2^m \ddot{q}_1 q_1 + d_3^m \ddot{q}_2 q_1 + d_4^m \ddot{q}_1 q_1 q_1 + d_5^m \dot{q}_1 \dot{q}_1 + d_6^m \dot{q}_2 \dot{q}_1 + d_7^m \dot{q}_1^2 q_1 = 0 \quad 2-50$$

Miles [79] calculated the damping ratio of m^{th} mode produced by viscosity of fluid sloshing in a rectangular container.

$$\xi_{w,m} = \left(\frac{1}{L}\right) \sqrt{\frac{\nu}{2\omega_m}} \left(\frac{L}{b} + 1 + m\pi \left[1 - 2\frac{h}{L}\right] \operatorname{cosech}\left(2\frac{m\pi}{L}h\right) + m\operatorname{coth}\left(\frac{m\pi}{L}h\right)\right) \quad 2-51$$

In which ν is fluid viscosity, b is tank width and ω_m is the natural angular frequency of m^{th} sloshing mode which is determined as

$$\omega_m^2 = \frac{m\pi g}{L} \tanh\left(\frac{m\pi h}{L}\right) \quad 2-52$$

The wave height at any x -coordinate in tank, (x, t) , is determined from

$$\eta(x, t) = \sum_{m=1}^{\infty} q_m(t) \cos\left(\frac{m\pi}{L} x\right) \quad 2-53$$

where $q_m(t)$ is the time dependent generalized coordinate of m^{th} sloshing mode. The wave height at the location of damping screens is used to determine the forces exerted on the screens by the fluid. Also, the maximum wave height at the walls of the tank defines the minimum freeboard to avoid overtopping of fluid or wave impact with the tank lid.

Using the principle of virtual work [86] the modal damping ratio produced by the damping screens can be calculated as

$$\xi_{s,m} = \frac{\tanh\left(\frac{m\pi h}{L}\right)}{2\omega_m L} C_l \left(\frac{1}{3} + \frac{1}{\sinh^2\left(\frac{m\pi h}{L}\right)} \sum_{j=1}^{ns} \left| \sin^3\left(\frac{m\pi x_j}{L}\right) \right| |\dot{q}_m(t)| \right) \quad 2-54$$

where $|q_m(t)|$ is the magnitude of fluid response, ns is the number of screens and x_j is the location of j^{th} screen.

Faltinsen and Timokha [97] showed the location of the sloshing fluid centroid (center of mass) can be expressed in terms of the time dependent generalized coordinates. The sloshing forces are determined via the acceleration of the centroid of mass of the sloshing fluid. By multiplying the obtained acceleration of fluid centroid by the fluid mass, the sloshing force can be expressed as

$$F_{sw} = -m_w \frac{L}{\pi^2 h} \sum_{m=1}^{\infty} \ddot{q}_m(t) \frac{1}{m^2} [1 + (-1)^{m+1}] \quad 2-55$$

m_w is the mass of fluid inside the tank defined as

$$m_w = \rho b h L \quad 2-56$$

By considering the fluid as a moving rigid mass for the conservative inertial component. The total base shear force exerted by TLD on the structure is expressed as

$$F_{TLD} = -m_w \{ \ddot{X} + \frac{L}{\pi^2 h} \sum_{m=1}^{\infty} \ddot{q}_m(t) \frac{1}{m^2} [1 + (-1)^{m+1}] \} \quad 2-57$$

The simultaneous ordinary differential equations in the model in this research are solved using Runge-Kutta-Gill method.

2.8 Base Isolation-Structure-Dynamic Vibration Absorber Systems

The increased deformability of isolated building can result in unacceptably large seismic and wind induced displacements at the isolator level and exceedance of serviceability limit state accelerations at the floor levels under wind loading. In fact, due to the floor acceleration exceeding the discomfort threshold, serviceability problems may occur during strong wind loads on buildings equipped with flexible base isolation systems. Past research work has examined the effectiveness of the base isolated systems equipped with TMDs and investigated optimal parameters for the design of a TMD. Although TMDs can reduce the displacement demand of the structure by 15-25%, the added extra mass to the structure can be as large as 5% of the total mass of the main structure.

Almost all of the previous work on hybrid systems consisting of passive damping devices and base isolation systems are restricted to the combined use of linear DVA-base isolation systems, such as TMD-linear SREI systems. Kareem has modelled base isolated buildings with passive dampers under wind loads [98]. A primary conclusion of this research was the location of the damper had little influence on the response of the structure. Taniguchi et al. [2] investigated the base isolated structures equipped with a TMD under white noise ground motion and also far field and near field earthquake records to determine the optimal mass, stiffness and damping parameters of the TMD that maximized the reduction in the seismic demand on the base isolated structure. The study revealed that the use of the TMD on a base isolated structure is most effective for lightly damped isolators and can reduce the displacement demand by up to 25 percent. Also, the efficiency of the coupled control system increases with an increase in the mass ratio, while increasing the damping was found to be less effective. Taniguchi et al. also found that while the response under the far field earthquakes is similar to the white noise response, in the case of near field earthquakes the

efficiency of the hybrid TMD-isolator system is significantly lower. This is due to the fact that in the near field ground motions the peak response usually occurs at the beginning of the record due to the near field pulse and as result this does not allow sufficient time for the TMD system to be mobilized.

Love et al. [3] introduced a TLD, which is a nonlinear DVA, as an effective control system for wind induced nonlinear base isolated structures. The schematic of a hybrid base isolation TLD system is shown in Figure 2-12. A linearized equivalent mechanical model and a form of the linearized Bouc-Wen model were utilized to represent the sloshing fluid in the TLD system and the hysteretic behaviour of the base isolation system, respectively. A preliminary design method to tune the TLD in the base isolated structure and determine the proper TLD dimensions and screen loss coefficient to perform optimally under the excitation were also presented. Additional studies [99], [100] and [101] have addressed the question of increased sensitivity of base isolated buildings to wind loads due to increased horizontal flexibility of a structure and its impact on the structure. Sinha and Li [102], [103] have studied the performance of base isolated structures with dynamic absorbers. Kareem [104] modelled the base isolated system with passive dampers under winds and conducted a parametric study to gain the influence of base isolation and damping system properties on the building response.

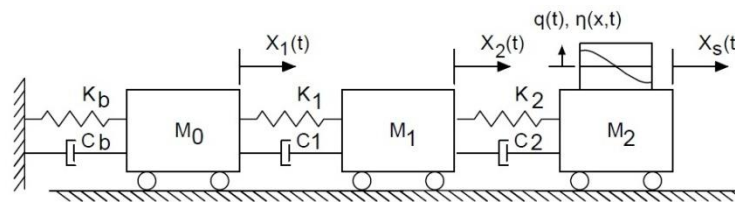


Figure 2-12 Schematic of BI-Structure-TLD

A passive tuned mass damper requires motion of the primary structure to react with. For an earthquake with substantially shorter duration than wind excitation, the tuned mass damper system may not have time to react [60]. Yong et al. [105] investigated combined tuned mass dampers-base isolation systems under earthquake loading. In the coupled tuned mass damper-base isolation systems, for damping ratios higher than critical damping using a TMD will result in increased structural response. The optimum tuning frequency and damping ratio of the tuned mass damper can be obtained from steady state response studies to reduce the seismic response of the base

isolated structure [106]. The frequency of the input earthquake also affects the performance of the tuned mass damper in the base isolated building. For input frequencies lower than the natural frequency of the structure, the addition of a tuned mass damper can increase the structural response. However, for the case of a base isolated structure this is not considered as serious as the natural frequency of base isolated structure is generally lower than the dominant frequency of the earthquake. Considering the fact that the fundamental mode of a base isolated structure is nearly a rigid body mode, which dominates in earthquake vibration, a single damper tuned to the fundamental mode is adequate for reducing the seismic response in combined system [106].

Chapter 3 Shake Table Test of a BI-Building-TLD System

3.1 Shake Table Test Set-up

Shake table tests were conducted on a $\frac{1}{4}$ scale two storey base isolated building model with a TLD attached to the roof. A single SU-FREI was located at each column-line between a flat steel plate welded to the base of the column and the shake table. A TLD with three identical tanks was mounted on the roof of the building. Damping screens were utilized in the TLD to increase the damping to an acceptable level. The first set of tests was conducted with no liquid inside the tanks. The tests were subsequently repeated with the tanks filled with water up to a height of 30 cm.

A schematic of test setup and the instrumentation used in this test program is shown in Figure 3-1 and Figure 3-2. A photograph of the shake table and test set-up is shown in Figure 3-3. Six displacement transducers were used to measure displacements of the structure at the locations shown in Figure 3-1 and Figure 3-2. A displacement transducer was connected at each floor level of the structure and to the table to record absolute displacements. In addition, the base floor level had two displacement transducers connected near the columns to allow both the rotational of the structure and deformation of the isolator to be measured during testing. Lateral in-plane accelerations were measured using unidirectional accelerometers, which were attached at each floor level and to the shake table. The free surface motion of the water was recorded using a

capacitance type wave probe installed at the end wall of the middle tank. All measurements were recorded at 200 Hz and filtered at 50 Hz [7].

3.2 Building Model

The test building consisted of a two-storey single-span moment-resisting steel frame. The plan dimensions of the building were 1500x1400 mm with total height of 1628 mm. Hollow steel sections were used for the columns (HSS 64x64x6.4 mm) and the beams were built-up sections consisting of a square hollow section (HSS 51x51x6.4 mm) welded to the top of a rectangular hollow section (HSS 76x51x6.4 mm). The floors consisted of 105 mm thick precast concrete two-way slabs. In order to satisfy dynamic similitude [107] additional mass is added using four steel plates bolted to each floor slab. The total weight of the test structure was 32.1 kN.

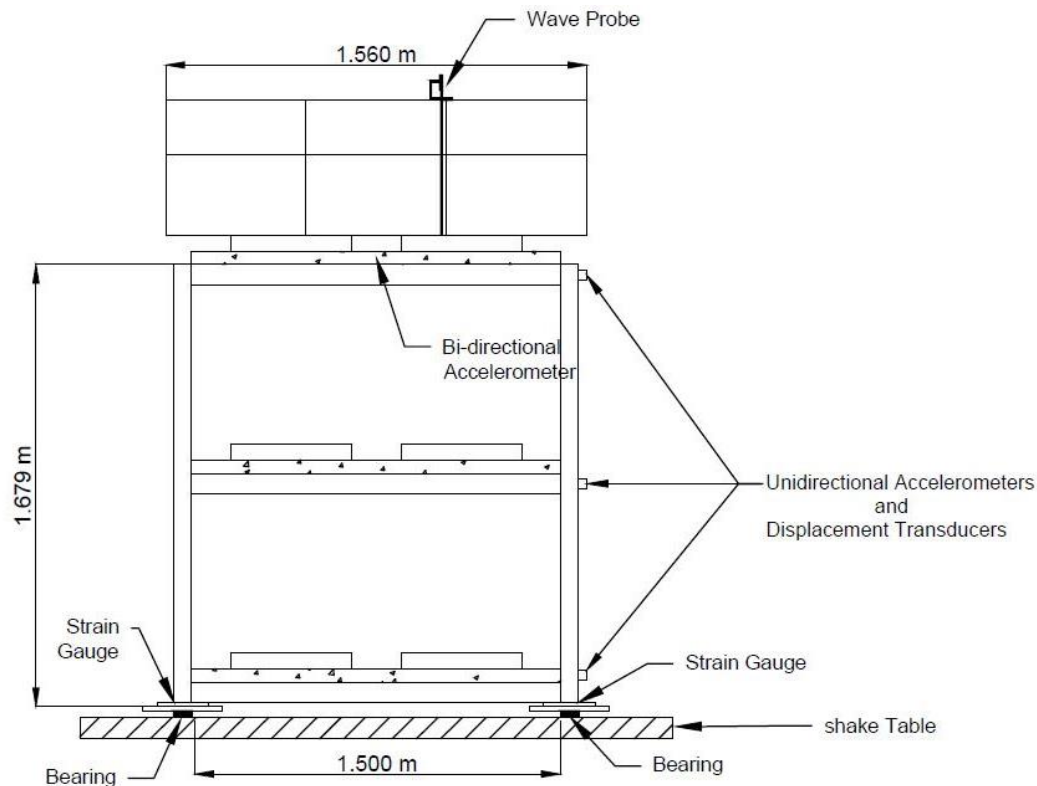


Figure 3-1 Schematic elevation view of test building

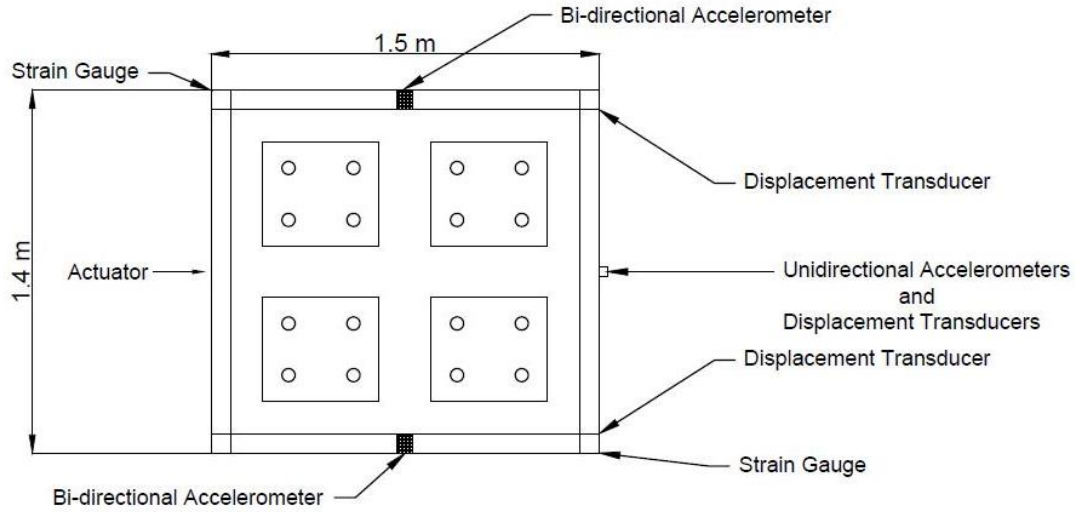


Figure 3-2 Schematic plan view of test building



Figure 3-3 Photograph of shake table test setup

The mass, stiffness and damping matrices for the fixed base (FB) building model are defined as follows.

$$M = \begin{bmatrix} m_1 & 0 \\ 0 & m_2 + m_{tank} \end{bmatrix} \quad 3-1$$

$$K = \begin{bmatrix} k_{11} & -k_{12} \\ -k_{12} & k_{22} \end{bmatrix} \quad 3-2$$

$$C = \begin{bmatrix} c_{11} & -c_{12} \\ -c_{12} & c_{22} \end{bmatrix} \quad 3-3$$

where the mass, stiffness and damping properties of the building model are as summarized in Tables 3-1, 3-2 and 3-3.

Table 3-1 Stiffness properties of FB building

Stiffness (kN/m)	
k_{11}	2.68E+04
k_{12}	1.25E+04
k_{22}	1.09E+04

Table 3-2 Damping properties of FB building

Damping (N.s/m)	
c_{11}	3.25E+03
c_{12}	1.06E+03
c_{22}	1.91E+03

Table 3-3 Mass properties of FB building (including TLD tank mass)

Mass (kg)	
m_0	1.09E+03
m_1	1.09E+03
m_2	1.09E+03
m_{tank}	7.64E+01

3.3 Base Isolation System

A single SU-FREI was located at each column-line under a flat steel plate that was welded to the base of the column. No bonding was introduced between the upper and lower contact surfaces between the shake table and the superstructure. The isolators had a total height of 22.35 mm and plan dimensions of 63mmx63mm and were comprised of seven elastomer layers and six carbon fiber fabric layers. The five interior elastomer layers had a thickness of 3.175 mm and the two outer elastomer layers had thickness of 1.5875 mm. The elastomer material was a neoprene rubber having a manufacturer specified nominal tensile modulus of 1.0 MPa at 100% elongation, a specified shear modulus of $G = 0.35$ MPa and a specified damping ratio of approximately 5%. Each of the bi-directional, plain weave carbon fiber fabric layers had a thickness of 0.55 mm. The total thickness of the rubber layers in the isolator, t_r , was equal 19.05 mm [7]. The 4 isolators used in the test program are shown in Figure 3-4. Additional details on the manufacturing of these isolators can be found elsewhere [7].



Figure 3-4 Photograph of SU-FREI

3.4 Tuned Liquid Damper

A multiple tuned liquid damper (MTLD) system, illustrated in Figure 3-5, was utilized in this test program. The MTLD system, which consisted of three identical tanks, was mounted on the roof

of the building as shown in Figure 3-3. It should be noted that this type of MTLTLD can be considered as an equivalent single TLD as all three tanks had the same properties.

In order to develop a sufficient level of damping in the tuned liquid damper, damping screens were installed. A single screen was placed at the middle of each tank. The solidity, S of the screens installed in the tanks was 40 %. The solidity value is defined as the ratio of the solid area of screen submerged in water normal to the flow, A_s to the gross area of the screen submerged in water, A_T

$$S = \frac{A_s}{A_T} \quad 3-4$$

The pressure loss coefficient for slat screen can be determined from the following equations [108].

$$C_l = \left(\frac{1}{C_c(1 - S)} - 1 \right)^2 \quad 3-5$$

where C_c is the construction coefficient. An estimate of this parameter can be made based on the solidity ratio and is expressed as [83].

$$C_c = 0.405 e^{-\pi S} + 0.595 \quad 3-6$$

Using the above relationships the loss coefficient of the screens was estimated to be 1.81.

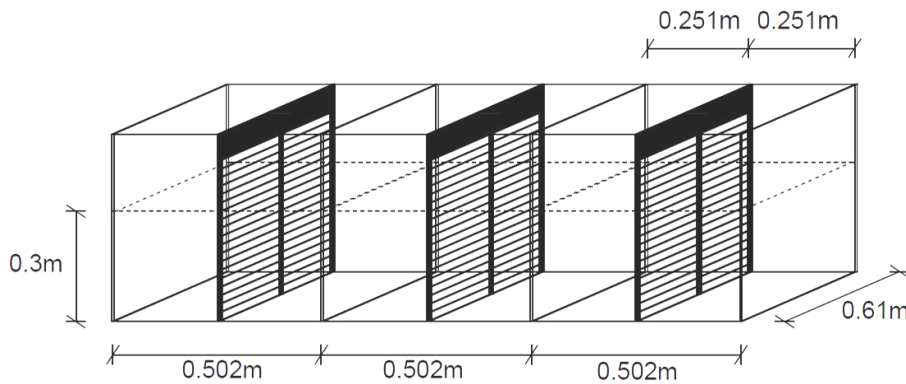


Figure 3-5 Schematic of the TLD

3.5 Test Results

3.5.1 Harmonic Base Excitation Tests

Discrete frequency sweep shake table tests were conducted at three amplitudes of excitation (1.3 mm, 2.5 mm and 3.8 mm). At each of the approximately 35 applied excitation frequencies, ranging between 0.8 Hz to 1.8 Hz for each excitation amplitude, the system was allowed to reach a steady-state response prior to recording a 60 s response history. Figure 3-6 shows sample response histories of the isolator displacement, $X_0(t)$, roof acceleration, $\ddot{X}_2(t)$ and TLD free surface wave height displacement, $\eta(t)$ corresponding to an excitation amplitude of 3.8 mm and excitation frequency of 1.22 Hz, which is near the expected resonant frequency of the system at an isolator displacement amplitude of approximately 75% t_r .

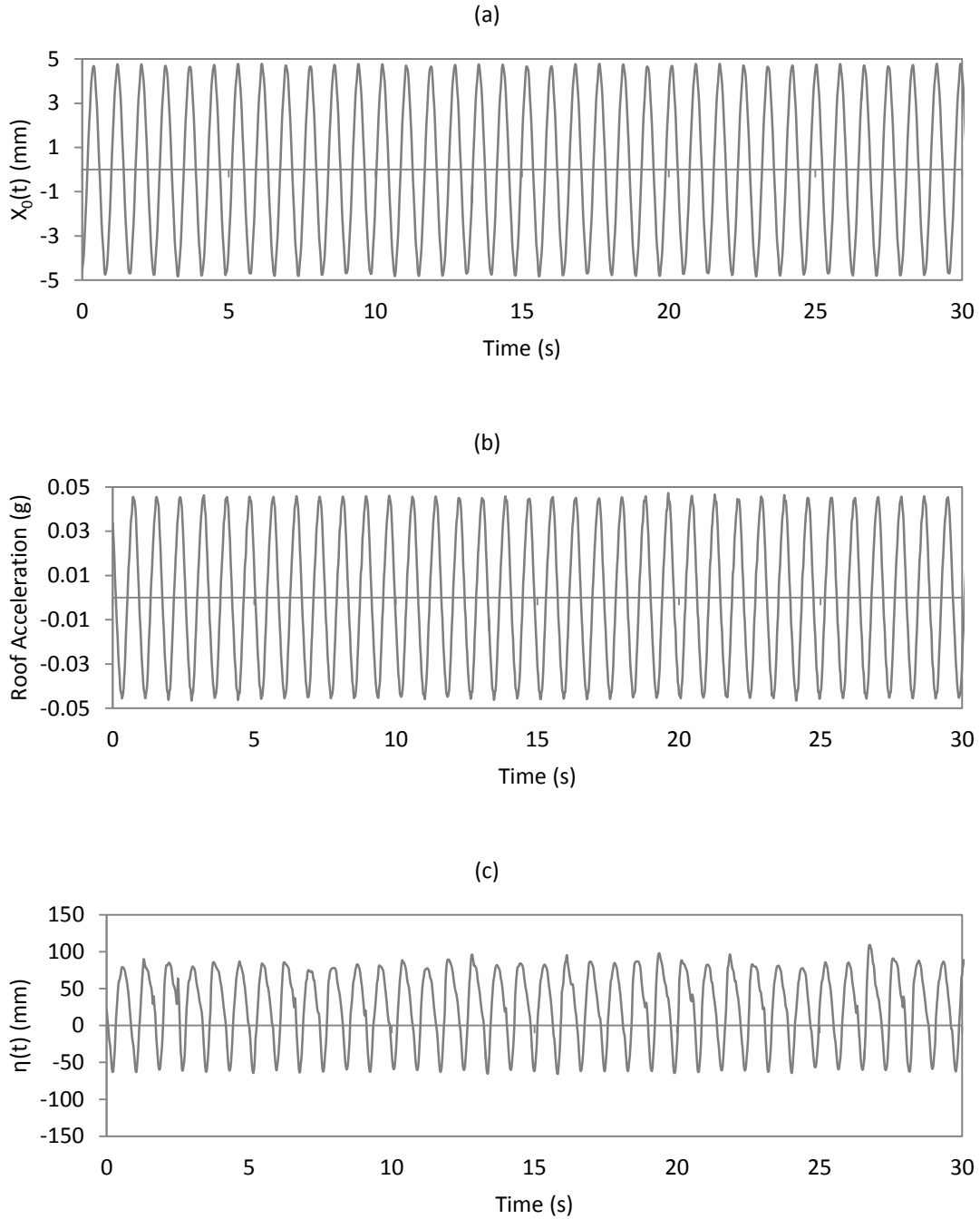


Figure 3-6 Response history plots of (a) isolator displacement, (b) roof acceleration and (c) TLD free surface motion (excitation amplitude=3.8 mm, excitation frequency=1.22 Hz)

From the response histories shown in Figure 3-6 it can be observed that steady-state response has been attained. In addition, it is evident that the isolator displacement and roof acceleration response

histories respond in a sinusoidal manner when subjected to a sinusoidal excitation. The wave height response history is more complex as a result of the nonlinear coupling of higher sloshing modes. This results in wave crests (positive peak free surface displacement) that are larger than the wave troughs (negative peak free surface displacement). This response characteristic is expected and is in agreement with that observed by other experimental research studies on TLDs under sinusoidal excitation [83].

3.5.2 Natural Frequencies and Modes Shapes

Free vibration tests on the building in both the fixed base and base isolated configurations have been conducted in a previous study [7]. The period of the first and second modes of the structure in the fixed base and isolated configurations were calculated using the mass and stiffness properties of the structure presented earlier, which include the mass of the TLD tank. Based on the dynamic properties of structure the period of the 1st and 2nd mode of the fixed base structure are calculated to be 0.106 s and 0.036 s, respectively. For the base isolated structure, due to the nonlinear stiffness of the isolators the period of the first mode ranges from approximately 0.65 s to 1.0 s for isolator displacement amplitudes between 25% to 250% t_r . At an isolator displacement of 75% t_r the period of the first mode is approximately 0.8 s. These periods are calculated based on effective stiffness values and assuming that the building responds as a rigid body.

The approximate fundamental mode shape of the base isolated test building, using experimental test results, is shown in Figure 3-7. The mode shape is determined based on the floor displacement response values of the building at an excitation frequency near that of the base isolated building. The displacement values at the floor levels have been normalized by the isolator displacement value and are presented in Table 3-4.

Figure 3-7(a) shows that the addition of the TLD does not significantly change the mode shape of the BI-building as the mode shapes obtained from shake table tests of the building with and without fluid in the TLDs are in close agreement. The difference between the first floor and isolator level values is approximately 2% and the difference between the roof and isolator level values is approximately 3%. As can be observed in Figure 3-7, the amplitude of the relative displacement

between first and second floor levels is approximately 50 times smaller than the amplitude of deformation experienced by the isolators. It can also be seen from Figure 3-7(a), for both the BI-building and BI-building-TLD, the building responds as a near rigid body with negligible inter-storey drift. This approximate mode shape is also in agreement with the theoretical mode shapes calculated by Foster [7].

The mode shape shown in Figure 3-7(b) includes the fluid response as well. The amplitude of the vertical response of the fluid has been indicated in the horizontal direction in this plot. It can be observed that the motion experienced by the fluid is significantly larger than that of the isolator and building. As shown in Table 3-4 the TLD free surface motion is almost 15 times larger than the motion that occurs in the isolator. These large sloshing motions in the fluid result in high energy dissipation in the TLD and thus provide an additional source of energy dissipation to the BI-building.

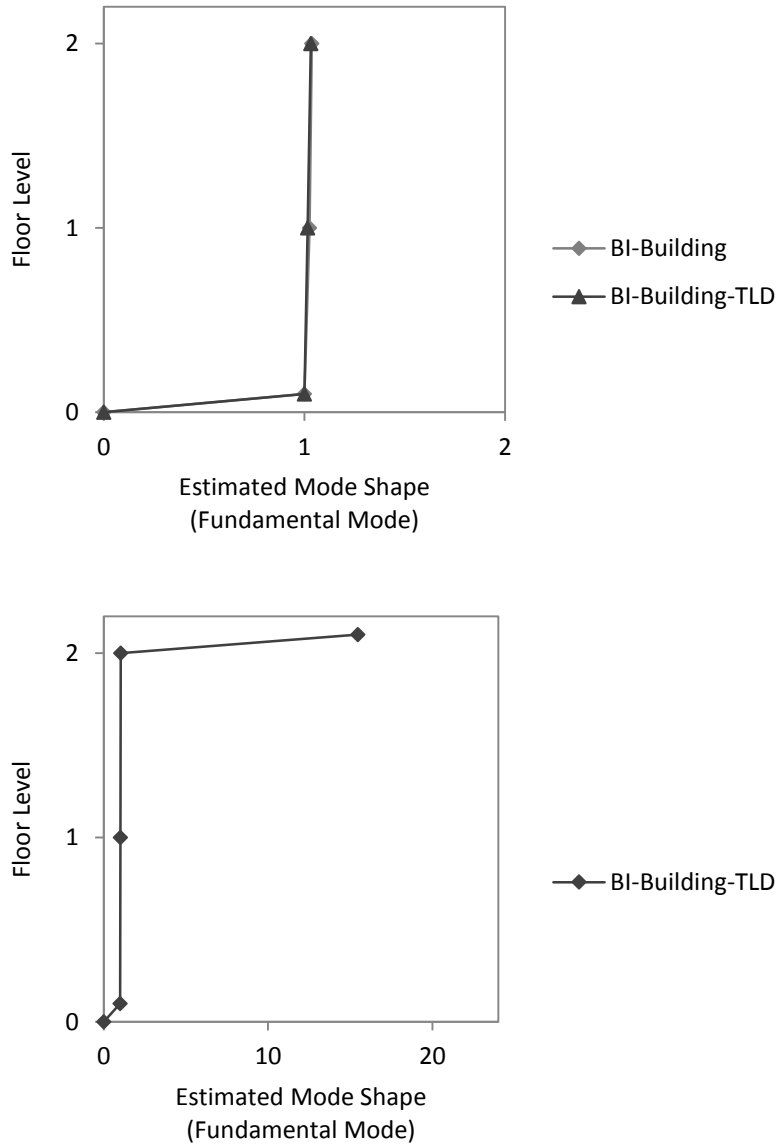


Figure 3-7 Approximate mode shape of (a) BI-building, (b) BI-building-TLD

Table 3-4 Estimated mode shape values

Floor Level	BI-Building	BI-Building-TLD
Base	1	1
1 st Floor	1.03	1.02
2 nd Floor	1.04	1.03
Wave Height	-	15.5

3.5.3 Frequency Response Plots

Frequency response plots for the base isolated building have been developed and are presented in Figures 3-8 to 3-10. In each figure the frequency response of the isolator displacement and the roof acceleration are presented for the case of the isolated building both with and without the TLD active for comparison purposes.

As indicated in Chapter 2, for the case of a base isolated structure subjected to lateral loading the majority of the system deformation occurs at the isolation layer and the structure itself moves as a near rigid body. Therefore, in this research the isolator displacement is selected as the primary response parameter of the BI-building and BI-building-TLD. The peak (maximum) steady state isolator displacement value, which is the displacement at the base of the building relative to the shake table displacement, has been determined at each excitation frequency. In addition, the peak roof acceleration has also been calculated at each excitation frequency and is presented as a second response parameter. Both of these parameters are shown for all three excitation amplitudes in Figures 3-8 to 3-10 for both the BI-building and BI-building-TLD.

Although the BI-building is a multi degree of freedom system it can be observed from the frequency response plots, the frequency response of the base isolated system corresponds to that of a typical of a single-degree of freedom having a single peak value. This is expected, as the higher modes are not anticipated to be excited over this frequency range. This single peak response for the BI-building is found to be consistent for all three excitation amplitudes.

The addition of the TLD, which adds another degree of freedom to the system, results in a double peak frequency response curve. This double peak frequency response curve is typical of a structure-DVA system, which results from the transfer of energy (coupling) between the building and the TLD.

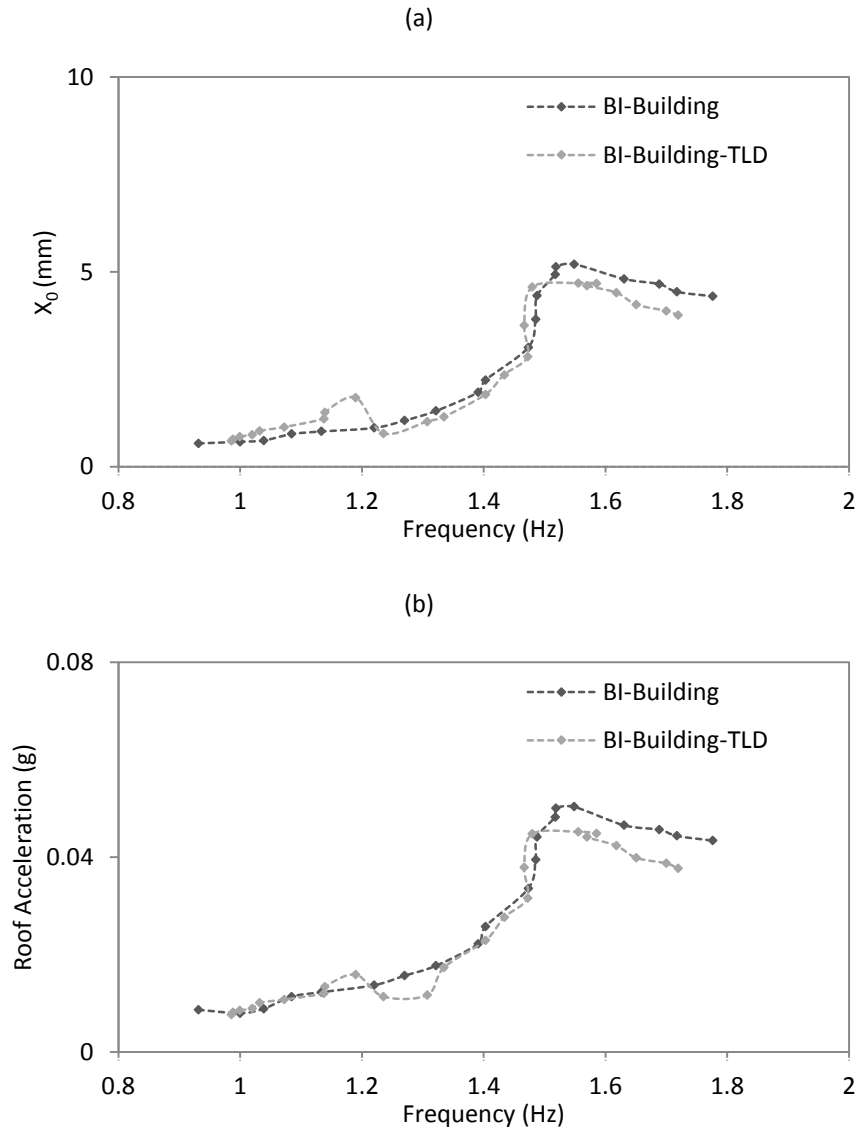


Figure3-8 Frequency response of BI-building and BI-building-TLD (a) isolator displacement and (b) roof acceleration at an excitation amplitude of 1.3 mm

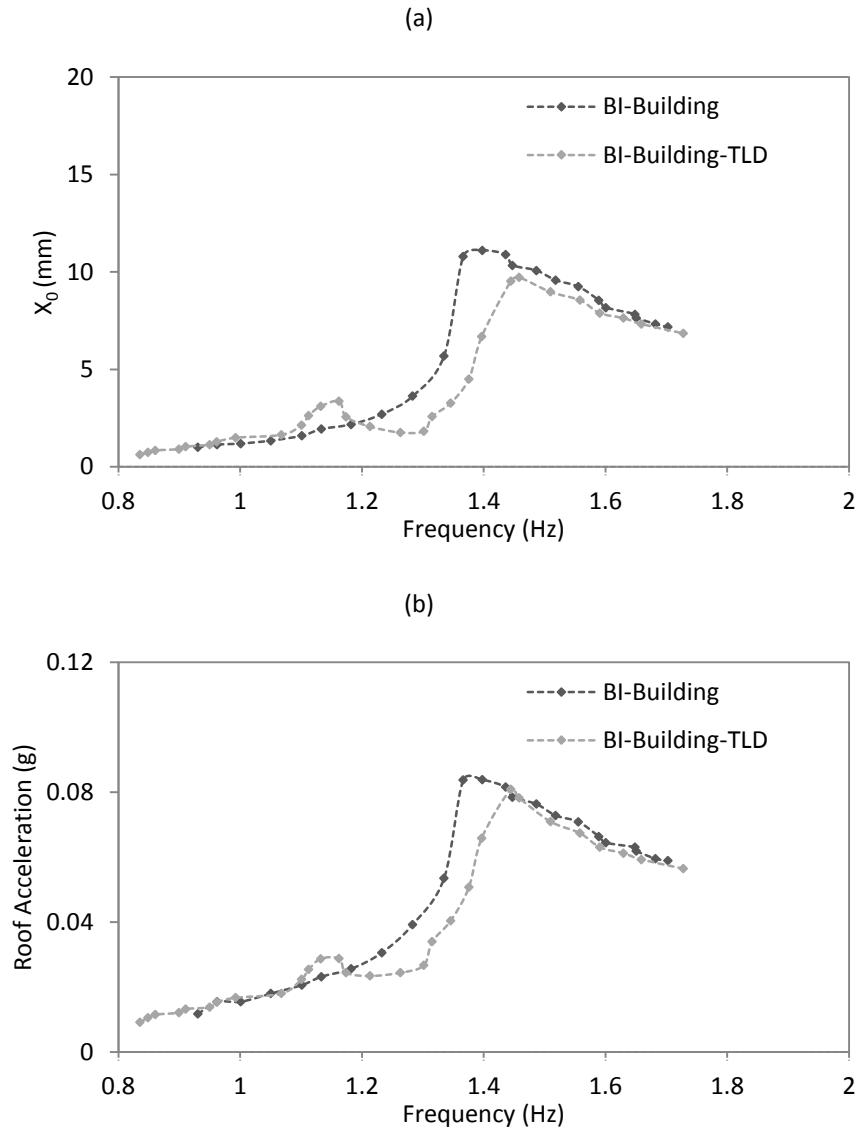


Figure 3-9 Frequency response of BI-building and BI-building-TLD (a) isolator displacement and (b) roof acceleration at an excitation amplitude of 2.5 mm

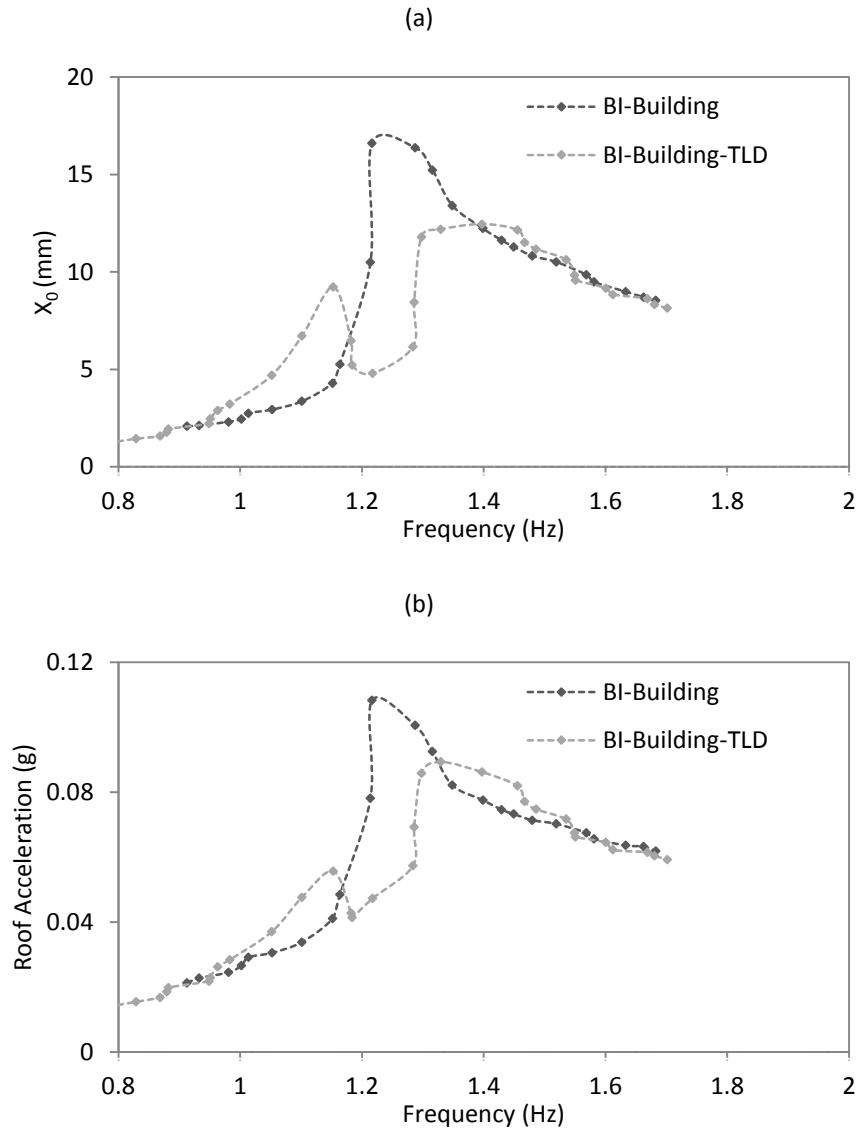


Figure 3-10 Frequency response of BI-building and BI-building-TLD (a) isolator displacement and (b) roof acceleration at an excitation amplitude of 3.8 mm

As both the isolators and the TLD are nonlinear devices, the frequency response of the system is expected to vary as a function of excitation amplitude. The stiffness of a SU-FREI decreases as the response of the system increases, which results in a decrease in the natural frequency (softening type behaviour) of the BI-building as the excitation amplitude is increased. This behaviour can be observed from the frequency response plots of the BI-building shown above. The isolator displacement amplitudes were found to occur at frequency values of 1.55 Hz, 1.40 Hz and 1.22 Hz for the 1.3 mm, 2.5 mm and 3.8 mm excitation amplitude tests, respectively. This corresponds to periods of 0.65 s, 0.71 s and 0.82 s, which is a result of the softening type behaviour. It should be noted that these periods fall within the expected range of periods for the BI-building given in Section 3.5.2.

As the natural frequency of the TLD is amplitude dependent, and for the water depth to tank length ratio employed in this study it is also expected to exhibit a softening type response behaviour. However, the rate at which the isolator and the TLD soften is not expected to be the same. As such, the tuning ratio of the TLD, which was determined using the preliminary design procedure outline in Chapter 2, is expected to be a function of applied excitation amplitude. The frequency response plots of the BI-building-TLD show that as the amplitude of applied excitation is increased a more pronounced double peak response occurs. This observed response is a direct result of the amplitude dependent tuning ratio. For all three excitation amplitudes the TLD has decreased both the peak isolator displacement and roof acceleration values. The peak isolator displacement has been reduced by 9%, 14% and 25% for the 1.3 mm, 2.5 mm and 3.8 mm excitation amplitudes, respectively. The peak roof acceleration has decreased by 10% after adding the TLD to the BI-building for the excitation amplitude of 1.3 mm. This decrease in peak roof acceleration increased to 3% for 2.5 mm excitation amplitude and 18% for the 3.8 mm excitation amplitude test.

Figure 3-11 shows the frequency response of the peak wave height for the three different amplitudes of excitation. It should be noted that the values shown are the average peak wave crest values (positive peak free surface motion) as these are found to exceed the peak wave trough (negative peak free surface motion) values as observed from Figure 3-6(c). It can be seen from this plot that as the amplitude of excitation increases the TLD free surface response amplitude increases significantly. As mentioned above, as the excitation amplitude is increased the TLD becomes

better tuned to the BI-building. This is expected to result in a significant increase in the TLD free surface response motion. This increase is reduced, to some extent, by the nonlinear velocity squared damping introduced by the damping screens. If the TLD possessed linear viscous damping, it would be expected that the increase in the free surface response would be larger. As the efficiency of a TLD is less sensitive to the damping ratio than the tuning ratio [86], the increased level of damping is not expected to reduce the efficiency of the TLD as significantly if the increase in excitation amplitude results in an overdamped TLD. Although the efficiency might be marginally degraded, the additional benefit due to the increased robustness to mistuning of the TLD, resulting from the increase in damping, is typically expected to negate or exceed the drawback of exceeding the optimal damping ratio value.

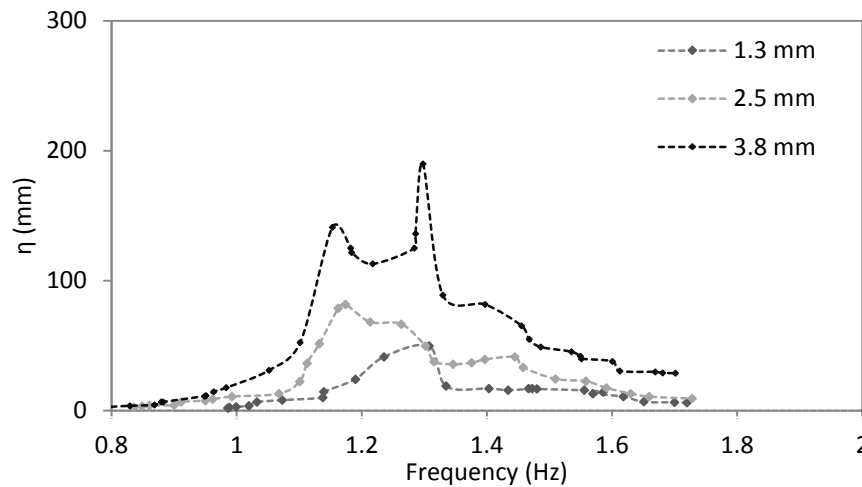


Figure 3-11 Frequency response of TLD free surface motion

3.5.4 Earthquake Excitation Tests

For the earthquake excitation component of this experimental study, a $\frac{1}{4}$ scaled record of the El Centro earthquake event was used and a total of three different peak ground acceleration (PGA) values (0.1 g, 0.2 g and 0.3 g) were applied. The acceleration time history of shake table input for PGA = 0.3 g is shown in Figure 3-12.

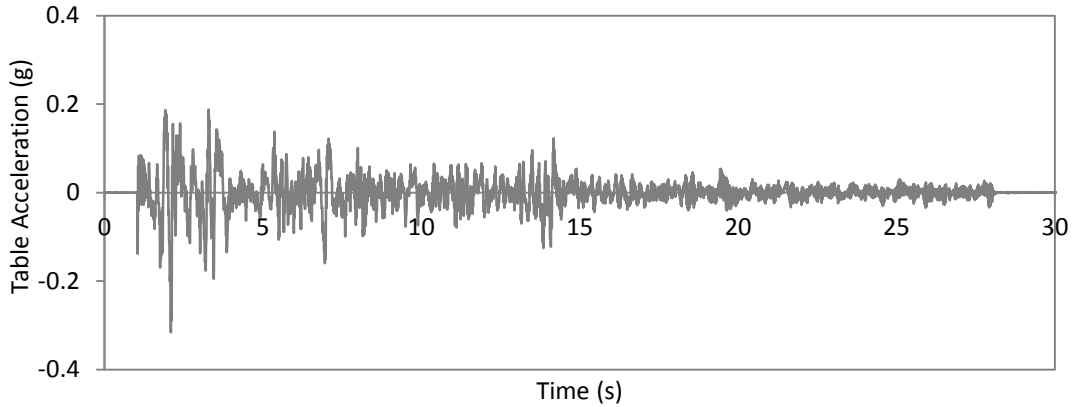


Figure 3-12 Acceleration time history of input excitation for El Centro earthquake (PGA = 0.3 g)

Figure 3-13 shows the acceleration and displacement response spectra for this input ground motion for a SDOF with 5% damping. The fixed base building period and the period range for the BI-building are also shown in response spectra plots. As discussed earlier, the fundamental period of the fixed base building was calculated to be 0.106 s and the range of periods for the BI-building was expected to fall between 0.65 s to 1.0 s. As can be observed from the acceleration response spectra shown in Figure 3-13, this increase in period of the base-isolated building shifts it into a region of lower spectral acceleration values, which will also lead to an increase in response displacement. However, the base isolated structure will have an increased damping value that will help to suppress the displacement.

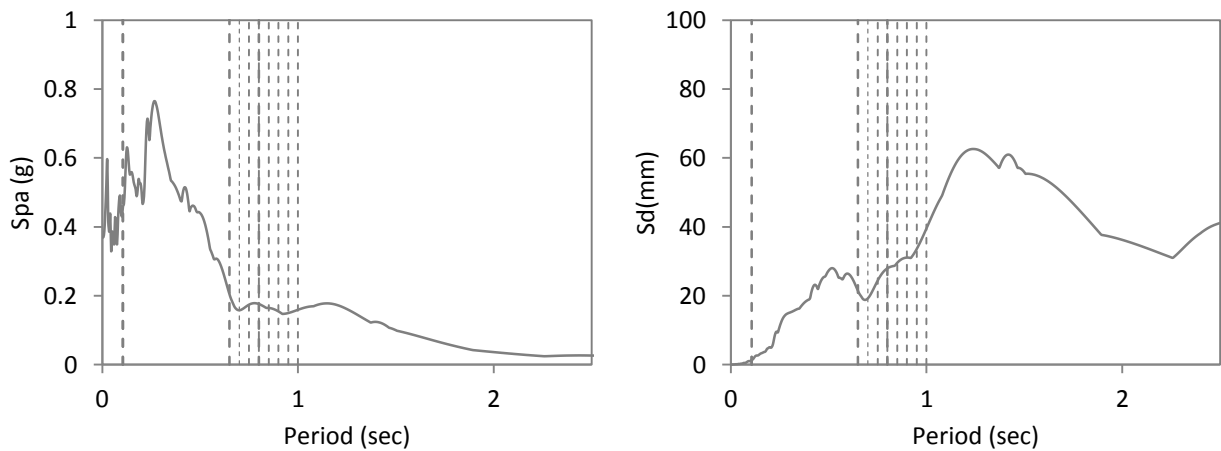


Figure 3-13 Pseudo acceleration and displacement spectra of shake table input (PGA=0.3 g)

Response histories of isolator displacement, roof acceleration and TLD free surface motion for 0.3 g PGA are shown in Figure 3-14 and Figure 3-15, respectively. Figure 3-14a shows the response of the BI-building and Figure 3-14b shows the response of the BI-building-TLD. The response histories look similar and no significant reduction in the peak isolator displacement can be observed. The same observations are made for the roof acceleration response histories. The peak response values for isolator displacement and roof acceleration for all three PGA levels for both the BI-building and BI-building-TLD are shown in Table 3-5.

Table 3-5 Summary of peak isolator displacement and roof acceleration values

	PGA=0.3 g		PGA=0.2 g		PGA=0.1 g	
	Without TLD	with TLD	Without TLD	with TLD	Without TLD	with TLD
Isolator Displacement (mm)	18.3	17.8	11.8	11.6	6.1	6.1
Roof Acceleration (g)	0.13	0.12	0.10	0.09	0.06	0.06

The values in Table 3-5 show that the TLD has negligible influence on peak isolator displacement and roof acceleration at a PGA=0.1g. At PGA=0.2g the TLD reduces the peak roof acceleration value by 10% but is not as effective in reducing the peak isolator displacement, as the reduction is approximately 1.7%. The TLD is found to have the greatest effect on reducing the peak isolator displacement value at the highest excitation input of PGA=0.3 g. At this PGA level the TLD has led to a decrease in the peak isolator displacement by 2.7% and peak roof acceleration by 7.7%.

The reduction in peak isolator displacement for the case of earthquake excitation is less than the reduction found for the case of harmonic excitation. A decrease in the effectiveness of a TLD under earthquake excitation is expected. For the case of harmonic excitation, the TLD has sufficient time to be activated. However, this typically is not the case for an earthquake type excitation. As the earthquake excitation approaches that of an impulse excitation it is expected that the TLD will be ineffective as the peak responses will occur before the TLD can be fully activated.

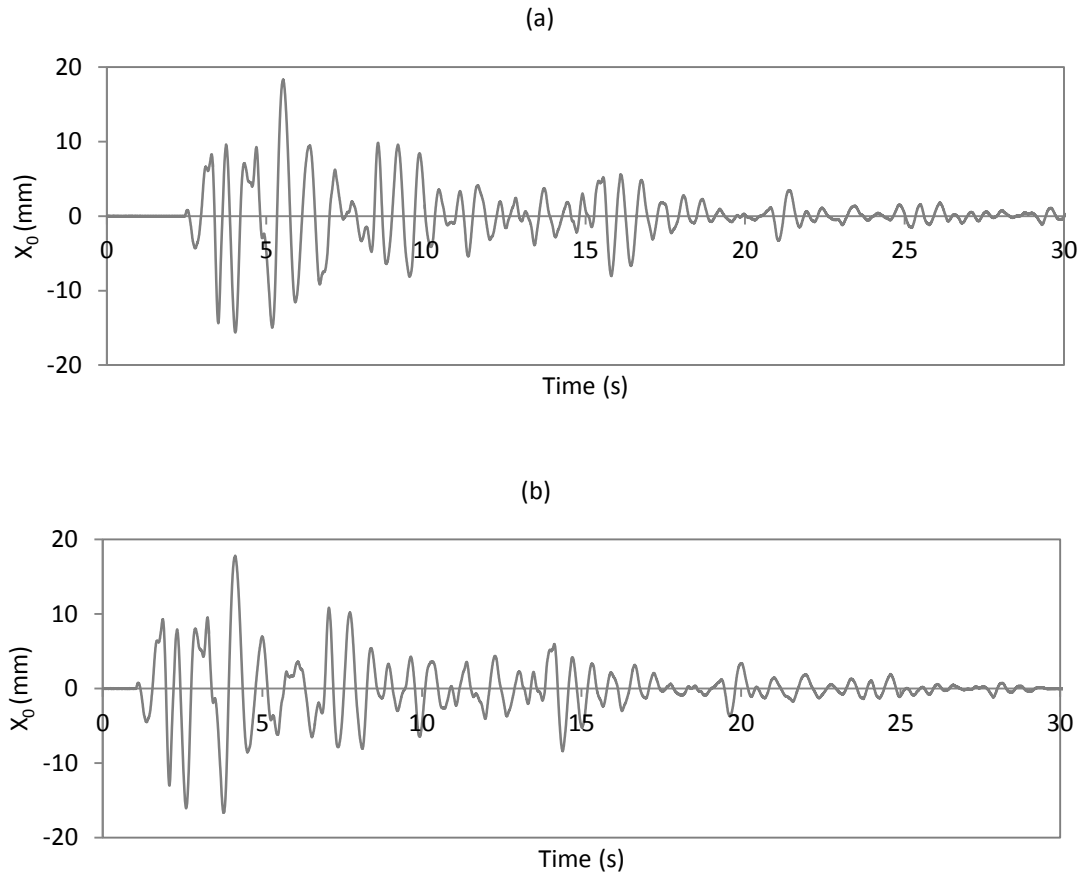


Figure 3-14 Response history of isolator displacement of (a) BI-building (b) BI-building-TLD at PGA of 0.3 g

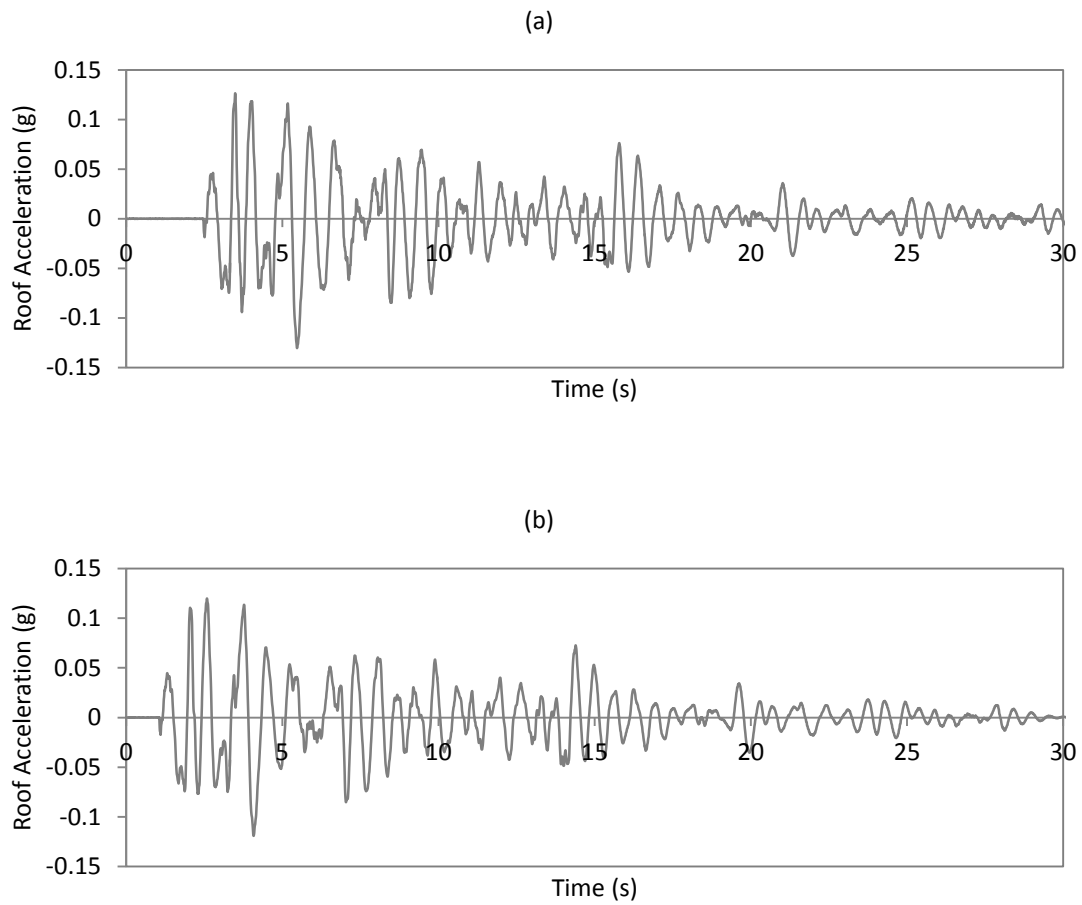


Figure 3-15 Response history of roof acceleration at PGA of 0.3 g (a) BI-building (b) BI-building-TLD

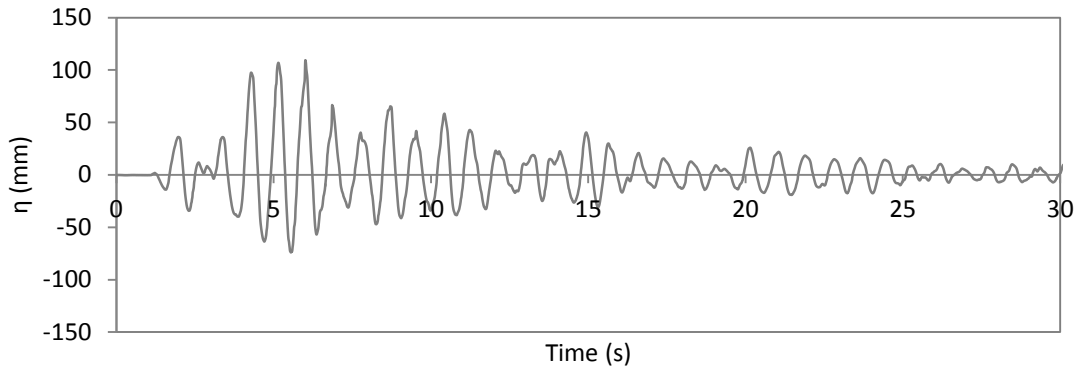


Figure 3-16 Response history of TLD free surface motion at PGA of 0.3 g

3.6 Summary

A BI-building-TLD system, which was developed for shake table testing, has been presented. A two-storey $\frac{1}{4}$ scale steel frame building was mounted on a shake table with four SU-FREIs placed underneath the building columns and TLD installed on its roof. Two sets of shake table tests were conducted with two different base excitations, sinusoidal excitation and earthquake excitation, respectively. For the sinusoidal excitation test program the BI-building and BI-building-TLD were tested under three amplitudes of excitation. For the earthquake test program both the BI-building and BI-building-TLD were subjected to the El Centro earthquake at 0.1 g, 0.2 g and 0.3 g PGA. In order to study the effect of a TLD on a BI-building all tests were first conducted with the TLD tanks, which were located at the top of the building, empty. The tanks were then filled with water up to a predetermined water depth level and the BI-building-TLD was then retested using the same input excitations.

Results from the shake table tests show that the TLD led to a reduction in the peak isolator displacement and roof acceleration response values under sinusoidal harmonic excitation. For this type of excitation, the effectiveness of the TLD was found to increase as the amplitude of excitation was increased. It was postulated that due to the softening behaviour of the SU-FREI the tuning ratio of the TLD improved resulting in increased effectiveness. The percent decrease in isolator

displacement increased from 9% at 1.3 mm excitation amplitude (the lowest excitation amplitude) to 25% at 3.8 mm excitation amplitude (the highest excitation amplitude).

The reduction in peak isolator displacement and roof acceleration was found to be significantly less for the case of earthquake excitation compared to harmonic excitation. For the earthquake excitation study, the TLD was found to be ineffective in reducing the peak isolator and peak roof acceleration values at 0.1 g PGA, however, as the level of excitation was increased the TLD was found to reduce both peak isolator and peak roof acceleration. For the highest PGA value (0.3 g) application of the TLD resulted in a decrease in the peak isolator displacement response of 2.7% and the peak roof acceleration by 7.7%. No general conclusions on TLD effectiveness for harmonic excitation or earthquake excitation could be drawn from this experimental study as it was limited to only a single BI-building-TLD configuration.

Chapter 4 **BI-Structure-DVA Systems under Harmonic Excitation**

4.1 **Introduction**

This chapter focuses on the numerical modelling of BI-Structure-DVA systems. An existing numerical model is first updated and evaluated for the BI-building-TLD tested under harmonic excitation and reported on in Chapter 3. Two numerical isolator models, a Bouc-Wen model and a Backbone Curve model, which have previously been used to simulate the force-displacement behaviour of a SU-FREI isolator, are considered. The isolators modelled in this study were constructed and tested under lateral cyclic loading in a previous study [7]. The hysteresis data obtained from that cyclic test program are used to generate parameters for the Bouc-Wen model. The predicted hysteretic response of the isolator using the Bouc-Wen model is compared with those of the experimental test results. In addition, a Backbone Curve (BC) model, previously calibrated by Foster [7] for the bearings utilized in the study, is also presented.

In the second part of this chapter a numerical model of a BI-Structure-TLD system, originally developed by Love et al. [3], is used to predict the response of the BI-building-TLD tested and reported on in Chapter 3. The numerical model consists of three individual modules, which model the structure (building), the base isolation (BI) system, and the dynamic vibration absorber (DVA), respectively. The base isolation module was modified in order to utilize the BC model. Details of each module in this numerical model as well as the input excitation and time history analyses are

presented. The predicted and measured results for three different amplitudes of excitation are then compared to experimental test results.

The BI-structure-DVA model is subsequently used to conduct a preliminary study on combinations of linear and nonlinear base isolation systems with linear and nonlinear dynamic vibration absorbers (DVA) systems. The design of the linear tuned mass damper (TMD) that is used in this study is based on the TLD system employed in the shake table study. A linear base isolator, having constant stiffness and damping values is also introduced. Analyses of these linear and nonlinear isolation and vibration absorber systems under harmonic excitation are subsequently carried out. The combinations of base isolators and dynamic vibration absorber (DVA) that are modelled in this chapter are as follows: nonlinear BI combined with a nonlinear DVA (TLD), nonlinear BI combined with a linear DVA (TMD), linear LBI combined with a linear DVA (TMD) and linear LBI combined with a nonlinear DVA (TLD).

4.2 Base Isolation-Structure-DVA Model

The BI-building investigated in the shake table study presented in Chapter 4 can be modelled as a three degree of freedom mass-spring-dashpot system as shown in Figure 4-1 [7]. The DVA located at the roof level, which is a TLD for the system shown Figure 4-1, can be modelled in a number of ways. For example, a TLD can be modelled as a fluid using shallow water wave theory or potential flow theory. Alternatively, the TLD can be modelled as an equivalent DVA, consisting of a mass, spring and dashpot attached to M_2 and the BI-structure-DVA system can be represented by 4 degree of freedom system as shown in Figure 4-2.

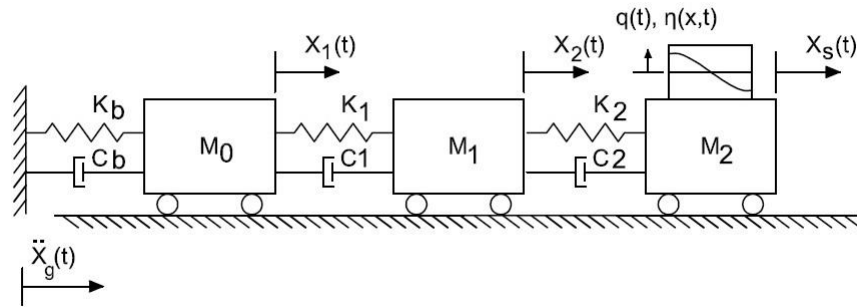


Figure 4-1 BI-structure-TLD model

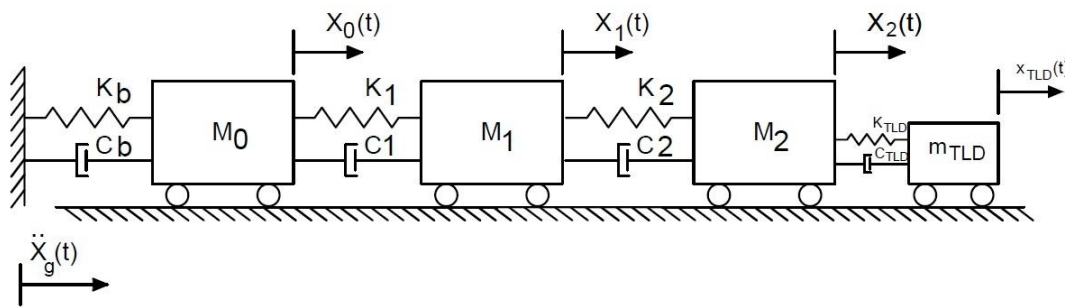


Figure 4-2 4DOF BI-structure-DVA model

The BI-structure-TLD model is comprised of three modules, which are shown in Figure 4-3. The base isolation module consists of the isolators (SU-FREI) and the base floor mass, the structure module consists of the first and second floors of the building and the DVA module simulates the TLD mounted on top of the second floor.

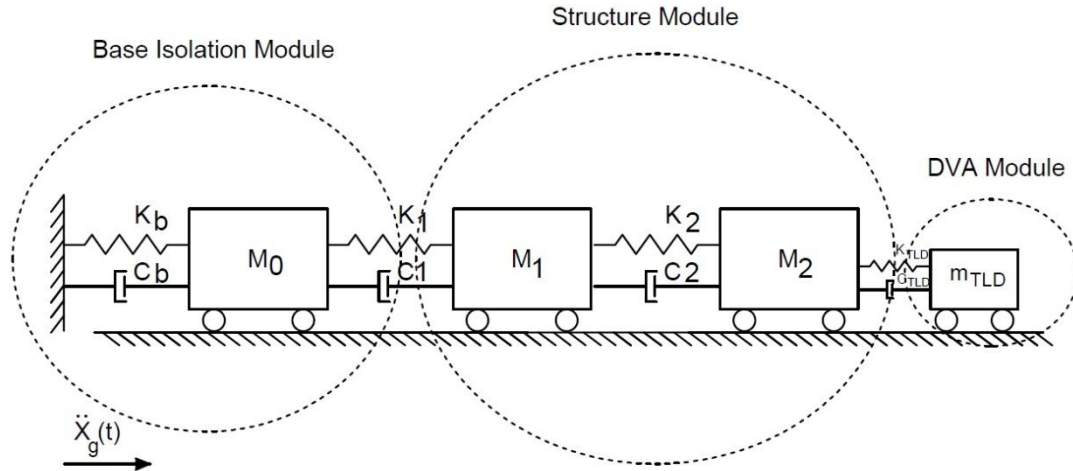


Figure 4-3 Individual modules comprising the BI-structure-TLD model

The base acceleration experienced by the building, shown in Figure 4-4, includes the ground acceleration \ddot{X}_g and the acceleration of the base mass \ddot{X}_0 multiplied by the corresponding mass at each floor level. In addition, a force, F_2 is transmitted from the TLD to the structure, which was located at the second floor mass for the BI-building tested on the shake table. The force from the DVA module is the inertial force of the accelerating fluid contained in the TLD that develops when it is subjected to lateral acceleration. For the BI-building tested on the shake table this is the total acceleration experienced by the second floor mass to which the TLD is attached. In the DVA module shown in Figure 4-4, the base acceleration is comprised of the ground acceleration \ddot{X}_g , the acceleration of the base mass \ddot{X}_0 and the acceleration of the second floor of the structure \ddot{X}_2 .

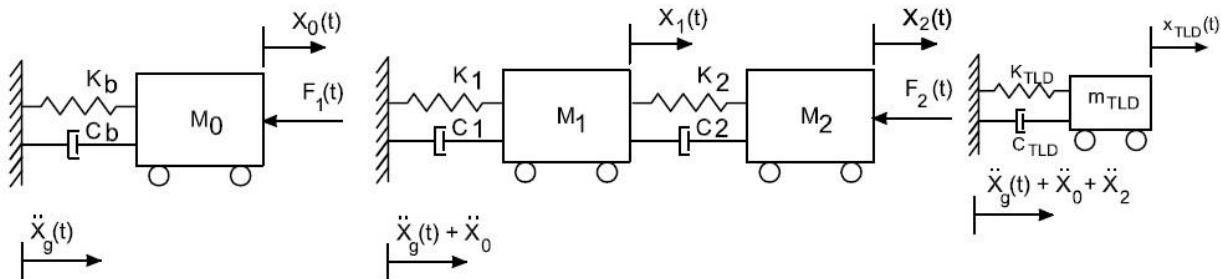


Figure 4-4 Force and acceleration transmission between different modules

In the BI-structure-DVA model there is the option to remove the effect of either the DVA and/or the base isolation system on the building. The mass of the empty tank is modelled as a part of the

mass of the second floor as the TLD tank remained attached to the structure during all shake table tests. The numerical time history analyses were carried out using the 4th order Runge-Kutta-Gill method with a time step of $dt = 0.0001$ s.

4.3 Structure Module

The Runge-Kutta-Gill method is employed to determine the building response at each time step under a specified base acceleration as well as corresponding TLD force applied to the building at the second floor level [3]. The force at each floor level of the building is determined at each time step by multiplying the total acceleration, consisting of the ground acceleration and the acceleration of the base mass, by the floor mass and accounting for the TLD force.

$$\begin{bmatrix} F_{s1} \\ F_{s2} \end{bmatrix} = \begin{bmatrix} -M_1(\ddot{X}_0 + \ddot{X}_g) \\ -M_2(\ddot{X}_0 + \ddot{X}_g) + F_2 \end{bmatrix} \quad 4-1$$

where F_{s1} and F_{s2} are the forces at first and second floor levels, respectively. These forces are the product of the ground and base mass accelerations and the TLD force, and M_1 and M_2 are the first and second floor masses. The equation of motion for the structure shown in Figure 4-4 can then be expressed as

$$\begin{bmatrix} M_1 & 0 \\ 0 & M_2 \end{bmatrix} \begin{bmatrix} \ddot{X}_1 \\ \ddot{X}_2 \end{bmatrix} + \begin{bmatrix} C_1 & 0 \\ 0 & C_2 \end{bmatrix} \begin{bmatrix} \dot{X}_1 \\ \dot{X}_2 \end{bmatrix} + \begin{bmatrix} K_1 & 0 \\ 0 & K_2 \end{bmatrix} \begin{bmatrix} X_1 \\ X_2 \end{bmatrix} = \begin{bmatrix} F_{s1} \\ F_{s2} \end{bmatrix} \quad 4-2$$

where X_1 is the relative displacement of M_1 and X_2 is relative the displacement of M_2 . As such, \dot{X}_1 , \dot{X}_2 , \ddot{X}_1 and \ddot{X}_2 correspond to relative velocity and acceleration at M_1 and M_2 , respectively. The damping C_1 and C_2 and stiffness K_1 and K_2 values of the structure have been reported in Chapter 3.

4.4 Base Isolation Module

The response of BI-structure is determined using the inertia force resulting from the ground acceleration, \ddot{X}_g , acting on the base mass, M_0 and the force, F_1 that accounts for the first storey stiffness and damping forces that develop between the structure and the base mass which is given by

$$F_1 = c_1 \dot{X}_1 + k_1 X_1 - M_0 \ddot{X}_g \quad 4-3$$

where c_1 and k_1 are damping and stiffness of the structure and \dot{X}_1 and X_1 are the relative velocity and displacement of the first floor.

Using the force as the input excitation the equation of motion for the isolation system can be expressed as

$$M_0 \ddot{X}_0 + F_0(\dot{X}, X) = F_1 \quad 4-4$$

where $F_0(\dot{X}, X)$ is a function of the isolator damping and stiffness. The base isolation module allows different isolation systems to be considered. In this chapter two isolators will be considered. A stable unbonded fiber reinforced elastomeric isolator is first modelled. Two SU-FREI models for $F_0(\dot{X}, X)$ were examined and are described below in Section 4.4.1. Subsequently, a linear isolation system, which consists of a linear spring, K_0 and dashpot, C_0 is modelled using the following equation of motion for the isolation system.

$$M_0 \ddot{X}_0 + C_0 \dot{X}_0 + K_0 X_0 = F_1 \quad 4-5$$

4.4.1 SU-FREI Models

The SU-FREI isolators used in this study were previously tested under cyclic lateral loading in order to evaluate their effective stiffness and damping properties using the recorded force-displacement data [7]

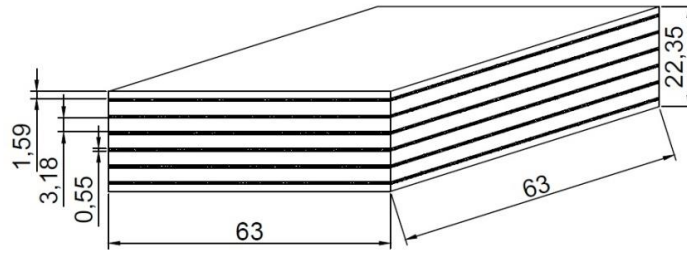


Figure 4-5 Schematic of the SU-FREI with theoretical dimensions (units mm)

For the lateral cyclic tests the isolators were monotonically loaded in the vertical direction to a design load of 8kN. After five seconds of sustained vertical load the isolator was subjected to three fully reversed sinusoidal cycles of lateral displacement for a total of seven different constant amplitude displacements, 25%, 50%, 75%, 100%, 150%, 200% and 250% of t_r . A time history of the lateral displacement from the cyclic tests conducted in [7] is illustrated in Figure 4-6. Figure 4-7 also shows example hysteresis loops obtained from these tests.

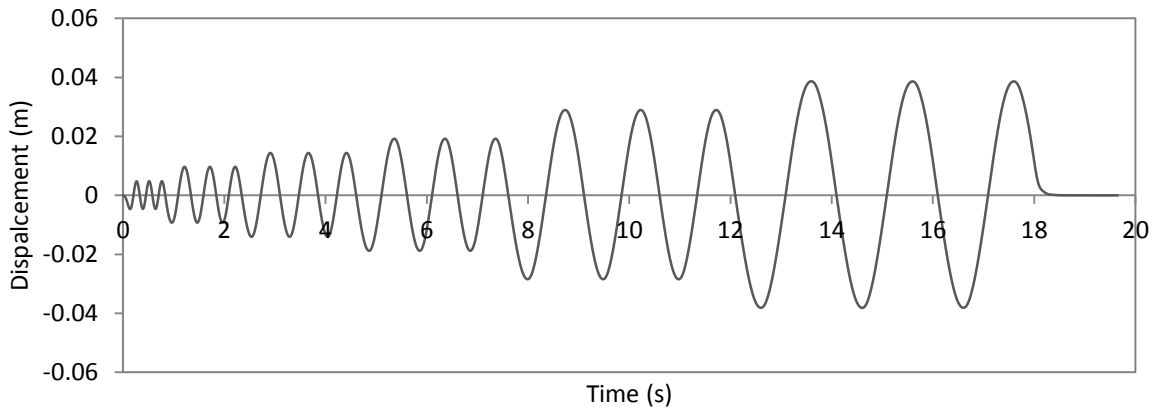


Figure 4-6 Displacement time history of the lateral cyclic test

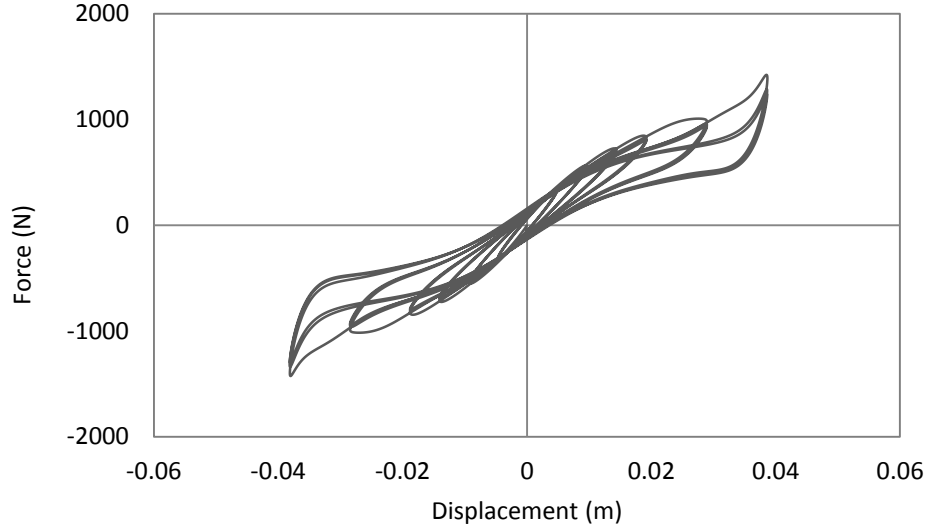


Figure 4-7 Measured force-displacement (hysteresis) loops from lateral cyclic test

The hysteresis data obtained from the lateral cyclic tests on the isolator were used to determine the Bouc-Wen model and Backbone Curve model parameters for the SU-FREI isolators as discussed in the following sections.

4.4.1.1 Bouc-Wen Model

A model commonly used to represent the hysteretic response of an isolator is the Bouc-Wen model. This model has been used to model base isolated buildings subjected to both wind [3] and earthquakes [101]. The model utilizes two time dependent variables to form two coupled equations. X is the displacement variable representing the displacement of the bearing, and Z is a hysteretic variable that has no physical meaning. A form of the Bouc-Wen model introduced by Chen Ahmadi [101] is expressed as

$$F_0(\dot{X}, X) = c\dot{X} + a_1X + a_2|X|X + a_3X^3 + b \left(1 - \frac{\beta}{A}|z|^n\right) z \quad 4-6$$

$$Y\dot{z} = -\gamma|\dot{X}|z|z|^{n-1} - \beta\dot{X}|z|^n + A\dot{X} \quad 4-7$$

The cubic polynomial in the above equation enables the softening behaviour of the isolator.

In order to capture the softening and subsequent hardening behaviour of a SU-FREI as it is displaced laterally a fifth order polynomial has been introduced [3]

$$F_0(\dot{X}, X) = c\dot{X} + a_1X + a_2|X|X + a_3X^3 + a_4|X|X^3 + a_5X^5 + b\left(1 - \frac{\beta}{A}|z|^n\right)z \quad 4-8$$

This modified Bouc-Wen model can be used to model the behaviour of a non-linear SU-FREI isolation system. The first cycle from each of the first six amplitudes applied in the lateral cyclic test program was used to evaluate the unscragged model parameters while the second and third cycles were used to evaluate scragged model parameters. Tables 4-1 shows the least squares fitted unscragged Bouc-Wen parameters at different amplitudes.

Table 4-1 Unscragged Bouc-Wen parameters (units N m)

Isolator Displacement	25%tr	50%tr	75%tr	100%tr	150%tr	200%tr
c	5.00E+02	7.96E+02	1.01E+03	4.83E+02	1.01E+02	-1.37E+03
a1	7.01E+04	5.85E+04	5.03E+04	4.88E+04	4.18E+04	4.14E+04
a2	0.00E+00	0.00E+00	0.00E+00	-2.30E+05	-1.75E+05	-3.09E+05
a3	2.42E+01	-1.43E+02	1.77E+01	-1.41E+08	-1.27E+07	-3.63E+07
a4	0.00E+00	0.00E+00	0.00E+00	1.55E+10	1.60E+08	1.01E+09
a5	2.00E+02	2.00E+02	2.00E+02	-4.55E+11	1.60E+09	-1.63E+09
b	9.98E+00	0.00E+00	-9.00E-02	2.59E+00	2.03E+00	1.77E+01
β	2.00E-02	-5.83E+00	0.00E+00	-3.10E-01	-3.70E-01	-2.90E-01
A	1	1	1	1	1	1
n	1	1	1	1	1	1
Υ	6.50E-02	6.50E-02	6.50E-02	4.40E-01	4.47E-01	4.46E-01
Υ	7.00E+00	7.00E+00	7.00E+00	1.15E-04	9.03E-05	1.13E-04

Figure 4-8 shows the force-displacement loops for 100% t_r and 200% t_r amplitude cycle from the experimental data and the Bouc-Wen model. It can be seen that there is good agreement between the predicted and experimental hysteresis loops at both amplitudes. Furthermore, the model is able to capture both the softening and hardening behaviour of the isolator.

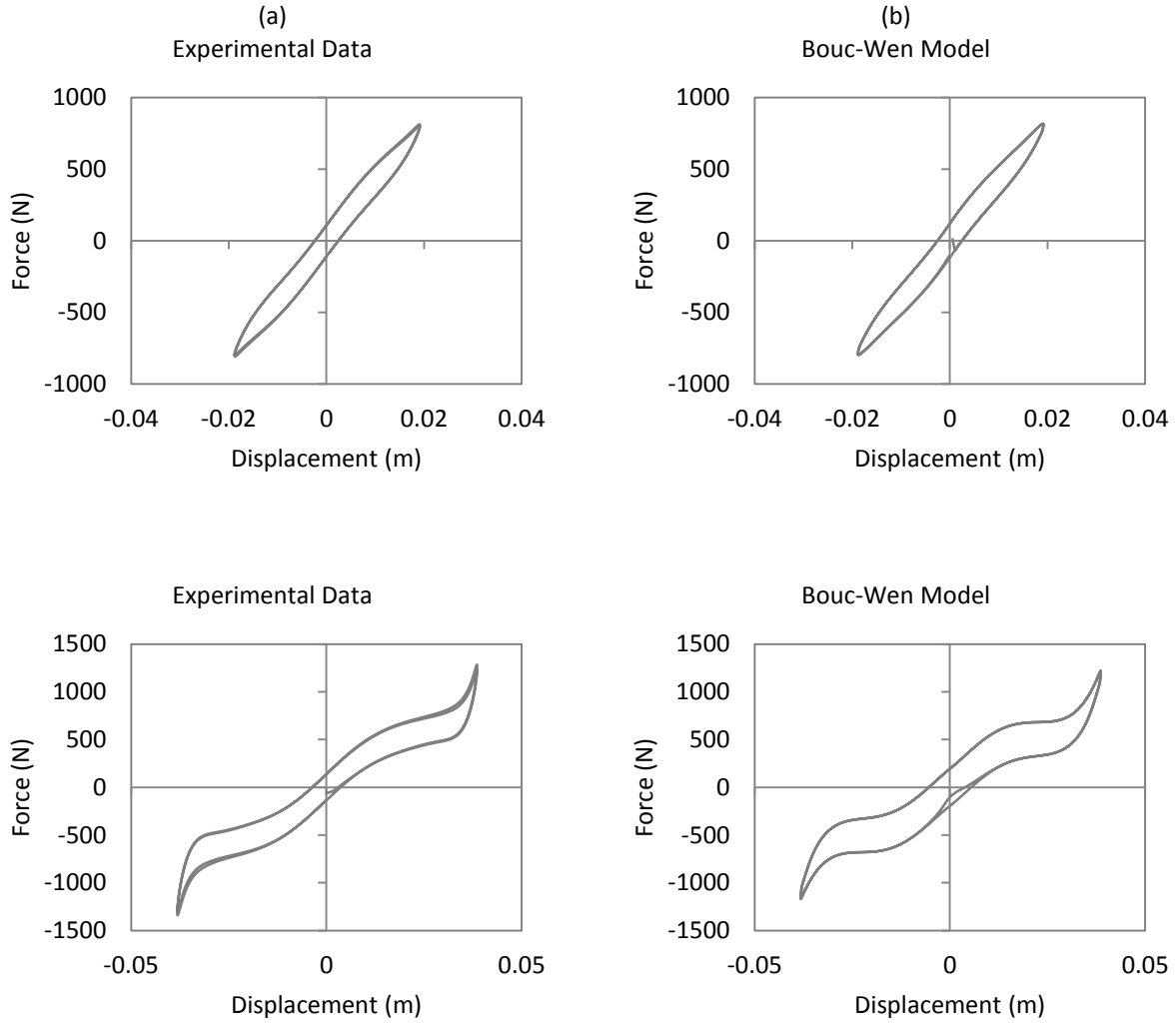


Figure 4-8 Hysteresis loops at 100% t_r and 200% t_r (a) experimental, (b) Bouc-Wen model

4.4.1.2 Backbone Curve Model

The Backbone Curve model employs a 4th order polynomial function for the elastic stiffness in combination with an amplitude dependent effective damping ratio to model the lateral force-displacement (hysteresis) of a SU-FREI. The fitted polynomial curve represents an idealized estimate of the lateral force-displacement response of the isolators (with the damping force

removed) and is referred to as the Backbone Curve. A least squares fit to the hysteresis loop data is carried out to determine the unknown polynomial coefficients. The effective damping values are also evaluated from lateral cyclic test results over the 25% to 250% displacement range.

The instantaneous SU-FREI lateral force can be expressed as [41]

$$F_0(\dot{X}, X) = \sum_{i=1}^N f_{si}(t) + f_{di}(t) \quad 4-9$$

where $f_{si}(t)$ and $f_{di}(t)$ are the isolator stiffness and damping force, respectively and N is the total number of isolators used in the isolation system. The stiffness component of the lateral force can be expressed as

$$f_{si}(t) = k_i(v_i(t))v_i(t) \quad 4-10$$

where $v_i(t)$ is the lateral displacement and $k_i(v_i(t))$ is the lateral stiffness of the isolator at time t . The stiffness is modelled using a 4th order polynomial expression given by

$$k_i(v_i(t)) = b_0 + b_1v_i(t) + b_2v_i^2(t) + b_3v_i^3(t) + b_4v_i^4(t) \quad 4-11$$

A least squares fitting method is used to fit the 5th order expression in Equation 4-10 to the experimentally obtained hysteresis loop in order to determine the five parameters of the model b_0 to b_4 .

The equivalent viscous damping is expressed using a Rayleigh damping idealization and is calculated as

$$f_{di}(t) = C_i(t)\dot{v}_i(t) \quad 4-12$$

where, at any instant in time, the damping coefficient $C_i(t)$ is calculated based on a constant effective damping value expressed as

$$C_i(t) = 2\zeta_{eff} \sqrt{\frac{k_i(v_i(t))P}{g}} \quad 4-13$$

where P is the applied load on an individual isolator, g is the acceleration due to gravity and ζ_{eff} is the effective damping ratio [45]. Using experimentally obtained force-displacement loops the effective damping was determined at each of the seven displacement amplitudes [7]. The nonlinear

stiffness and amplitude dependent damping forces are combined to obtain the hysteretic behaviour of the isolator at particular displacement amplitude.

The Backbone Curve stiffness coefficient values and effective damping values obtained by Foster [7] for the isolators (at each of the displacement amplitudes) are shown in Table 4-2. It can be observed that the damping ratio, listed in the first row, decrease as the displacement amplitude is increased.

Table 4-2. Backbone Curve Model Parameters [7]

Isolator Displacement	25%tr	50%tr	75%tr	100%t	150%tr	200%tr	250%tr
ζ (%)	1.02E+01	9.40E+00	9.10E+00	8.90E+00	8.70E+00	7.40E+00	7.45E+00
b_0 (N/m)	7.30E+04	7.02E+04	6.38E+04	5.94E+04	5.62E+04	5.25E+04	4.49E+04
b_1 (N/m ²)	7.13E+05	1.55E+05	-1.77E+05	-1.56E+05	-9.71E+04	-9.84E+04	-4.10E+04
b_2 (N/m ³)	-1.55E+08	2.71E+08	-1.15E+08	-7.81E+07	-6.08E+07	-4.84E+07	-2.79E+07
b_3 (N/m ⁴)	-2.39E+10	4.57E+08	3.52E+08	2.54E+08	8.45E+07	8.94E+07	3.74E+07
b_4 (N/m ⁵)	3.42E+12	1.78E+12	2.63E+11	1.01E+11	4.33E+10	2.54E+10	1.16E+10

Plots of the hysteresis loops generated using the Bouc-Wen model and the Backbone Curve model at 100% t_r amplitude are shown in Figure 4-9 along with the measured force-displacement results obtained from lateral cyclic tests [7].

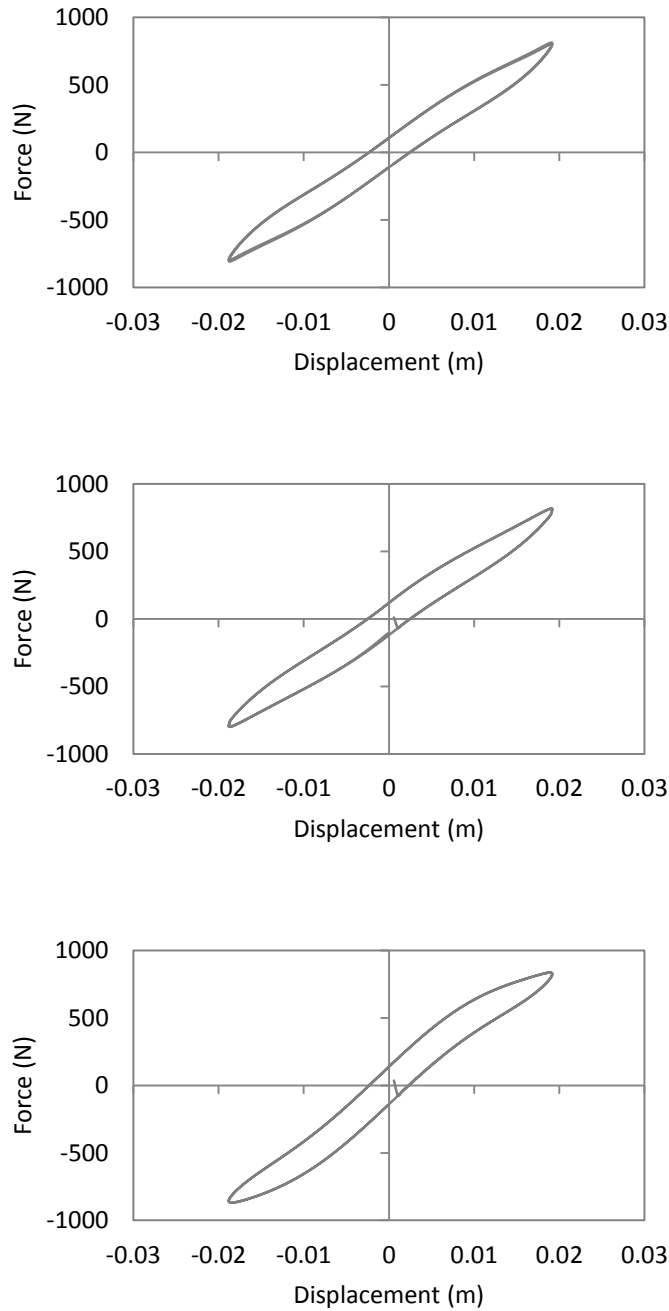


Figure 4-9 Hysteresis loops (a) experimental, (b) Bouc-Wen model and (c) Backbone Curve model (100% t_r)

Both the Bouc-Wen model and the Backbone Curve model were able to reproduce the hysteresis loops with reasonable accuracy. These models were calibrated at discrete displacement amplitudes, corresponding to the cyclic lateral test amplitudes, and as a result the isolator stiffness and damping

parameters are functions of amplitude. In order to accurately model the nonlinear stiffness and damping behaviour of the isolator under a general type of loading the stiffness coefficients and damping ratio must be determined by interpolating between the nearest displacements amplitudes for which model parameters are known.

Although the hysteretic response predicted by the Bouc-Wen model was in good agreement with experimental results, a suitable interpolation technique to update the model parameters over each isolator displacement response cycle, which is required for time history analysis, was not found. In addition, the Bouc-Wen model requires more computational effort than the Backbone Curve model. Finally, Toopchi-Nezhad et al. [41] and Foster [7] have successfully used the Backbone Curve model to model the response of a SU-FREI base isolated building. As a result the Backbone Curve model, using the parameters determined by Foster, was selected as the model to be used in this study.

The Backbone Curve model, with parameters determined at seven displacement amplitudes, expressed as percent of t_r (25%, to 250%) was incorporated into the base isolation module of the BI-structure-DAV model. A linear interpolation technique, which uses the calculated peak isolator displacement value to update the base isolator stiffness coefficients and damping ratio, is employed. The program interpolates between the isolator restoring forces for each of the two bracketing amplitudes after the completion of each response cycle based on the peak isolator displacement value of that cycle.

4.5 Dynamic Vibration Absorber (DVA) Module

Two DVA models were considered in this study and incorporated into the DVA module. One is a linear DVA model, representing a linear tuned mass damper (TMD), which consists of a linear spring and dashpot as shown in Figure 4-4. The second DVA model, which is described in detail below, is a tuned liquid damper (TLD).

4.5.1 Tuned Liquid Damper Model

In this study the TLD is located at the roof level. As such, the total acceleration, \ddot{X}_{TLD} , at the roof level of the building is used as the input excitation exerted on the TLD and is expressed as

$$\ddot{X}_{TLD} = \ddot{X}_g + \ddot{X}_0 + \ddot{X}_2 \quad 4-14$$

For the BI-structure-DVA model the input acceleration is calculated by adding the ground acceleration, the isolator acceleration and the relative acceleration of the building at the roof level.

The response of the fluid is calculated using a modal expansion method, which accounts for the coupling between sloshing modes through the nonlinear free surface boundary conditions [96], [97]. The TLD fluid model used in this study was developed by Love and Tait [96] and considers the first three sloshing modes. The equation of motion of the m^{th} sloshing mode is expressed as [3]

$$\begin{aligned} \ddot{q}_m + 2\omega_m(\xi_{\omega,m} + \xi_{s,m})\dot{q}_m + \omega_m^2 q_m + P_m \ddot{X}_{TLD} + d_1^m \dot{q}_1 \dot{q}_2 + d_2^m \dot{q}_1 q_1 \\ + d_3^m \ddot{q}_2 q_1 + d_4^m \dot{q}_1 q_1 q_1 + d_5^m \dot{q}_1 \dot{q}_1 + d_6^m \dot{q}_2 \dot{q}_1 + d_7^m \dot{q}_1^2 q_1 = 0 \end{aligned} \quad 4-15$$

The coupled equations of motion for the first three sloshing modes can be expressed as

$$\begin{aligned} \ddot{q}_1 + 2(\xi_{w,1} + \xi_{s,1}|\dot{q}_1|)\omega_1 \dot{q}_1 + \omega_1^2 q_1 + d_1 \dot{q}_1 \dot{q}_2 + d_2 \dot{q}_1^2 q_1 + d_3 \ddot{q}_2 q_1 - d_1 \dot{q}_2 \\ - 2d_2 q_1 \dot{q}_1 - P_1 \ddot{X}_{TLD} = 0 \end{aligned} \quad 4-16$$

$$\ddot{q}_2 + 2(\xi_{w,2} + \xi_{s,2}|\dot{q}_2|)\omega_2 \dot{q}_2 + \omega_2^2 q_2 + d_4 \dot{q}_1 q_1 + d_5 \dot{q}_1^2 = 0 \quad 4-17$$

$$\begin{aligned} \ddot{q}_3 + 2(\xi_{w,3} + \xi_{s,3}|\dot{q}_3|)\omega_3 \dot{q}_3 + \omega_3^2 q_3 + d_6 \dot{q}_1 \dot{q}_2 + d_7 \dot{q}_1 q_1^2 + d_8 \ddot{q}_2 q_1 \\ + d_9 \dot{q}_1 \dot{q}_2 + d_{10} \dot{q}_1^2 q_1 - P_3 \ddot{X}_{TLD} = 0 \end{aligned} \quad 4-18$$

where

$$\begin{aligned} \xi_{w,m} = \left(\frac{1}{L}\right) \sqrt{\frac{v}{2\omega_m}} \left(\frac{L}{b} + 1 + m\pi \left[1 - 2\frac{h}{L}\right] \operatorname{cosech}\left(2\frac{m\pi}{L}h\right) \right. \\ \left. + m\operatorname{coth}\left(\frac{m\pi}{L}h\right)\right) \end{aligned} \quad 4-19$$

and

$$\xi_{s,m} = \frac{\tanh\left(\frac{m\pi h}{L}\right)}{2\omega_m L} C_l \left(\frac{1}{3} + \frac{1}{\sinh^2\left(\frac{m\pi h}{L}\right)} \sum_{j=1}^{ns} \left| \sin^3\left(\frac{m\pi x_j}{L}\right) \right| |\dot{\beta}_m(t)| \right) \quad 4-20$$

The coefficients d_i are defined as follows [109]

Table 4-3 Equations to calculate d_i coefficients

Coefficients d_i			
d_1	$\frac{2E_0}{E_1} + E_1$	d_6	$3E_3 - 6\frac{E_0}{E_1}$
d_2	$2E_0(-1 + 4\frac{E_0}{E_1 + E_2})$	d_7	$-3E_0 - 9\frac{E_0 E_3}{E_1} + 24\frac{E_0^2}{E_1 E_2}$
d_3	$-\frac{2E_0}{E_2} + E_1$	d_8	$-6\frac{E_0}{E_2} + 3E_3$
d_4	$-\frac{4E_0}{E_1} + 2E_2$	d_9	$-6\frac{E_0}{E_1} - 6\frac{E_0}{E_2} - 6\frac{E_0 E_3}{E_1 E_2} + 3\frac{E_3 E_1}{E_2}$
d_5	$E_2 - 2\frac{E_0 E_2}{E_1^2} - 4\frac{E_0}{E_1}$	d_{10}	$-6E_0 - 24\frac{E_0 E_3}{E_1} + 48\frac{E_0^2}{E_1 E_2} + 24\frac{E_0^2 E_3}{E_1^2 E_2}$

The E_i coefficients are given by

$$E_0 = \frac{1}{8} \left(\frac{\pi}{L} \right)^2 \quad 4-21$$

$$E_n = \left(\frac{\pi}{2L} \right) \tanh\left(\frac{n\pi}{Lh}\right) \quad , \quad n = 1, 2, 3, 4 \quad 4-22$$

and P_i values are expressed as

$$P_1 = -8 \frac{E_1 L}{\pi^2} \quad 4-23$$

$$P_2 = 0 \quad 4-24$$

$$P_3 = -8 \frac{E_3 L}{3\pi^2} \quad 4-25$$

The resultant inertial fluid force, which is a function of the anti-symmetric sloshing modes, is calculated by multiplying the mass of the fluid by the acceleration of its centre of mass [97].

$$F_{tank} = m_w \frac{L}{h\pi^2} \left(2\ddot{q}_1 + \frac{2}{9}\ddot{q}_3 \right) \quad 4-26$$

where m_w is the mass of the fluid. The TLD free surface response and corresponding fluid inertia force is calculated at each time step using the above set of equations. The TLD force is then applied to the second floor mass to determine the building response in the following time step.

4.6 Input Excitation

The BI-structure-DVA response is evaluated under harmonic excitation at the frequencies and amplitudes used in the shake table test program. The measured table displacement amplitude values and excitation frequencies, determined from the shake table test results, were used to generate the excitation acceleration time history. A plot of the calculated harmonic acceleration time history used as the input excitation is shown in Figure 4-10. It should be noted that although this input matches the frequencies used in the shake table study it is not a record of the actual input applied during testing.

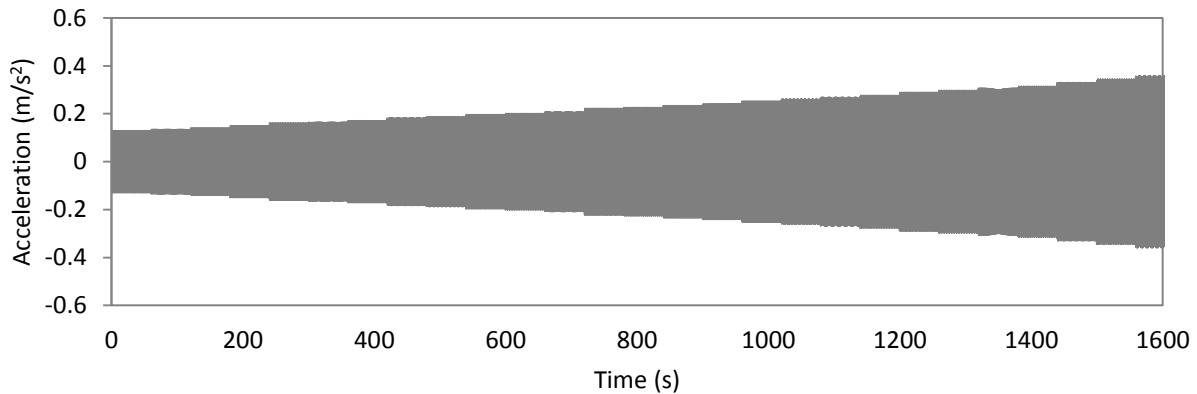


Figure 4-10 Input harmonic base acceleration time history (3.8 mm excitation amplitude)

4.7 Model Evaluation

Results from shake table tests conducted under harmonic excitation are compared to results obtained from the BI-structure-TLD model described above. The model is evaluated for both the

BI-building and BI-building-TLD as experimental tests were conducted both with and without water in TLD tanks.

The predicted steady-state lateral displacement amplitude experienced by the isolation system (isolator displacement amplitude, X_0) is compared with results obtained from shake table tests. Frequency response plots of both the measured and predicted normalized isolator displacement amplitude, corresponding to excitations amplitudes of 1.3 mm, 2.5 mm and 3.8 mm, for the BI-building are shown in Figure 4-11. At higher and lower excitation frequencies the predicted and experimental isolator displacement amplitude values match well for all three excitation amplitudes. For the BI-building the model predicts a more pronounced jump phenomenon, where the isolator response rapidly changes from one response amplitude to a much higher or lower response amplitude. Due to the nonlinear behaviour of the isolator, more than a single response amplitude can exist for a given excitation frequency. It should be noted that the jump phenomenon is dependent upon the direction the frequency sweep (ascending or descending) is carried out. In the model and in experimental testing the frequency sweep was carried out in ascending order. However, as the actual applied excitation history was not recorded, this adds an additional challenge to accurately capturing the BI-building response near resonance. In all cases the model predicts higher peak isolator displacement values near resonance in comparison to shake table test results. For the lowest and highest excitation amplitudes the model over predicts the peak response by approximately 16% and 20%, respectively.

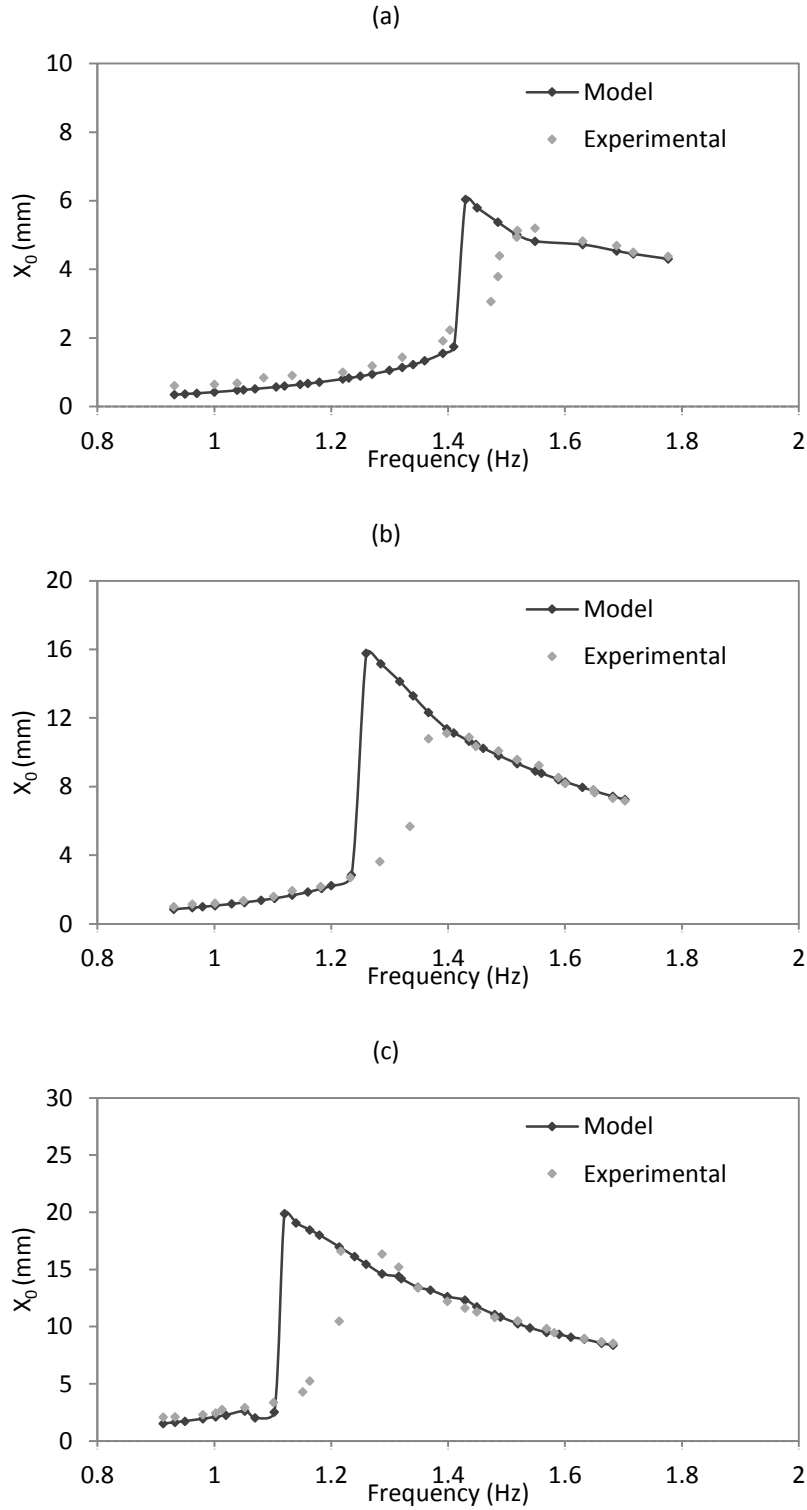


Figure 4-11 BI-building isolator displacement at (a) 1.3 mm (b) 2.5 mm and (c) 3.8 mm excitation amplitude

Figure 4-12 shows frequency response plots of the measured and predicted isolator displacement for the BI-building-TLD. Overall, reasonable agreement is found between the values predicted by the model and the experimentally measured values. The rapid increase in isolator displacement amplitude near the natural frequency is captured by the model. Discrepancies between the model and measured values are found to increase with increased excitation amplitude.

For the lowest excitation amplitude considered (1.3 mm), results from the model are found to be overall in good agreement with the experimental results. The presence of a second smaller peak, which is related to the TLD is also predicted by the model. At the 2.5 mm excitation amplitude, although the results from the shake table test display a frequency response behaviour that is characteristic of a nonlinear system under harmonic excitation, the jump phenomenon is not as pronounced as predicted by the model. At this excitation amplitude the model over predicts the peak response value by approximately 17%. At the largest excitation amplitude of 3.8 mm the model is able to capture the distinct two-peaked frequency response behaviour, which indicates increased coupling between the TLD and the BI-structure. However, the model over predicts the peak response amplitude by approximately 28%.

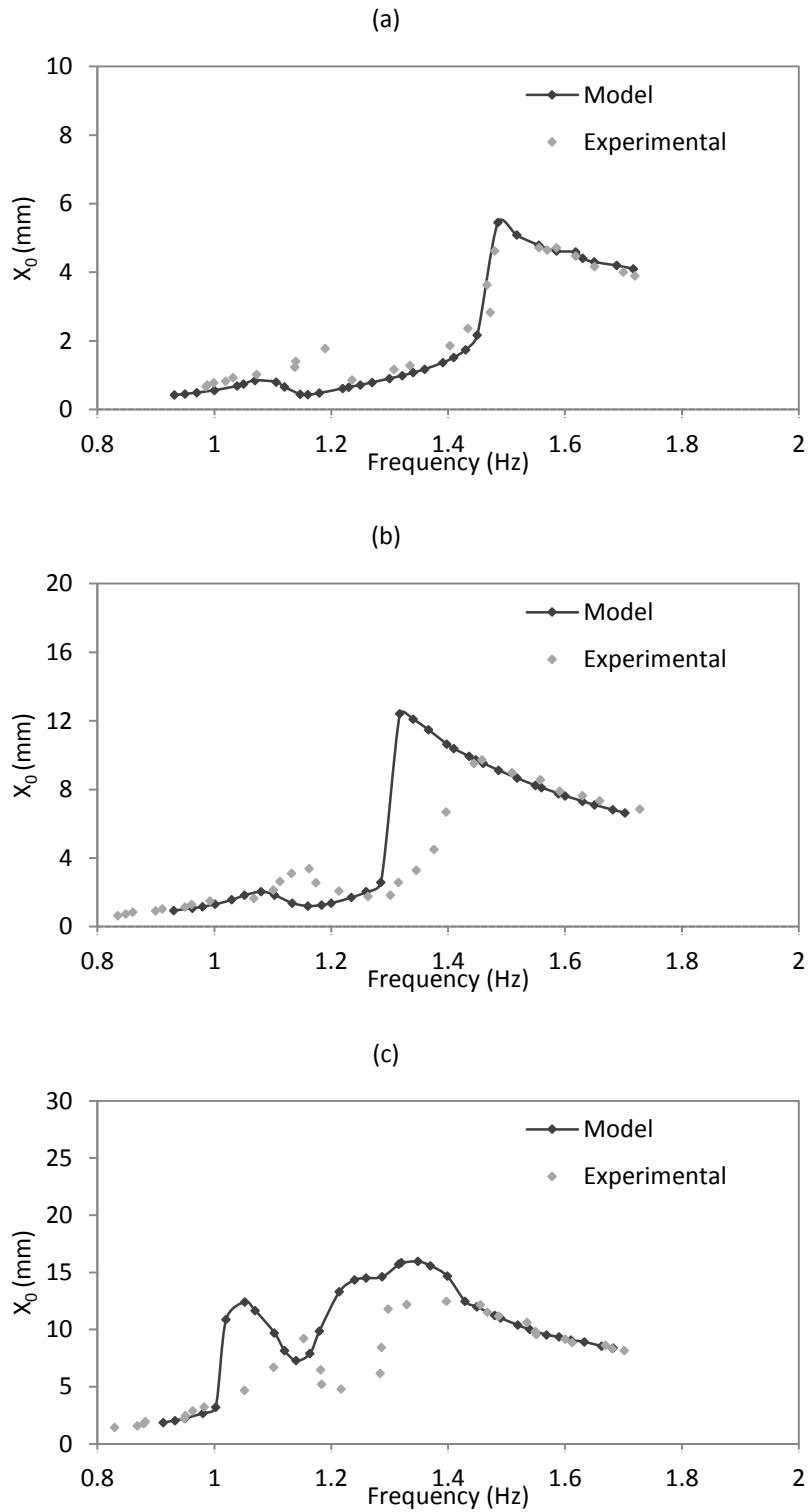


Figure 4-12 BI-building-TLD isolator displacement at (a) 1.3 mm (b) 2.5 mm and (c) 3.8 mm excitation amplitude

Figure 4-13 shows frequency response plots of both the measured and predicted TLD free surface response amplitude for the lowest (1.3 mm) and highest (3.8 mm) excitation amplitudes. It can be seen from this figure that at the highest excitation amplitude the model was able to predict the double-peaked response of the BI-building-TLD system. The model was found to under-predict the peak free surface response amplitude by approximately 26%, 31% and 10% for the 1.3 mm, 2.5 mm and 3.8 mm excitation amplitudes, respectively.

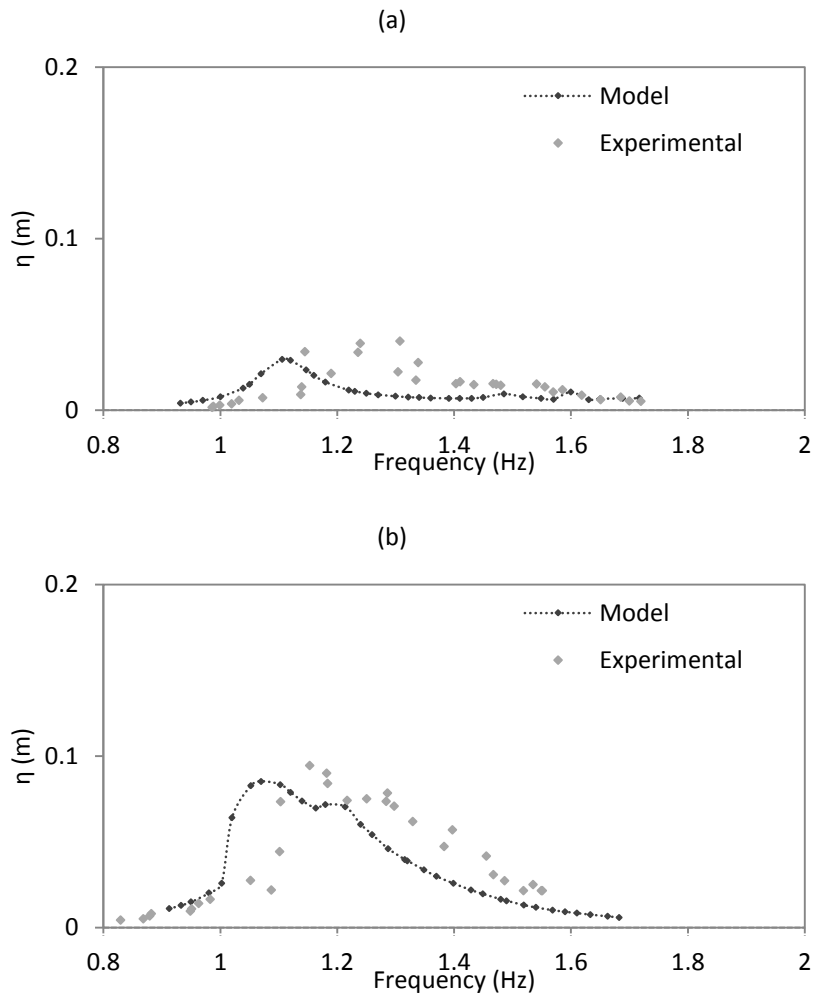


Figure 4-13 BI-building-TLD free surface response at (a) 1.3 mm and (b) 3.8 mm excitation amplitude

4.8 Linear Base Isolation System Model

The response of a (linear) LBI-structure-DVA system is investigated considering two different isolator stiffness values for the base isolation system. The linear systems are modelled in the Base Isolation module using Equation 4-5. The constant stiffness values, K_0 , for the two isolation systems considered, are taken to as the linear stiffness for the 100% t_r and 150% t_r backbone curves shown in Table 4-2, which approximately bracket the effective stiffness of the SU-FREI base isolation system between the 50% t_r and 75% t_r response amplitudes. The isolators used in both linear isolation systems were assumed to have a constant effective damping value of 8.9%.

4.9 Linear DVA –Linear Tuned Mass Damper Model

It can be observed from Figure 4-4, that a linear TMD can be modelled in the DVA module as a linear single degree of freedom system. As discussed in Chapter 3, equivalent linear mass, stiffness and damping parameters for a TLD can be determined allowing it to be represented by an equivalent mechanical system. The equivalent, mass, stiffness and damping can be calculated using the following equations [86]

$$m_{eq} = \frac{8\rho bL^2}{\pi^3} \tanh\left(\frac{\pi h}{L}\right) \quad 4-27$$

$$k_{eq} = \frac{8\rho bLg}{\pi^2} \tanh^2\left(\frac{\pi h}{L}\right) \quad 4-28$$

$$\xi_{eq} = C_l \frac{16}{3\pi^2} \tanh^2\left(\frac{\pi h}{L}\right) \Delta \Xi \frac{x_r}{L} \quad 4-29$$

The equivalent viscous damping, given by Equation 4-28, is for the case of harmonic excitation and is dependent on the response parameter x_r . As such, x_r values of 8.6 mm, 17 mm and 45 mm were selected for the 1.3 mm, 2.5 mm and 3.8 mm excitation amplitudes, respectively and the damping ratio was assumed to remain constant for a given excitation amplitude. The TMD parameters, determined using Equations 4-27 to 4-29, are shown in Table 4-5.

Table 4-4 Linearized Equivalent TLD Parameters at the frequency of excitation equal to natural frequency of the TLD

m_{eq} (kg)	113.6
k_{eq} (N/m)	6649
ξ_{eq} (%) (1.3 mm)	0.7
ξ_{eq} (%) (2.5 mm)	1.3
ξ_{eq} (%) (3.8 mm)	3.4

4.10 Response of Linear and Nonlinear Base Isolation and DVA Systems

The following section presents the results of a preliminary study on combined linear and nonlinear base isolation and dynamic vibration absorber systems. The linear DVA and isolators described in Sections 4.8 and 4.9, respectively, are used in combination with the SU-FREI Backbone Curve model and the Tuned Liquid Damper model. The following combinations of systems are considered, a BI-structure-TMD, a LBI-Structure-TLD and a LBI-structure- TMD.

4.10.1 BI-Structure-TMD System

This BI-structure-DVA system is comprised of the nonlinear SU-FREI BI-building described in earlier and a linear DVA having equivalent linear TMD system properties, determined in Section 4.9. For the BI-building-TMD, additional simulations were carried out, which are shown as a different data series in the plots. For these simulations, the system was excited from rest to a steady state response in order to investigate the influence of initial conditions.

Frequency response plots of BI-building-TMD and BI-building-TLD isolator displacement, X_0 are shown in Figure 4-14. For the 1.3 mm excitation amplitude, shown in Figure 4-14 (a), both systems are found to be in agreement at a majority of excitation frequency values. The largest discrepancies were found to occur at a frequency of approximately 1.2 Hz, which is near the natural frequency of the DVA, and at excitation frequencies greater than 1.6 Hz. However, it can be observed that

better agreement was obtained when discrete frequency simulations, starting with at rest initial conditions, were carried out on the BI-building-TMD. This shows the sensitivity of this system to initial condition values, particularly when the damping ratio of the absorber is low.

At an excitation amplitude of 2.5 mm the isolator displacement of the BI-building-TMD and BI-building-TLD are in good agreement, except at frequency values near the first smaller peak near 1.2 Hz. Similar to the 1.3 mm excitation case, better agreement is found at higher and lower excitation frequency values. Discrete frequency results again highlight the sensitivity of the system to the initial conditions.

At an excitation amplitude of 3.8 mm the response of the BI-building-TMD and BI-building-TLD differ over a greater range of frequencies. Greater discrepancy is expected to occur at larger excitation amplitudes as the nonlinear behaviour of the TLD becomes more pronounced. The peak isolator displacement value for the BI-building-TLD is approximately 7% less than the peak response value of the BI-building-TMD. The greater reduction in response can be explained, in part, by the fact as the amplitude of excitation increases the TLD achieves a higher damping ratio structure compared to the linear TMD making it a more robust DVA.

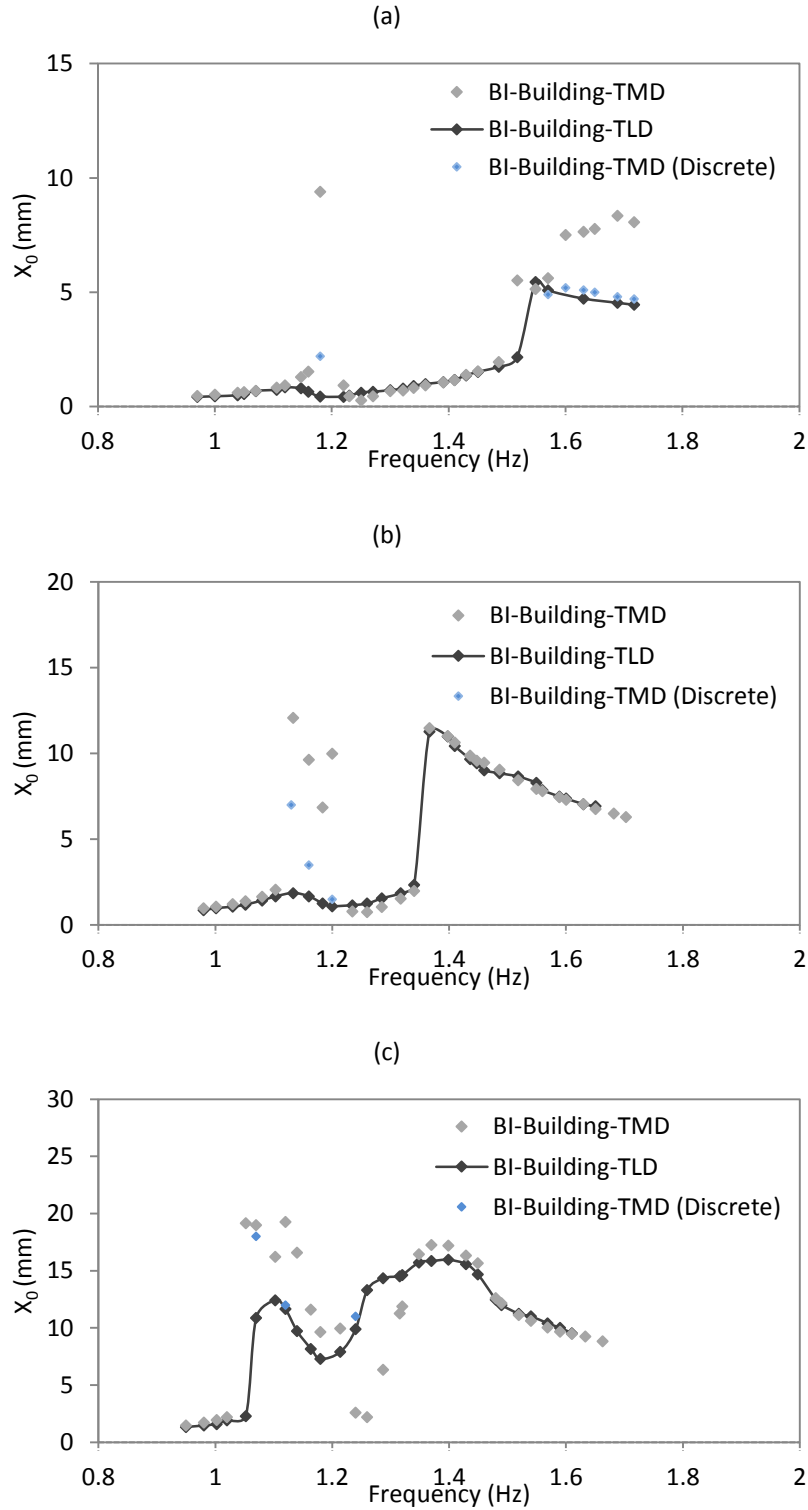


Figure 4-14 BI-building-TMD and BI-building-TLD isolator displacement at (a) 1.3 mm, (b) 2.5 mm and (c) 3.8 mm excitation amplitude

4.10.2 LBI-Structure-TLD System

In the following simulations the nonlinear SU-FREI isolators are replaced with two different linear isolators having properties described in Section 4-8. The behaviour of a TLD attached to a LBI-building is expected to match that of a typical structure-TLD system. Figure 4-15 shows frequency response plots of the two LBI-building-TLD for the lowest (1.3 mm) and highest (3.8 mm) excitation amplitudes.

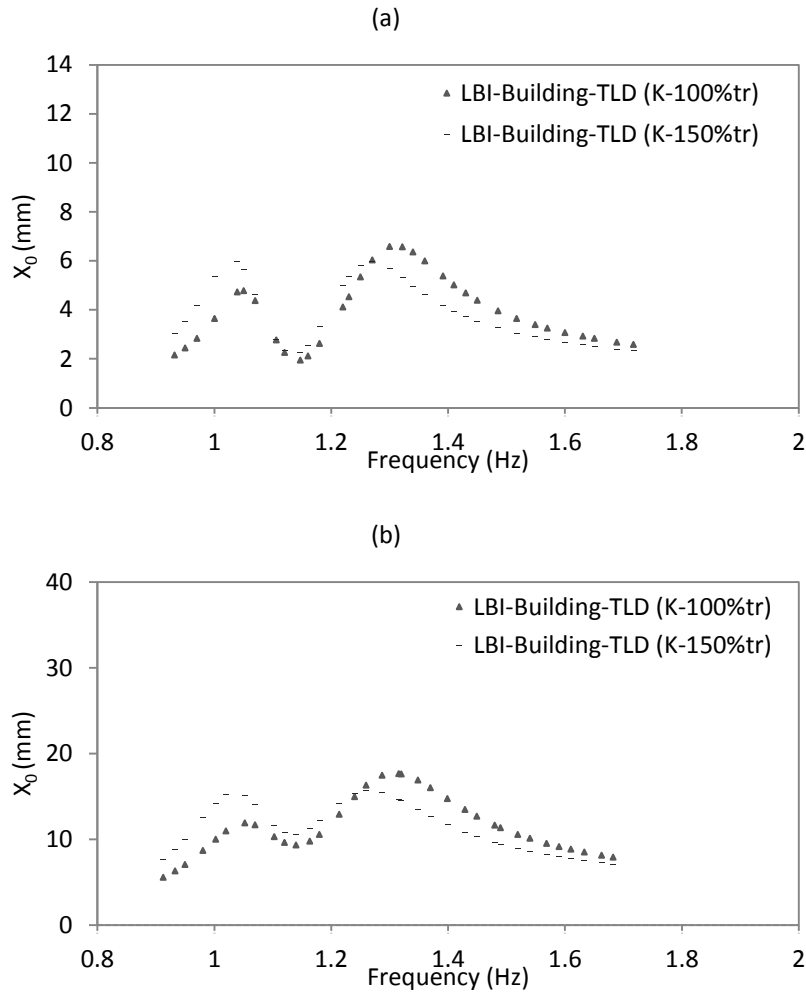


Figure 4-15 LBI-building-TMD isolator displacement at (a) 1.3 mm and (b) 3.8 mm excitation amplitude

It can be observed from these figures that as the stiffness of the linear isolation system is increased the peak isolator displacement reduced, which indicates the TLD is better tuned to the LBI-building having a higher isolator stiffness value. In addition, as the excitation amplitude is increased it can be observed that the shape of the frequency response curves change. In particular, the first peak of the double peaked curve is found to reduce. This observed change in the frequency response curve is attributed to the amplitude dependent damping ratio of the TLD.

4.10.3 LBI-Structure-TMD System

The response of the two LBI-buildings is investigated in combination with a TMD. Frequency response plots of the two systems are shown in Figure 4-16 for the lowest (1.3 mm) and highest (3.8 mm) excitation amplitudes. Negligible difference between the isolator displacement values of the two systems is observed. In addition, as the both systems are linear, the frequency response curves are found to remain consistent at both levels of excitation.

Table 4-5 Ratio of peak isolator displacement

Peak isolator displacement TLD/ Peak isolator displacement TMD		
Excitation Amplitude (mm)	100% t_r	150% t_r
1.3	0.97	0.91
2.5	0.98	0.91
3.8	1.10	1.02

Table 4-7 summarizes the ratio of the peak isolator displacement of the LBI-building-TLD and linear BI-building-TMD systems for the two different isolator stiffness values at three different amplitudes of excitation. These findings indicate that the effectiveness of the TMD is less than or equal to the TLD at lower excitation amplitudes and exceeds the TLD at higher excitation amplitudes.

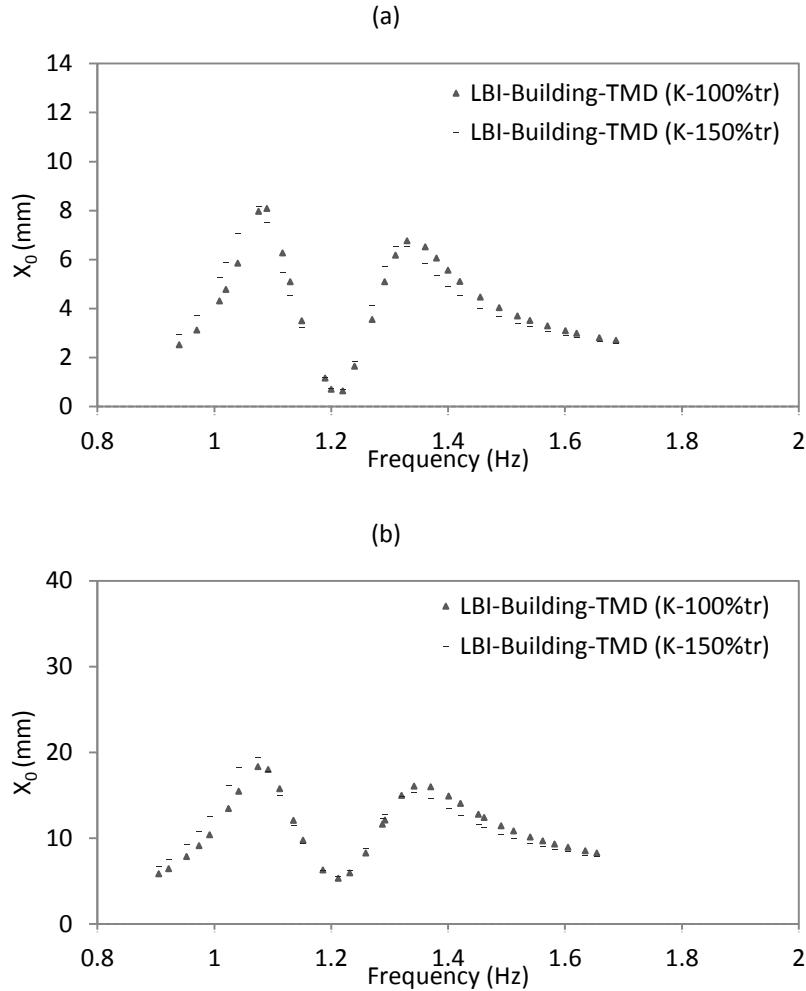


Figure 4-16 LBI-building-TMD isolator displacement at (a) 1.3 mm and (b) 3.8 mm excitation amplitude

4.11 Summary

A numerical model of a BI-structure-DVA system for time history analysis under harmonic base excitation was presented and discussed in this chapter. Details of the SU-FREI were presented, including the hysteresis loops obtained from lateral cyclic tests conducted in a previous research study. Two models, the Bouc-Wen model and the Backbone Curve model were used to model the hysteretic behaviour of SU-FREI. The parameters of the Bouc-Wen model were determined by conducting a least squares fit to the hysteresis loops. As both models were able to simulate the

experimental force-displacement loops with reasonable accuracy, the Backbone Curve model, which has previously been used to model SU-FREI, was selected. This model allowed the amplitude dependent stiffness and damping BC model properties to be interpolated between two bracketing amplitudes at the end of each isolator response cycle. The TLD was modelled using a modal expansion method, which considers the first three sloshing modes, allowing the nonlinear response of the fluid to be simulated.

The BI-structure-DVA model was evaluated by comparing model results with shake table test results presented in Chapter 3. Reasonable agreement was found between the predicted and measured isolator displacement response under harmonic excitation. The BI-structure-DVA was subsequently used to carry out a preliminary study on combined linear and nonlinear base isolation and dynamic vibration absorber systems. In addition to the BI-building-TLD system, which was used to evaluate the model a BI-building-TMD System, LBI-building-TLD and a LBI-building-TMD were analyzed.

It was found that for LBI systems a TMD led to lower isolator displacements and for a BI system a TLD led to lower isolator displacement at higher excitation amplitudes. At lower excitation amplitudes, it was found that the isolator displacement of a LI-building-TLD was lower than that of a LI-building-TMD. Finally, at the lowest excitation amplitude the TLD and TMD had a similar effect on a BI- building. As this study was limited in scope, no general conclusions about the performance of these various systems under harmonic base excitation could be drawn from these findings.

Chapter 5 **BI-Structure-TLD under Earthquake Excitation**

5.1 Introduction

This chapter investigates the response of BI-structure-DVA systems under earthquake excitation using the base isolation-structure-DVA model that was introduced and evaluated in Chapter 4 using harmonic excitation. For the case of harmonic excitation, the amplitude dependent properties of the isolators were updated based on the isolator response amplitude, X_0 , of the previous response cycle. For harmonic loading the amplitudes of successive cycles are the same under a steady state response condition, however, for the case of earthquake excitation, the peak amplitude at a particular cycle can be considerably different than the peak amplitude of the previous cycle. As a result, different approaches to update the isolator amplitude dependent properties in the base isolation module for the case of earthquake excitation were investigated. Three different updating methods were evaluated by comparing BI-building-TLD predicted results with shake table test results. The method deemed most suitable was then selected and used in the analyses conducted in the remainder of this chapter.

The response of the BI-building-TLD system is then investigated using 8 different earthquake ground motion records. The ground motion records selected have peak ground acceleration (PGA) values ranging from 0.21 g to 0.97 g. Each record was scaled to four different PGA levels (0.1 g, 0.2 g, 0.4 g and 0.6 g) and a total of 32 time history analyses of the BI-building, both with and

without a TLD, were carried out. The displacement of the isolator (and base isolation system), X_0 and the roof acceleration of the structure, \ddot{X}_2 are the primary response parameters reported in this study. A linear base isolation system, introduced in Chapter 4, is also investigated and its response is compared to that of the BI-building-TLD.

5.2 Evaluation of BI-Structure-TLD Model for Earthquake Excitation

The equation of motion for the base isolation system, originally introduced in Chapter 4, is expressed as

$$M_0\ddot{X}_0 + F_0(\dot{X}, X) = F_1 \tag{5-1}$$

where, M_0 is the mass of the isolation system, \ddot{X}_0 is the relative acceleration of the isolation system, F_1 is the applied excitation and $F_0(\dot{X}, X)$ is a function of the damping and stiffness properties of the isolators. The BI-structure-DVA model, introduced in Chapter 4, utilizes the Backbone Curve model (BCM) to simulate the behaviour of a SU-FREI isolator. The model updates the BCM stiffness coefficients and damping ratio, which are used to determine $F_0(\dot{X}, X)$ in Equation 5-1. For harmonic excitation, the BCM stiffness coefficients and damping ratio that are used to calculate the response of the isolation system are updated after the completion of each isolator response cycle, these updated values are then used in the calculation of the following response cycle. This approach yields a reasonable estimate of SU-FREI behaviour under harmonic excitation. However, for the case of earthquake excitation, changes in the displacement amplitude of the base isolation system can occur rapidly under this type of transient loading in comparison to harmonic loading. As a result, the peak amplitude of a particular cycle can be considerably different than the peak amplitude of the previous cycle. Therefore, using the BCM stiffness coefficients and damping ratio that are updated based on the response amplitude of the previous cycle may not be suitable.

In order to modify the base isolation module to obtain a more accurate estimate of the response of a BI-structure-TLD system under earthquake excitation, three different methods are investigated for updating the BCM.

In the first method (Method 1), the BCM stiffness coefficients and damping ratio were updated based on the peak displacement amplitude, $X_{0\text{-peak}}$, of the isolator that occurred over the entire earthquake record. The following iterative procedure was applied. First, the stiffness coefficients and damping ratio of the isolator were assumed to have initial values corresponding to a lateral displacement of $X_0 = 75\% t_r$. Next, a nonlinear time history analysis was carried out using these stiffness coefficients and damping ratio and the value of $X_{0\text{-peak}}$ from the time history results determined. The BCM stiffness coefficients and damping ratio were then updated based on this new value of $X_{0\text{-peak}}$. This process was repeated until the peak displacement amplitude $X_{0\text{-peak}}$ from two successive analysis converged to within a predefined error value. This updating method has previously been used by Toopchi-Nezhad et al. [45] to model a structure isolated with SU-FREI bearings under earthquake loading.

The second method (Method 2) is the one that was employed for the case of harmonic excitation. The BCM stiffness coefficients and damping ratio were updated at the end of each response cycle based on the peak base displacement of that cycle, $X_{0\text{-cycle_peak}}$. These updated values were then used to calculate the response of the isolation system over the next cycle. For the case of harmonic excitation this method was found to be more efficient and converged to the same solution as Method 1 more rapidly.

The third method (Method 3) also employs an iterative technique. For every isolator response cycle the initial conditions for the BI-structure-TLD system were stored, the response of the system was then calculated using the stiffness coefficients and damping ratio from the previous cycle and the $X_{0\text{-cycle_peak}}$ value determined for this current response cycle. The stiffness coefficients and damping ratio were then updated and the response of the isolation system recalculated using the initial conditions for the current response cycle. The stiffness coefficients and damping ratio were updated in an iterative manner until the $X_{0\text{-cycle_peak}}$ converged to within a predefined error value. This process was repeated for all cycles of response over the entire time history.

Each of these three methods was used to calculate the response of the BI-building-TLD subjected to the El Centro earthquake ground motion record that was used in the shake table study at PGA levels of 0.1 g, 0.2 g and 0.3 g, which match those used in the experimental shake table study. The results were then compared with the results from the shake table tests in order to evaluate the different updating methods.

Table 5-1 shows the relative difference in peak isolator displacement and peak roof acceleration between the calculated values using the three updating methods and the experimental values recorded from the shake table study. For the highest PGA (0.3 g), the peak isolator displacement values calculated using Method 2, which was for harmonic excitation, are up to 102% higher than the experimental results. For the BI-building-TLD at this PGA level Method 1 overestimates peak response by approximately 132%. These differences in the measured and predicted displacement response values indicate that these two methods are not as accurate at this higher PGA level. For the 0.3 g PGA level Model 3 also overestimates the peak displacement response by 40% for BI-structure and 64% for BI-building-TLD and underestimates the peak acceleration response by approximately 17% for both systems.

Table 5-1 Relative percentage difference between predicted and measured BI-building-TLD peak isolator displacement and roof acceleration values

	PGA Level (g)	0.1		0.2		0.3		
		DVA	No TLD	TLD	No TLD	TLD	No TLD	TLD
Peak Base Isolation Displacement (X_0)	Method 1		9.2	-1.9	38.4	37.4	45.8	132.2
	Method 2		32.7	24.4	22.0	29.7	102.8	60.2
	Method 3		6.8	8.4	35.0	25.7	40.5	64.8
Peak Roof Acceleration (\ddot{X}_2)	Method 1		-25.0	-30.3	-17.4	-21.3	-16.6	61.0
	Method 2		3.7	4.0	22.4	7.7	69.8	101.4
	Method 3		-24.5	-16.7	-19.2	-22.4	-16.5	-16.8

For the lowest PGA value (0.1 g), Method 1 and Method 3 are found to provide similar results. At this PGA level Method 2 is found to better predict the roof acceleration response in comparison to Method 1 and Method 3, however, Method 1 and Method 3 are found to better predict the peak isolator displacement.

It can be seen that all three methods overestimate the peak isolator displacement amplitude for all three PGA levels considered. Method 1 provides better estimates of X_0 at the lower PGA values than at the higher PGA value. As already indicated, the discrepancy between the predicted peak isolator displacement using Method 2 and the experimental value is quite significant at the highest PGA value.

Based on the results presented in Table 5-1 Method 3 was considered to provide the best overall estimate of the response and was found to have the lowest average relative difference for both the BI-building and the BI-building-TLD system. As a result, Method 3 was chosen to analyze the BI-building-TLD system subjected to earthquake excitation in this chapter.

Response histories of the BI-building-TLD system generated using Method 3 for the El Centro earthquake excitation at $\text{PGA} = 0.1 \text{ g}$ are shown Figure 5-1 along with the corresponding shake table test results. At this PGA level good agreement between the model and experimental normalized isolator displacement (X_0/t_r) and roof acceleration response histories is found. However, it can be seen that there is greater discrepancy between the model and experimental normalized wave height response (η/h) time histories.

Model and experimental response histories of the BI-building for the El Centro earthquake excitation at $\text{PGA} = 0.1 \text{ g}$ are shown in Figure 5-2. Similar to the BI-building-TLD findings, good agreement is found between the model and experimental normalized isolator displacement (X_0/t_r) and roof acceleration response histories.

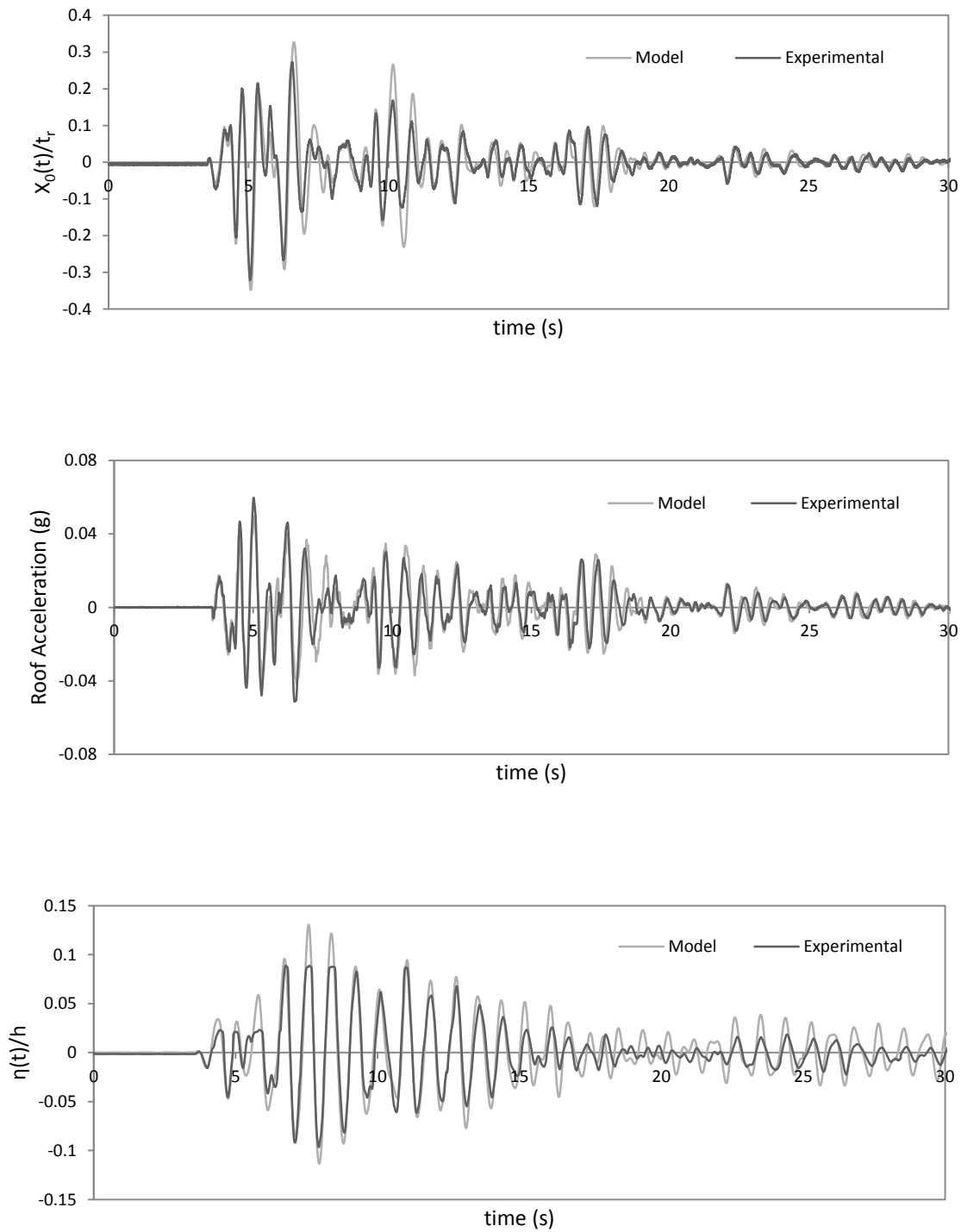


Figure 5-1 Normalized Isolation displacement, roof acceleration and normalized wave height time histories, BI-structure-TLD model compared to shake table test results, El Centro earthquake, PGA = 0.1 g

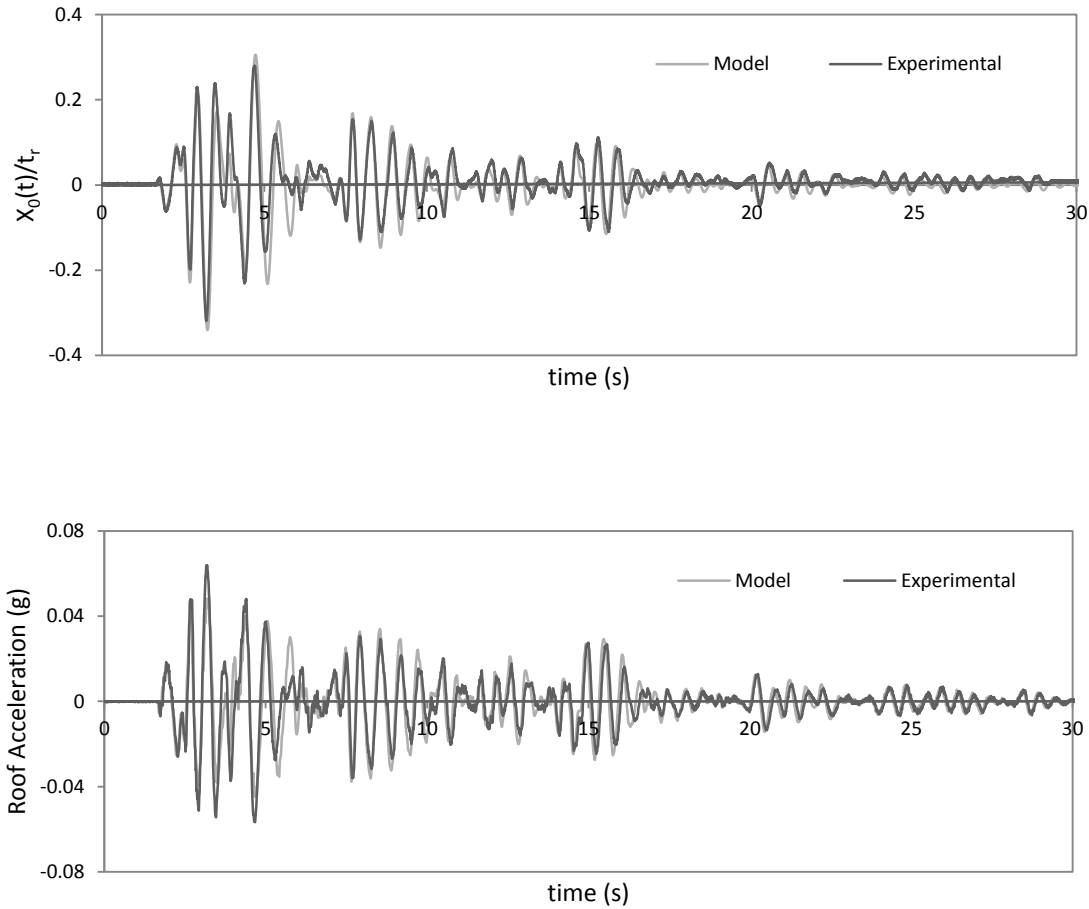


Figure 5-2 Normalized Isolation displacement, roof acceleration and normalized wave height time histories, BI-structure model compared to shake table test results, El Centro earthquake, PGA = 0.1 g

5.3 Nonlinear Base Isolation-Structure-TLD Subjected to Earthquake Excitation

A total of eight earthquake ground motion records with different magnitude, energy content, soil class and epicentral distances were used to conduct a preliminary study on the seismic response behaviour of the BI-building-TLD. The earthquakes and their properties are given in Table 5-2.

Table 5-2 Ground motion records

Earthquake/ Year	Station/Component	Epicentral Distance (km)	Station site Class	Magnitude (Richter)	PGA (g)
El Centro/1940	117 USGS/ S00E	8	Stiff Soil (D)	6.9	0.35
San Fernando, 1971	CDMG 24303, LA/ PEL090	39.49	Stiff Soil (D)	6.61	0.21
Friuli, Italy/ 1976	8012 Tolmezzo/ TMZ000	20.23	Rock (B)	6.5	0.35
Loma Prieta, 1989	CDMG 47379, Gilroy Array/ G01090	28.64	Hard Rock (A)	6.93	0.47
Manjil, Iran/ 1990	BHRC, Abbar/ L	40.43	Stiff Soil (D)	7.37	0.52
Northridge, 1994	CDMG 24538, Santa Monica/ STM090	22.45	Stiff Soil (D)	6.69	0.88
Kobe, Japan/ 1995	CUE, Nishi-Akashi/ NIS000	8.7	Rock (B)	6.9	0.51
Duzce, Turkey/ 1999	Lamont 375/ E	24.05	Rock (B)	7.14	0.97

*The abbreviations ELC, SFN, FRL, LPT, MNJ, NTR, KOB and DZC will be used for El Centro, San Fernando, Friuli, Loma Prieta, Manjil, Northridge, Kobe and Duzce earthquakes

The ground motion records of the original earthquakes were compressed in time by a factor of 2 to satisfy the dynamic similitude requirements. The acceleration response spectra for these eight earthquakes are shown in Figure 5-3 and Figure 5-4. In addition, the periods corresponding to the fixed based building (0.106 s) and period range corresponding to the BI-building at different displacement amplitudes (0.65 s to 1.0 s) are also indicated with a dashed line and a hatched area, respectively. Some of the earthquakes, including Manjil, Northridge, El Centro and San Fernando have a significant portion of the energy content concentrated in the low period range. In particular, for Manjil and Northridge, the bulk of the energy is concentrated near the period of the fixed based building. The introduction of a base isolation system to the building, resulting in a shift in the natural period of the system, is expected to substantially reduce the seismic demand on the building. However, for other earthquakes such as Kobe, Duzce, Friuli and Loma Prieta the energy is spread over a larger range of periods. For these earthquakes the introduction of a base isolation system may not lead to the same level of reduction in seismic demand on the building. It should be noted that the focus of this study is on the effect of adding a TLD to a base isolated building. As such, comparing the response results with a fixed base building is not considered in this study.

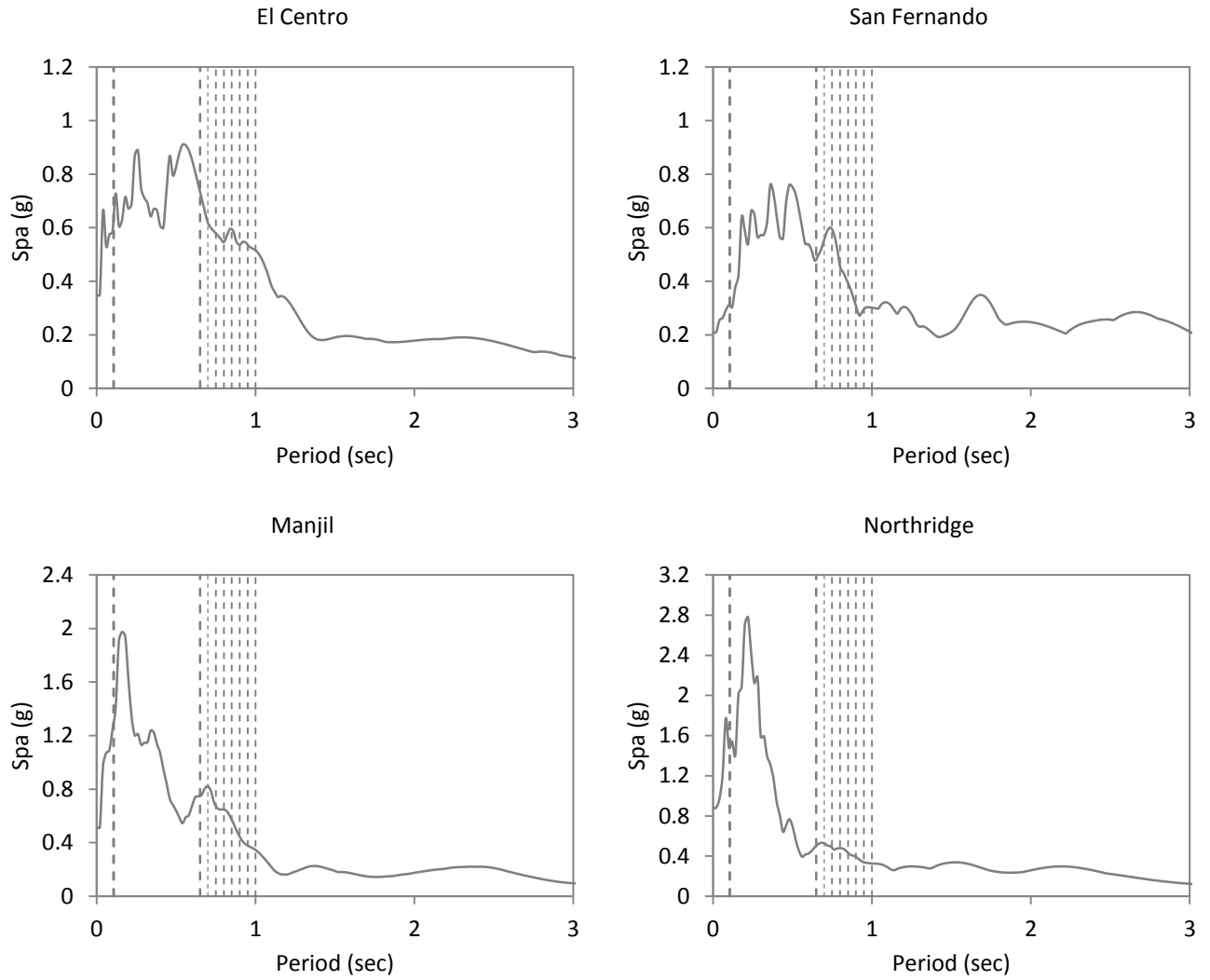


Figure 5-3 Pseudo acceleration response spectra of earthquakes

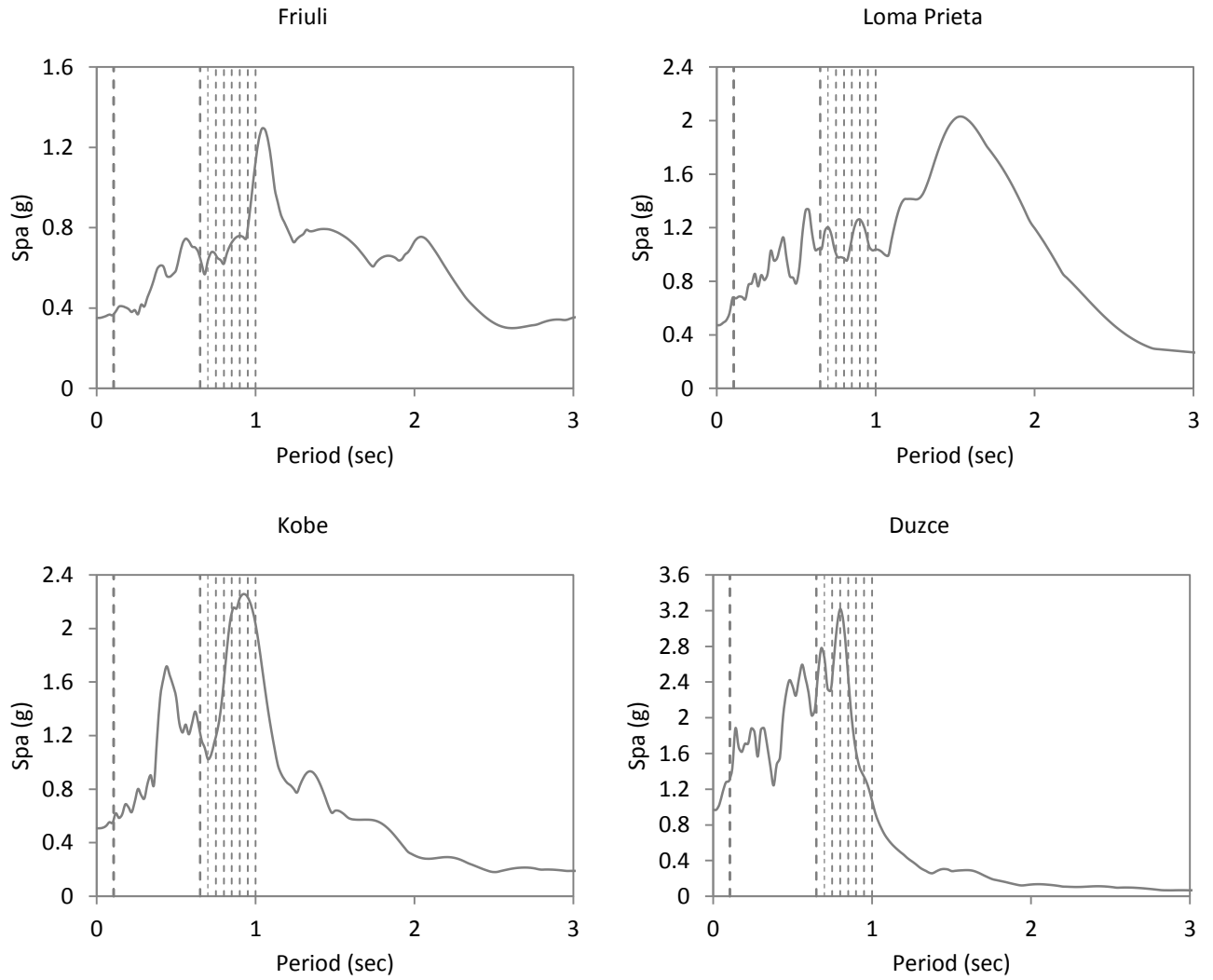


Figure 5-4 Pseudo acceleration response spectra of earthquakes

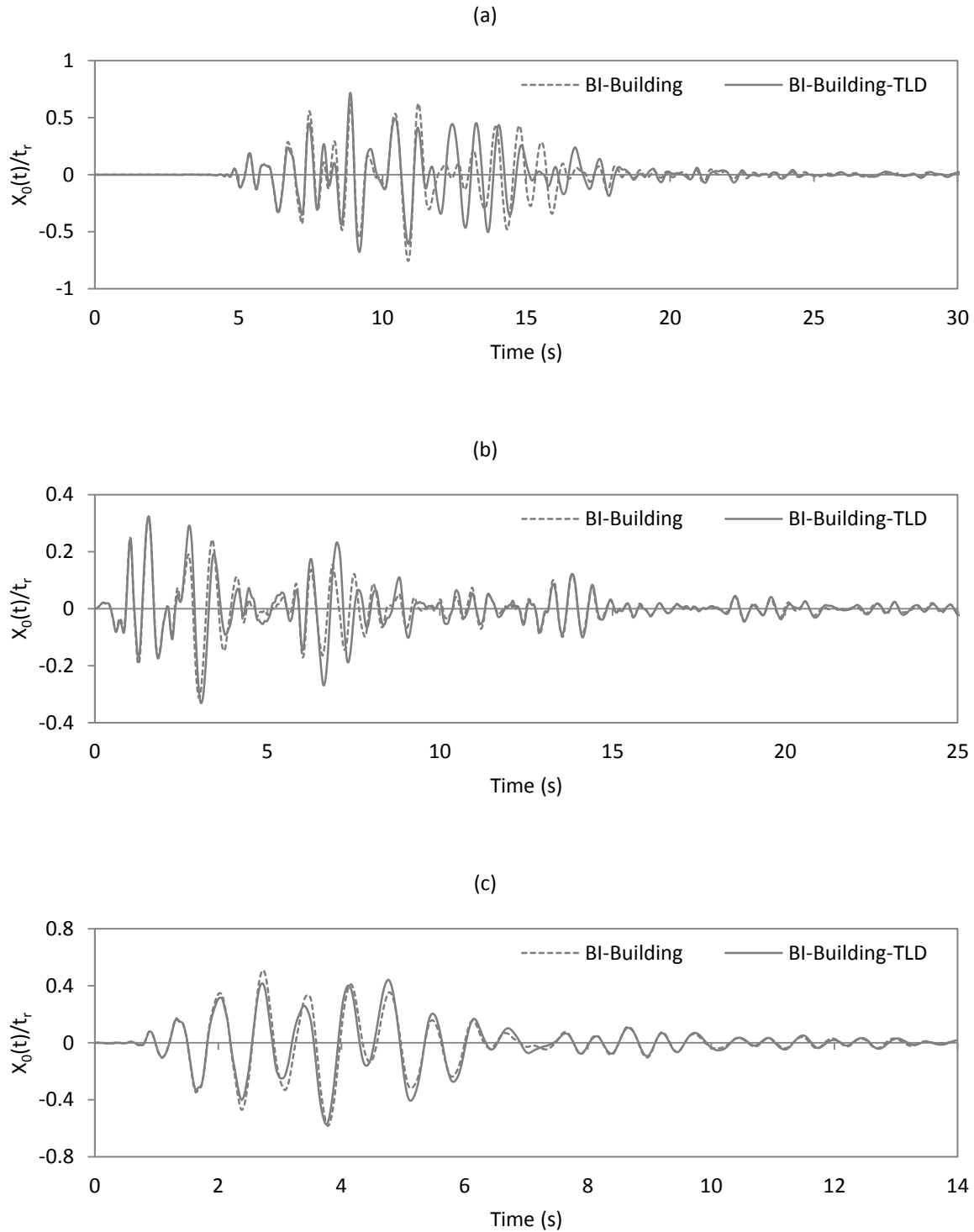


Figure 5-5 Response history of isolation displacement for (a) Kobe (b) El Centro and (c) San Fernando at PGA = 0.1 g

For each earthquake the response of both the nonlinear BI-building and nonlinear BI-building-TLD were calculated for PGA of 0.1 g, 0.2 g, 0.3 g and 0.6 g. Figure 5-5 shows sample response histories of the normalized isolator displacement for the Kobe, El Centro and San Fernando at a PGA of 0.1 g for both the BI-building and BI-building-TLD. It can be seen in Figure 5-5 (a) that there is a reduction in peak isolator displacement of approximately 5% for the Kobe earthquake. The effect of the TLD on peak isolator displacement is less for the San Fernando earthquake, with a reduction of only 2%. Finally, for the El Centro earthquake, the TLD is found to have a negative impact on peak isolator displacement, resulting in an increase of approximately 2%.

Figure 5-6 shows the normalized free surface response of the TLD for Kobe, El Centro and San Fernando at a PGA of 0.1 g for the BI-building-TLD system. It can be observed that for all three earthquakes the fluid is responding under the earthquake induced motion of the BI-building, however, the impact of the resulting fluid inertia forces on the peak response of the isolation system is quite different for these three earthquakes.

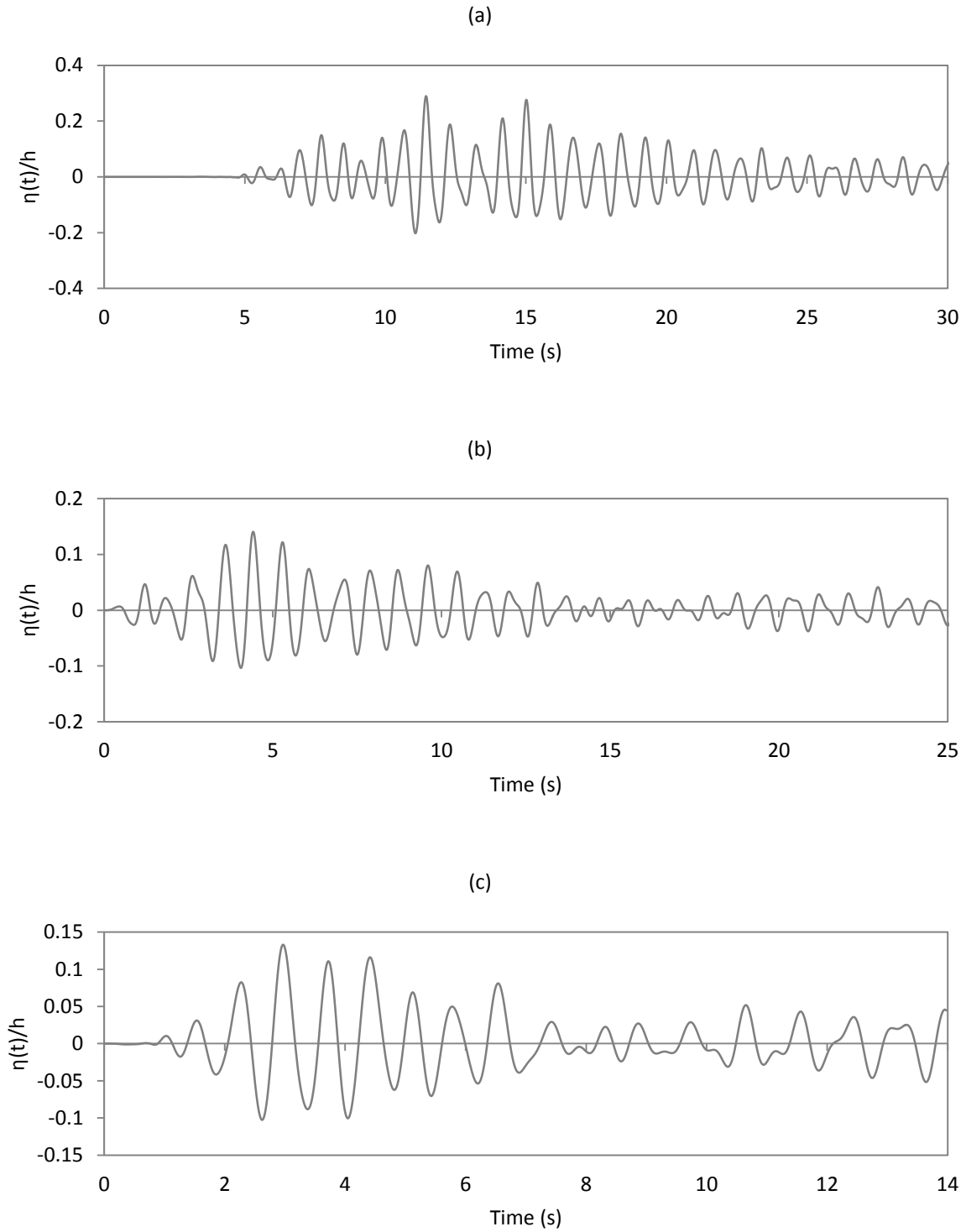


Figure 5-6 Response history of TLD wave height for (a) Kobe earthquake (b) El Centro earthquake and (c) San Fernando earthquake at PGA = 0.1 g

Reductions in peak isolator displacement and peak roof acceleration are shown in Table 5-3 and Table 5-4, respectively. A positive value indicates that the addition of a TLD has led to a reduction in the peak response value while a negative value indicates that the addition of the TLD has resulted in an increase in the peak response value.

Table 5-3 Reduction in peak isolator displacement for nonlinear BI-building with the addition of a TLD

(%)								
PGA	ELC	SFN	FRL	LPT	MNJ	NTR	KOB	DZC
0.1	-2	2	1	0	8	-6	5	7
0.2	3	-18	5	3	8	11	13	-4
0.4	-10	-10	7	6	-5	10	18	-4
0.6	3	-2	9	8	-1	4	-69	7

Table 5-4 Reduction in peak roof acceleration for nonlinear BI-building with the addition of a TLD

(%)								
PGA	ELC	SFN	FRL	LPT	MNJ	NTR	KOB	DZC
0.1	0	-3	11	3	6	4	-3	7
0.2	4	-15	9	11	3	8	5	16
0.4	-46	-44	11	6	4	11	11	-3
0.6	25	-7	6	9	-11	21	-215	4

Results presented in the above tables indicate that the effectiveness of a TLD in reducing the response of the BI-building under seismic excitation is highly dependent on the ground motion record. For example, at a PGA of 0.4 g the TLD has reduced the peak isolator displacement by 18% and the acceleration by 11% for the Kobe earthquake. However, at the same PGA level, the TLD has led to an increase in peak isolator displacement for the El Centro earthquake by 10% and peak roof acceleration by 46%. The PGA value also influences the effectiveness of the TLD. For example, for Kobe the addition of a TLD led to a 17% reduction in the peak isolator displacement at 0.4 g PGA; however an increase in the peak isolator displacement of 69% was found at 0.6 g PGA. From the results in Table 5-4 it can be seen that the influence of PGA level had an even greater impact on the peak roof acceleration, particularly for Kobe earthquake, where the TLD reduced the peak roof acceleration by 11% at 0.4 g PGA but resulted in an increase of 215% at 0.6 g PGA.

The addition of a TLD was found to consistently decrease both the peak isolator displacement and peak roof acceleration responses for the Loma Prieta and Friuli earthquakes at all PGA levels. The addition of the TLD was also found to consistently increase the peak roof acceleration response for the San Fernando earthquake. It can be seen that the effect of a TLD on the response of a BI-structure is highly dependent on the earthquake and the PGA level and as such no general conclusions on the effectiveness of a TLD can be derived from these results.

5.4 Linear Base Isolation-Structure-TLD Subjected to Earthquake Excitation

This section reports on the response of a linear (L)BI-building-TLD system subjected to the 8 earthquake ground motions listed in Table 5-2 at two PGA levels (0.1 g PGA and 0.2 g PGA). The linear BI-building-TLD system investigated in Chapter 4, having a constant stiffness value equal to the linear stiffness coefficient of the 150% t_r BC model curve and a constant effective damping ratio of 8.9%, was selected for this study. The response of this system is compared to the BI-building-TLD.

The ratio of LBI-building-TLD peak isolator displacements and peak roof accelerations to BI-building-TLD peak isolator displacements and peak roof accelerations for each of the 8 different earthquake records are reported in Table 5-5 and Table 5-6, respectively. From Table 5-5 it is found that peak isolator displacements are larger for the LBI-building for the El Centro, Loma Prieta, Manjil, Northridge, Kobe and Duzce earthquakes and lower for the San Fernando and Friuli earthquakes, at both PGA levels. When the TLD was added to the LBI-building, the peak isolator displacement ratio values were found to consistently decrease for 0.1g PGA. An increase in the PGA level had a significant effect on the peak isolator displacement ratio value for the Manjil, Northridge, Kobe and Duzce earthquakes. The peak isolator displacement ratio was found to decrease for the Manjil and Northridge earthquakes and increase significantly for the Kobe and Duzce earthquakes. Sample response histories of normalized isolator displacement for Kobe, El Centro and San Fernando are shown in Figure 5-7 and the corresponding normalized TLD free surface response motion in Figure 5-8.

It can be observed from Table 5-6 that the peak roof accelerations are lower for the LBI-building, both with and without a TLD, for both the Friuli and Loma Prieta earthquakes at both PGA levels. On average, the peak roof acceleration is lower for the LBI-building at 0.1 g PGA and higher at 0.2 g PGA. Finally, although both the isolator displacement and peak acceleration ratio values were found to be lower for the San Fernando and Friuli earthquakes a different trend was found for the Loma Prieta and Manjil earthquakes where the LBI-building, both with and without a TLD, resulted in higher peak isolator displacement but lower peak roof acceleration ratio values.

Table 5-5 Ratio of LBI-building-TLD peak isolator displacement to BI-building-TLD peak isolator displacement

PGA	Earthquake	ELC	SFN	FRL	LPT	MNJ	NTR	KOB	DZC
0.1 g	No TLD	1.3	0.82	0.88	1.2	1.5	2.3	1.1	1.1
	TLD	1.2	0.86	0.86	1.2	1.8	2.0	0.99	0.89
0.2 g	No TLD	1.1	0.97	0.92	1.0	1.1	1.4	4.3	5.9
	TLD	1.1	0.85	0.92	1.0	1.3	1.5	4.2	4.3

Table 5-6 Ratio of linear BI-building-TLD peak roof acceleration to SU-FREI BI-building-TLD peak roof acceleration

PGA	Earthquake	ELC	SFN	FRL	LPT	MNJ	NTR	KOB	DZC
0.1 g	No TLD	0.98	0.79	0.67	0.93	0.84	1.0	1.3	0.66
	TLD	0.90	0.82	0.70	0.88	0.97	0.96	0.96	0.55
0.2 g	No TLD	1.2	1.2	0.87	0.98	0.94	1.2	3.7	1.6
	TLD	1.1	1.1	0.88	0.96	1.0	1.2	3.0	1.5

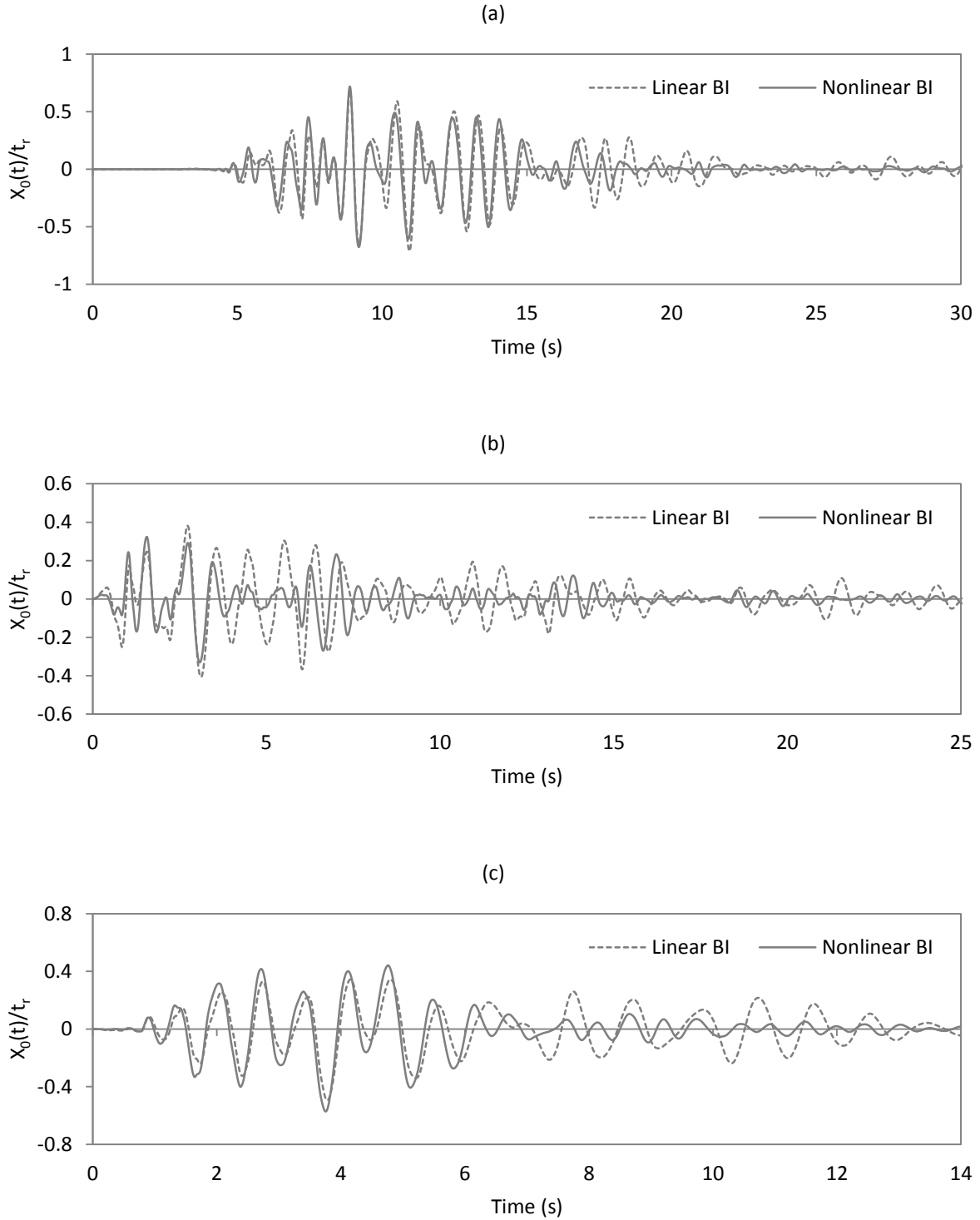


Figure 5-7 Response history of isolation displacement for linear base isolation system for (a) Kobe earthquake (b) El Centro earthquake and (c) San Fernando earthquake at PGA = 0.1 g

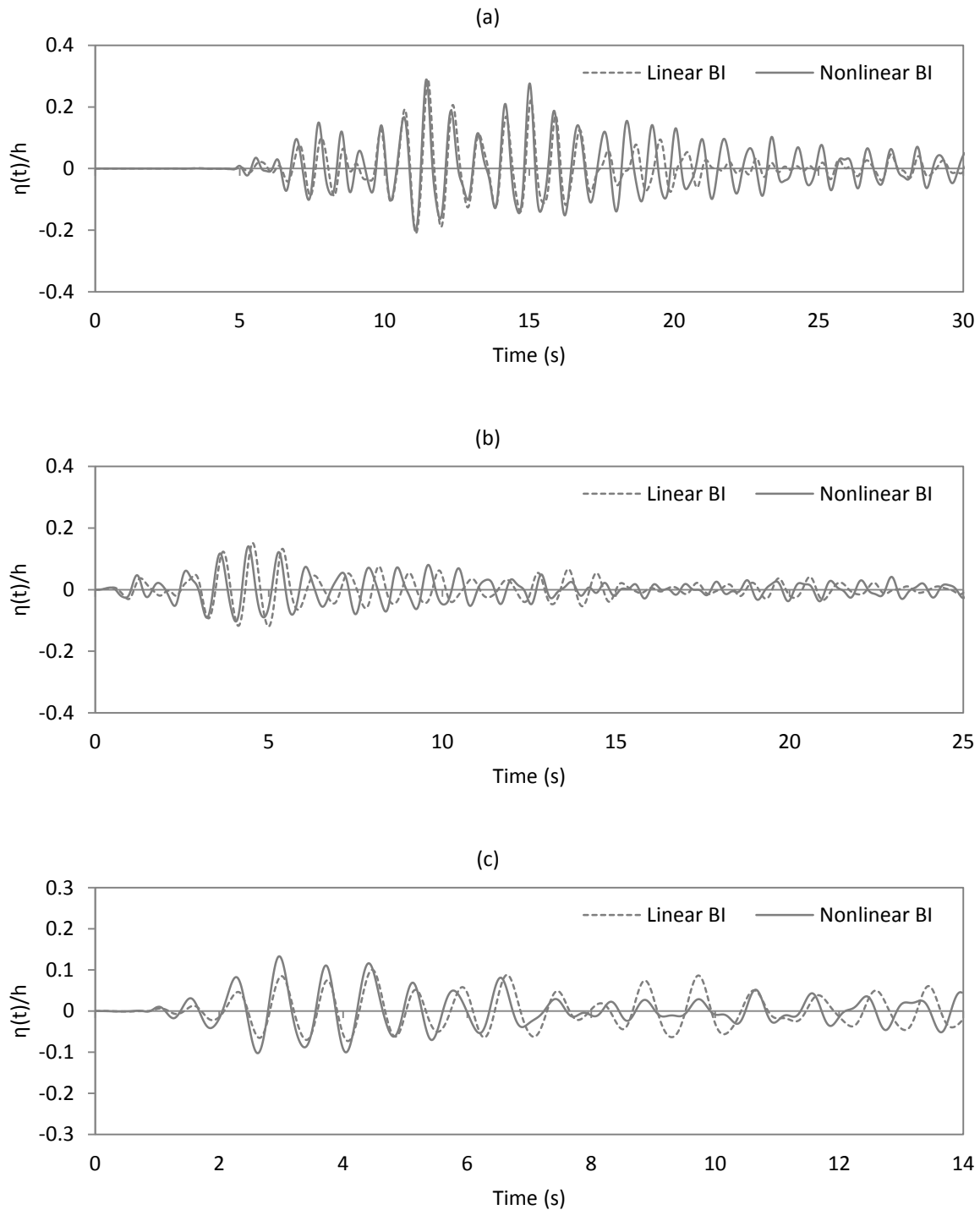


Figure 5-8 Response history of wave height for linear base isolation for (a) Kobe earthquake (b) El Centro earthquake and (c) San Fernando earthquake at PGA = 0.1 g

The change in peak isolator displacement and roof acceleration values with the addition of the TLD is shown in Tables 5-7 and Table 5-8, respectively, in terms of percent decrease in the peak response values. It should be noted that a negative value indicates an increase in response.

Table 5-7 Percent decrease in peak isolator displacement response for LBI-building with addition of TLD

PGA	Earthquake	ELC	SFN	FRL	LPT	MNJ	NTR	KOB	DZC
0.1 g	LBI-building	5	-3	4	5	-8	7	17	25
	BI-building	-2	2	1	0	8	-6	5	7
0.2 g	LBI-building	4	-3	5	5	-7	7	15	24
	BI-building	3	-18	5	3	8	11	13	-4

Table 5-8 Percent decrease in peak roof acceleration response for linear LBI-building with addition of TLD

PGA	Earthquake	ELC	SFN	FRL	LPT	MNJ	NTR	KOB	DZC
0.1 g	LBI-building	10	-8	8	12	-6	10	22	24
	BI-building	0	-3	11	3	6	4	-3	7
0.2 g	LBI-building	10	-6	8	12	-6	10	23	24
	BI-building	4	-15	9	11	3	8	5	16

* a negative value shows increase in response after turning TLD on

It is evident from the results presented in Table 5-7 and 5-8 that the addition of the TLD does not always lead to a reduction in peak isolator displacement or peak roof acceleration. In fact, for the San Fernando earthquake the addition of a TLD resulted in larger peak roof accelerations for both isolation systems and both PGA levels. For most of the earthquake ground motions considered in this study the TLD was found to be more effective in reducing peak isolator displacements and roof accelerations when combined with the LBI-building. For both the LBI-building and the BI-building the TLD was found to be more effective at the lower PGA level.

5.5 Summary

The response of both BI-structure and BI-structure-TLD under earthquake loading was investigated in this chapter. As the isolator module of the BI-structure-TLD numerical model was originally developed for harmonic base excitation different methods to update the stiffness coefficients and damping ratio of the BC model were investigated. Three different methods to update the Backbone Curve model stiffness coefficient values were investigated and evaluated

using results from the experimental test program presented in Chapter 3. An iterative method, which converges to a unique set of stiffness coefficients and damping ratio, was subsequently selected.

The updated BI-Structure-TLD model was used to study the response of the BI-building and BI-building-TLD from Chapter 3 under eight different earthquake ground motion records and at four different PGA levels. Unlike the case of harmonic excitation, the effectiveness was dependent not only on the level of excitation but also on the earthquake ground motion record. The addition of the TLD was found to reduce both the peak isolator displacement and peak roof acceleration values for the Friuli and Loma Prieta earthquakes and increase the peak roof acceleration for the San Fernando earthquake. For all other ground motion records the addition of the TLD led to a combination of increased and decreased peak response values, which depended on the earthquake and the PGA level.

The response of a linear base isolated building (LBI-building), both with and without a TLD, was also investigated and compared to the response of the BI-building. The properties of the linear isolation system were chosen to match that of the linear isolation system investigated under harmonic excitation. The response of the LBI-building, both with and without a TLD, was investigated at two different PGA levels for each of the eight earthquake ground motion records. Results showed for the systems and earthquake ground motions considered in this study the TLD was more effective for the LBI-building. Overall, the effect of the TLD on the response of the base isolated buildings was found to be highly dependent on the earthquake ground motion record and PGA level and, as such, no general conclusions on the overall effectiveness of BI-structure-DVA systems could be drawn from the results presented in this chapter.

Chapter 6 Summary and Recommendations

6.1 Overview of the Research

A significant amount of research effort has focused on increasing the seismic performance of structures using innovative earthquake resistant systems. The majority of these systems can be divided into two main categories, supplemental damping devices that dissipate seismic energy, and base isolation systems. Base isolation decouples the structure from the ground motion by introducing a flexible layer between the structure and the foundation. The introduction of this flexible layer increases the period of the structure beyond the critical period range of earthquake ground motions expected in the region the structure is located. Due to their high flexibility the isolators experience large lateral deformations when a base isolated structure is subjected to base excitation, such as earthquake, as the majority of lateral deformation occurs in the isolation layer rather than the superstructure. Dynamic Vibration Absorbers (DVA), including Tuned Mass Dampers (TMD) and Tuned Liquid Dampers (TLD) have been used to reduce excessive wind-induced resonant vibration motions in flexible structures. However, only a limited number of studies have focused on utilizing DVA in base isolated structures to reduce resonant motions under seismic excitation.

The objective of this research was to investigate, both experimentally and numerically, passive structural control base isolation (BI) systems subjected to base excitation. The response of a base

isolated building equipped with TLD (BI-building-TLD) subjected to both harmonic and seismic base excitation was experimentally investigated through shake table testing (Chapter 3). An existing numerical model of a BI-building-TLD was modified and evaluated for harmonic base excitation and earthquake excitation. This modified model was used to investigate the response behaviour of linear and nonlinear DVA in combination with linear and nonlinear base isolators under harmonic (Chapter 4) and earthquake (Chapter 5) base excitation.

6.2 Shake Table Tests

A series of shake table tests of a $\frac{1}{4}$ scaled model base isolated building, without (BI-building) and with (BI-building-TLD) tuned liquid dampers (TLD) were conducted. The isolation system comprised of four unbonded fiber reinforced elastomeric isolators (SU-FREI), which were placed underneath the columns of the building. Each of the three identical TLD, mounted on the roof of the building, contained a single damping screen with solidity of 40% installed in the mid-length of each tank in order to provide sufficient damping. Two different types of base excitation, harmonic excitation and earthquake ground motion were employed in the shake table test program.

The BI-building and BI-building-TLD were tested under three amplitudes of harmonic excitation. For the earthquake ground motion tests both the BI-building and BI-building-TLD were subjected to the El Centro earthquake ground motion at peak ground accelerations of 0.1g, 0.2g and 0.3g. To determine the effect of a TLD on a BI-building under harmonic and earthquake ground motion loading all tests were first conducted with the TLD tanks empty, the tanks were then filled to a predetermined water depth level and the BI-building-TLD was retested.

Shake table test results showed that the addition of the TLD to the BI-building led to a reduction in both the peak isolator displacement and roof acceleration response values under harmonic excitation. The percent decrease in isolator displacement increased from 9% at 1.3 mm excitation amplitude (the lowest excitation amplitude) to 25% at 3.8 mm excitation amplitude (the highest excitation amplitude). These findings indicate that for this BI-building-TLD the TLD becomes better tuned to the base isolated building and thus more efficient in reducing peak responses as the excitation amplitude increased.

The effect of the TLD on both peak isolator displacement and roof acceleration was found to be significantly less when the BI-building-TLD was tested under earthquake excitation. The TLD was found to have no effect on the peak isolator displacement and peak roof acceleration response at 0.1 g PGA. At 0.3 g the addition of the TLD led to a decrease in the peak isolator displacement of 2.7% and the peak roof acceleration by 7.7%.

The results of the study showed that the effectiveness of the TLD on the BI-building considered in this study was significantly more effective in reducing the peak isolator displacement and roof acceleration under harmonic excitation. However, no general conclusions on TLD effectiveness for harmonic excitation or earthquake excitation can be drawn from this experimental study as it was limited to only a single BI-building-TLD configuration.

6.3 Numerical Base Isolation-Structure-Dynamic Vibration Absorber Model

An existing BI-structure-DVA numerical model was modified and used to conduct time history analyses of the BI-building-TLD system tested under harmonic excitation. In order to simulate the force-displacement behaviour of SU-FREI isolators two isolator numerical models, a Bouc-Wen model and a Backbone Curve model, were investigated. The numerical model of the BI-building-TLD system was then evaluated through the comparison of the predicted response with measured results from shake table tests. The evaluated BI-building-DVA model was subsequently used to investigate different combinations of linear and nonlinear base isolation systems with linear and nonlinear dynamic vibration absorbers (DVA) systems under harmonic base excitation.

To model the BI-building-TLD subjected earthquake excitation, different approaches were investigated to update the SU-FREI amplitude dependent properties under this transient type of loading. Three different methods were evaluated using shake table test results and the most suitable model was then utilized to investigate the response of a BI-building-TLD system under different earthquake ground motions. The model was also used to carry out a preliminary study on combined linear and nonlinear base isolation and dynamic vibration absorber systems.

6.3.1 Base Isolation-Building-DVA Subjected to Harmonic Excitation

The response of a building employing different combinations of linear and nonlinear isolators and linear and nonlinear dynamic vibration absorber systems were investigated under harmonic base excitation. It was found that for linear base isolated systems a TMD leads to lower isolator displacements and for a nonlinear isolation system a TLD leads to lower isolator displacements at higher excitation amplitudes. At lower excitation amplitudes, it was found that the isolator displacement of a linear isolated building was lower when equipped with the TLD compared to the TMD. Also, at the lowest excitation amplitude the TLD and TMD had a similar effect on a nonlinear base isolated building. Although findings from this study provided insight into the response of these different systems no general conclusions on their performance under harmonic excitation could be drawn due to the limited number of systems investigated.

6.3.2 Base Isolation-Building-DVA Subjected to Earthquake Excitation

The response of a linear base isolated building, both with and without a TLD under earthquake excitation, was also investigated. The properties of the linear isolation system were chosen to match the linear system investigated under harmonic excitation. The response of the LBI-building, both with and without the TLD, was investigated at two different PGA levels for each of the eight earthquake ground motion records. Results showed for the systems and earthquake ground motions considered in this study the TLD was more effective for the LBI-building. Overall, the effect of the TLD on the response of base isolated buildings was found to be highly dependent on the earthquake ground motion record and PGA level and, as such, no general conclusions on the overall effectiveness of a TLD could be drawn from this study.

6.4 Recommendations for Future Studies

Based on the findings from this research study the following recommendations are suggested for future research work:

- Results from the BI-building-DVA model indicated a more pronounced change in the response amplitude of the BI-building near resonance than observed in the experimental tests. This jump phenomenon occurs due to the existence of more than single response for the nonlinear isolation system. The influence of initial conditions on the predicted response was investigated to a very limited extent. Further investigation into the response of nonlinear base isolated buildings under harmonic base excitation is recommended.
- The results of the shake table tests were used to evaluate the numerical model developed for BI-building-DVA systems under harmonic excitation. However, for earthquake excitation the results of the numerical study showed that the structural response is highly dependent on the earthquake ground motion and PGA level. Only one earthquake (El Centro) was employed in the experimental test program and the response of the BI-building-TLD subjected to the single earthquake ground motion was used to evaluate the BI-structure-DVA model for earthquake input excitation. Additional shake table tests using different input earthquake ground motions is recommended to permit the calibration and evaluation of both the existing numerical model and future numerical models.
- Although a Bouc-Wen model was calibrated and used to simulate the force-displacement behaviour of SU-FREI, it was not implemented into the BI-structure-DVA model using the iterative updating methods employed in this study. The development of a suitable interpolation technique to update the amplitude dependent properties of the Bouc-Wen model under any general type of loading is recommended. In addition, other hysteretic models should be investigated.

- A more comprehensive study of different isolation systems having different linear stiffness and damping properties is required. Furthermore, DVAs with different design parameters (i.e. tuning ratio, mass ratio and damping ratio), different depth to length ratios and different tuning strategies need to be investigated in order to further understand the behaviour of BI-structure-DVA systems.

References

- [1] A. Taylor and T. Igusa, “Primer on seismic isolation,” *ASCE publications*, 2004.
- [2] T. Taniguchi, A. Kiureghian and M. Melkumyanc, “Effect of tuned mass damper on displacement demand of base isolated structures,” *Engineering Structures*, vol. 30, 2008.
- [3] J. Love, M. Tait and H. Toopci-Nezhad, “A hybrid structural control system using a tuned liquid damper to reduce wind induced motion of a base isolated structure,” *Engineering Structures*, vol. 33, 2011.
- [4] T. Soong and G. Dargush, *Passive energy dissipation systems in structural engineering*, Chichester, UK.: Wiley, 1997.
- [5] Y. Ho, *Performance of dynamic vibration absorbers on buildings with coupled modes*, Canada: McMaster University, 2009.
- [6] A. Kareem, T. Kijewski and Y. Tamura, “Mitigation of motions of tall buildings with specific examples of recent applications,” *Wind and Structures, An International Journal*, vol. 2, no. 3, 1999.

- [7] A. Foster, Base isolation using stable unbonded fibre reinforced elastomeric isolators (SU-FREI), M.A.Sc Thesis McMaster University, December 2011.
- [8] M. de Raaf, Experimental study of unbonded fiber reinforced elastomeric bearings, Masters Thesis, McMaster University, 2009.
- [9] F. Naeim and J. M. Kelly, Design of seismic isolated structures: from theory to practice, New York: John Wiley & Sons Inc., 1999.
- [10] Vulcano and S. Alfonso, "Comparative study of the earthquake and wind dynamic responses of base-isolated buildings," *Journal of Wind Engineering and Industrial Aerodynamics*, Vols. 74-76.
- [11] B. Liang, X. Shishu and Jiaxian.T.S., "Wind effects on habitability of base-isolated buildings," *Journal of Wind Engineering and Industrial Aerodynamics*, vol. 90, 2002.
- [12] L. Tashkov, K. Manova and L. Krstevska, "Bulletin of earthquake engineering," vol. 7, 2009.
- [13] L. Li, "Base-isolation measure for aseismic buildings in China," in *Proceedings of 8th world conference on earthquake engineering*, San Francisco, USA, 1984.
- [14] L. Li, "Base isolation measure for aseismic building in China," in *Proc. 8 WCEE*, San Francisco, 1984.
- [15] M. Dolce, D. Cardone and G. Palermo, "Bulletin of Earthquake Engineering," vol. 5, 2007.
- [16] Y. Huang, J. Kong and X. Zhang, "Earthquake resistant engineering," vol. 3, 2000.
- [17] B. Myslimaj, M. Midorikawa, M. Liba and M. Ikenaga, "Seismic behaviour of a newly developed base isolation system for houses," *Journal of Asian Architecture and Building Engineering*, vol. 17, no. 24, 2002.

- [18] N. Mostaghel, "Resilient-friction base isolator," in *Report No. UTEC 84-097, The University of Utah*, 1984.
- [19] R. S. Datta and T. K. Jangid, "Seismic response of structure isolated by R-FBI system," *Indian Society of Earthquake Technology*, vol. 30, 1993.
- [20] B. Lin, I. Tajbakhsh, A. Papageorgiou and G. Ahmadi, "Performance of earthquake isolation systems," *ASCE Journal of Engineering Mechanics*, vol. 116, 1990.
- [21] N. Khodaverdian and M. Mostaghel, "Seismic response of structures supported on R-FBI system," *Earthquake Engineering and Structural Dynamics*, vol. 16, 1998.
- [22] Y. Ahmadi and G. Chen, "Stochastic earthquake response of secondary systems in base isolated structures," *Earthquake Engineering and Structural Dynamics*, vol. 21, 1992.
- [23] N. Khodaverdian and H. Mostaghel, "Dynamics of resilient-friction base isolator (R-FBI)," *Earthquake Engineering and Structural Dynamics*, vol. 15, 1987.
- [24] L. Su, G. Ahmadi and I. Tadjbakhsh, "A comparative study of base isolation systems," *ASCE Journal of Engineering Mechanics*, vol. 115.
- [25] F. Naiem and J. M. Kelly, "Stability of elastomeric seismic isolation bearings," *Journal of Structural Engineering*, Vols. 125 (9), 946-954, 1999.
- [26] Y. Zhang, Y. Wang and Y. Shi, "Parameters optimization of sliding base-isolation structure under the action of coupling earthquake," *Advanced Materials Research*, Vols. 243-249, 2011.
- [27] W. H. Robinson, "Lead-rubber hysteretic bearings suitable for protecting lead-rubber hysteretic bearings suitable for protecting," *Earthquake Engineering & Structural Dynamics*, vol. 10, no. 4, 1982.
- [28] J. M. Kelly, "Aseismic base isolation: review and bibliography," *Soil Dynamics and Earthquake Engineering*, vol. 5, 1986.

- [29] J. M. Kelly and S. B. Hodder, "Experimental study of lead and elastomeric dampers for base isolation systems in laminated neoprene bearings," *Bulletin of New Zealand National Society for Earthquake Engineering*, vol. 15, 1982.
- [30] I. Buckle, "New Zealand seismic base isolation concepts and their application to nuclear engineering," *Nuclear Engineering and Design*, vol. 84, 1985.
- [31] R. Skinner, J. Kelly and A. Heine, "Hysteretic dampers for earthquake-resistant structures," *Earthquake Engineering Structural Dynamics*, vol. 3, 1975.
- [32] W. Robinson and A. Tucker, "A lead-rubber shear damper," *Bulletin of New Zealand National Society of Earthquake Engineering*, vol. 10, 1977.
- [33] J. M. Kelly, "Analysis of fiber-reinforced elastomeric isolators," *Journal of Seismology and Earthquake Engineering*, Vols. 2 (1), 19-34, 1999.
- [34] A. Mordini and A. Strauss, "An innovative earthquake isolation system using fibre reinforced rubber bearings," *Engineering Structures*, Vols. 2739-2751, 2008.
- [35] M. Kelly and S. M. Takhirov, "Analytical and experimental study of fiber-reinforced elastomeric isolators," *University of California Berkely, PEER Report 201/11*, 2001.
- [36] B. Moon, G. Kang, B. Kang and J. M. Kelly, "Design and manufacturing of fiber reinforced elastomeric isolator for seismic isolation," *Journal of Material Processing Technology*, Vols. 130-131 , 145-150, 2002.
- [37] S. D. Campbell, "Carbon fiber-reinforced elastomeric pads for building isolation," *The 33rd International Congress and Exposition on Noise Control Engineering*, 2004.
- [38] G. D. Ashkezari, A. A. Aghakouchak and M. Kokabi, "Design, manufacturing and evaluation of the performance of steel like reinforced elastomeric seismic isolators," *Journal of Materials Processing Technology*, Vols. 197,140-150, 2008.

- [39] B. Kang, G. Kang and B. Moon, "Hole and lead plug effect on fiber reinforced elastomeric isolator for seismic isolation," *Journal of Materials Processing Technology*, Vols. 592-597, 2003.
- [40] A. Dorfmann and R. Ogden, "A constitutive model for the mullins effect with permanent set in particle-reinforced rubber," *International Journal of Solids and Structures*, pp. 1855-1878, 2004.
- [41] H. Toopchi-Nezhad, Stable unbonded fiber reinforced elastomeric isolators, Doctoral Thesis, McMaster University, 2008.
- [42] H. Toopchi-Nezhad, M. J. Tait and R. G. Drysdale, "Testing and modeling of square carbon fiber-reinforced elastomeric seismic isolators," *Structural Control and Health Monitoring*, Vols. 15, 876-900, 2008.
- [43] H. Toopchi-Nezhad, M. J. Tait and R. G. Drysdale, "Lateral response evaluation of fiber-reinforced neoprene seismic isolators utilized in an unbonded application," *Journal of Structural Engineering*, Vols. 134(10), 1627-1637, 2008.
- [44] H. Toopchi-Nezhad, M. Tait and R. Drysdale, "Simplified analysis of a low-rise building seismically isolated with stable unbonded fiber reinforced elastomeric isolators," *Canadian Journal of Civil Engineering*, vol. 36, 2009.
- [45] H. Toopchi-Nezhad, M. Tait and R. Drysdale, "A novel elastomeric base isolation system for seismic mitigation of low-rise buildings," in *The 14th World Conference on Earthquake Engineering*, Beijing, China, October 2008.
- [46] C. Christopoulos and A. Filiatrault, *Principals of Passive Supplemental Damping and Seismic Isolation*, Italy: IUSS Press, 2006.
- [47] T. T. Soong and G. F. Dargush, *Passive Energy Dissipation Systems in Structural Engineering*, John Wiley & Sons: West Sussex, England, 1997.
- [48] "Taipei financial center corporation," <http://www.taipei-101.com>, 2005.

- [49] R. Rana, "Response control of structures by tuned mass dampers and their generalizations," in *Eleventh World Conference of Earthquake Engineering*, 1996.
- [50] S. Randall, D. Halsted and D. Taylor, "Optimum vibration absorbers for linear damped systems," *Journal of Mechanical Design*, vol. 103, 1981.
- [51] J. Den Hartog, *Mechanical vibrations*, vol. 4th edition, New York: McGraw-Hill, 1956.
- [52] R. Rana and T. Soong, "Parametric study and simplified design of tuned mass dampers," *Engineering Structures*, vol. 20, 1998.
- [53] J. Den Hartog, *Mechanical vibrations*, 4th Edition, New York: McGraw-Hill, 1985.
- [54] G. Warburton and E. Ayorinde, "Optimum absorber for simple systems," *Earthquake Engineering and Structural Dynamics*, vol. 8, 1980.
- [55] T. Asami, T. Wakasono, K. Kameoka and M. Hasegawa, "Optimal design of dynamic absorbers for a system subjected to random excitation," *JSME international Journal*, vol. 34, no. 2, 1991.
- [56] T. Asami, O. Nishihara and A. Baz, "Analytical solutions to H_∞ and H_2 optimization of dynamic vibration absorbers attached to damped linear system," *Journal of Vibration and Acoustics*, vol. 124, no. 2, 2002.
- [57] F. Sadek, B. Mohraz, A. Taylor and R. Chung, "A method of estimating the parameters of tuned mass dampers for seismic applications," *Earthquake Engineering and Structural Dynamics*, vol. 26, 1977.
- [58] Y. Gupta and A. Chandrasekaran, "Absorber system for earthquake excitation," *Proc. 4th World Conference on Earthquake Engineering*, vol. II, 1969.
- [59] A. Kaynia, D. Veneziano and J. Biggs, "Seismic effectiveness of tuned mass dampers," *Journal of Structural Dynamics*, vol. 107, 1981.

- [60] J. R. Sladek and R. E. Klingner, "Effect of tuned mass damper on seismic response," *Structural Engineering*, vol. 109, 2004.
- [61] P. Wirsching and J. Yao, "Safety design concepts for seismic structures," *Computational Structures*, vol. 3, 1973.
- [62] P. Wirsching and G. Campbell, "Minimal structural response under random excitation using vibration absorber," *Earthquake Engineering and Structural Dynamics*, vol. 2.
- [63] S. Ohno, A. Watari and I. Sano, "Optimum tuning of the dynamic damper to control response of structures to earthquake ground motion," *Proceedings of 6th World Conference on Earthquake Engineering*, vol. 3, 1977.
- [64] R. Villaverde, "Reduction in seismic response with heavily-damped vibration absorbers," *Earthquake Engineering and Structural Dynamics*, vol. 13, 1985.
- [65] R. Villaverde, "Seismic control of structures with damped resonant appendages," *Proceedings of 1st World Conference on Structural Control*, 1994.
- [66] R. Villaverde and L. Koyama, "Damped resonant appendages to increase inherent damping in buildings," *Earthquake Engineering and Structural dynamics*, vol. 22, 1993.
- [67] R. Villaverde and S. Martin, "Passive seismic control of cable-stayed bridges with damped resonant appendages," *Earthquake Engineering and Structural Dynamics*, vol. 24, 1995.
- [68] T. Miyama, "Seismic response of multi-storey frames equipped with energy absorbing storey on its top," *Proceedings of 10th World Conference on Earthquake Engineering*, vol. 7, 1992.
- [69] R. Soto-Brito and S. Ruiz, "Influence of ground motion intensity on the effectiveness of tuned mass dampers," *Earthquake Engineering and Structural Dynamics*, vol. 28, 1999.
- [70] T. Pinkaew, P. Lukkunaprasit and P. Chatupote, "Seismic effectiveness of tuned mass dampers for damage reduction of structures," *Engineering Structures*, vol. 25, 2003.

- [71] C. Lin, J. Wang and J. Ueng, "Vibration control identification of seismically excited MDOF structure-PTMD systems," *Journal of Sound and Vibration*, vol. 240, 2001.
- [72] R. Villaverde, "Reduction in seismic response with heavily-damped vibration absorbers," *Earthquake Engineering and Structural Dynamics*, vol. 13, 1985.
- [73] J. C. Miranda, "On tuned mass dampers for reducing the seismic response of structures," *Earthquake Engineering and Structural Dynamics*, vol. 34, 2005.
- [74] M. Maravani and M. Hamed, "Numerical modeling of sloshing motion in a tuned liquid damper outfitted with a submerged slat screen," Thermal Processing Laboratory (TPL), Department of Mechanical Engineering, McMaster University, Canada, 2009.
- [75] P. Bhuta and L. Koval, "A viscous ring damper for a freely precessing satellite," *International Journal of Mechanical Science*, vol. 8, 1966.
- [76] G. Carrier and J. Miles, "On the annular damper for a freely precessing gyroscope," *Journal of Applied Mechanics*, vol. 27, 1960.
- [77] L. Sun, Semi-analytical modelling of TLD with emphasis on damping of liquid sloshing, Japan: Ph.D., University of Tokyo, 1991.
- [78] P. Warnitchai and T. Pinkaew, "Modeling of liquid sloshing in rectangular tanks with flow restricting damping devices," *Engineering Structures*, vol. 20, no. 7, 1998.
- [79] J. Miles, "Surface wave damping in closed basins," *Proceedings of the Royal Society of London*, vol. 297, 1967.
- [80] H. Bauer, "Nonlinear propellant sloshing in a rectangular container of infinite length," *Developments in Theoretical and Applied Mechanics*, vol. 3, 1964.
- [81] H. Abramson, The dynamic behaviour of liquid in moving containers, Washigton, D.C.: NASA SP-I06, 1967.

- [82] S. Kaneko and O. Yoshida, "Modeling of deep water-type rectangular tuned liquid damper with submerged nets," *ASME Journal of Pressure Vessel Technology*, vol. 121, 1999.
- [83] M. Tait, A. El Damatty, Isyumo and M. Siddique, "Numerical flow models to simulate TLDs with slat screens," *Journal of Fluids and Structures*, vol. 20, no. 8, 2005.
- [84] M. Tait, A. El Damatty and N. Isyumov, "Testing of tuned liquid damper with screens and development of equivalent TMD model," *Wind and Structures*, vol. 7, no. 4, 2004.
- [85] T. Shimizu and S. Hayama, "Nonlinear responses of sloshing based on shallow water wave theory," *JSME international Journal*, vol. 30, no. 263, 1987.
- [86] M. Tait, "Modelling and preliminary design of a structure-TLD system," *Engineering Structures*, vol. 30, 2008.
- [87] T. Caughey, "Equivalent linearization techniques," *Journal of the Acoustical Society of America*, vol. 35, 1963.
- [88] F. Sakai, S. Takaeda and T. Tamaki, "Tuned liquid column damper, new type device for suppression of building vibrations," in *Proc. Int. Conf. on Highrise Buildings*, Nanjing, China, 1989.
- [89] C. Chang and Q. W.L., "Unified dynamic absorber design formulas for wind-induced vibration control of tall buildings," *The Structural Design of Tall Buildings*, vol. 7, 1998.
- [90] E. Graham and A. Rodriguez, "The characteristics of fuel motion which affect airplane dynamics," *Journal of Applied Mechanics*, vol. 19, 1952.
- [91] J. Hamelin, The effect of screen geometry on the performance of a tuned liquid damper, M.A.Sc., McMaster University, 2007.
- [92] H. Morsy, A numerical study of the performance of tuned liquid dampers, McMaster University, M.A.Sc Thesis, 2010.

- [93] H. Lamb, *Hydrodynamics*, Cambridge, England: The University Press, 1932.
- [94] A. K. Chopra, *Dynamics of structures: Theory and applications to earthquake engineering*, 2nd Edition, Upper Saddle River, NJ: Prentice-Hall Inc., 2000.
- [95] O. Faltinsen, O. Rognebakke, I. Lukovsky and A. Timokha, "Multi-dimensional modal analysis of nonlinear sloshing in a rectangular tank with finite water depth," *Journal of Fluid Mechanics*, vol. 407, 2000.
- [96] J. Love and M. Tait, "Nonlinear simulation of a tuned liquid damper with damping screens using a modal expansion technique," *Journal of Fluids and Structures*, vol. 26, 2010.
- [97] O. Faltinsen and A. Timokha, "An adaptive multi-modal approach to nonlinear sloshing in a rectangular tank," *Journal of Fluid Mechanics*, vol. 432, 2001.
- [98] A. Kareem, "Modeling of base isolated buildings with passive dampers under winds," *Journal of Wind Eng and Industrial Aerodynamics*, vol. 72, 1997.
- [99] P. Henreson and M. Noval, "Response of base isolated buildings to wind loading," *Journal of Earthquake Engineering and Structural Dynamics*, vol. 18, 1989.
- [100] A. Kareem and M. J. Deklotz, "Dynamics of wind exited base isolated buildings with passive dampers," Notre Dame, Indiana : Technical report, Department of Civil Engineering, University of Notre Dame, 1991.
- [101] Y. Chen and G. Ahmadi, "Wind effects on base isolated structures," *Journal of Engineering Mechanics*, vol. 118, 1992.
- [102] S. Sinha and G. Li, "Optimal design of base isolated structure with dynamic absorbers," *Journal of Engineering Mechanics*, vol. 120, 1993.
- [103] J. Yang and D. Wong, "On seismic hybrid control system, structural safety and reliability," in *Proc. ICOSSAR89*, San Francisco, 1989.

- [104] A. Kareem, "Modelling of base isolated buildings with passive dampers under winds," *Journal of Wind Engineering and Industrial Aerodynamics*, vol. 72, 1997.
- [105] J. N. Yang, A. Danielians and S. Liu, "Aseismic hybrid control system for building structure," *Journal of Engineering Mechanics*, vol. ASCE 117, 1991.
- [106] H. Tsai, "The effect of tuned mass dampers on the seismic response of base isolated structures," *International Journal of Solids and Structures*, vol. 32, 1995.
- [107] H. Harris and G. Sabnis, *Structural modeling and experimental techniques*, CRC Press, 1999.
- [108] W. Baines and E. Peterson, "An investigation of flow through screens," *ASME Transactions*, vol. 73, 1951.
- [109] O. Faltinsen and A. Timokha, *Sloshing*, Cambridge: Cambridge University Press, 2009.